NUMERICAL MODELLING OF ROCK ANCHOR PULLOUT AND THE INFLUENCE OF DISCRETE FRACTURE NETWORKS ON THE CAPACITY OF FOUNDATION TIEDOWN ANCHORS

by

BRAD PANTON

A THESIS SUBMITTED IN PARTIAL FULFILLMENT OF
THE REQUIREMENTS FOR THE DEGREE OF
MASTER OF APPLIED SCIENCE

in

THE FACULTY OF GRADUATE AND POSTDOCTORAL STUDIES
(Mining Engineering)

THE UNIVERSITY OF BRITISH COLUMBIA
(Vancouver)

April 2016

ABSTRACT

Numerous studies presented in this thesis have reported failure of the rock mass surrounding an anchor, as a result of applied external tensile loads (i.e. pullout loads) transferred to rock mass from the anchor and the overlying structure. Resistance to this failure mechanism is provided in design by assuming that the dead weight of a uniformly shaped inverted "cone", with an assumed initiation point and breakout angle, provides resistance to the design loads. In some cases, a minor contribution of rock mass tensile or shear strength is considered by designers across the area of the assumed pullout cone. Strength estimates for this additional resistance are based primarily on sparse historic testing data, rock mass rating type relationships developed for other applications, and engineering judgement. However, rock mass rating systems assume that the rock mass is homogenous and isotropic, and at the scale of the anchor this assumption may not be valid since individual fractures may influence anchor stability.

As an alternative to the current foundation anchor design method, this research presents a new approach to the rock cone pullout problem using Discrete Fracture Networks (DFN) combined with numerical simulations. The simulations presented in the research investigate the influence of fractures in a synthetic rock mass on ultimate anchor strength, with the purpose of developing a method for incorporation of scale effects of jointing in anchor design.

By using numerical simulations that allow the load transfer mechanism from the anchor to the rock mass to vary with stiffness, it is contended that the failure mechanism of the rock mass under the applied loading can be considered more appropriately in anchor designs. It is also contended that some aleatory variability associated with fractures can be quantified using a DFN-based approach. Fractures are observed to have an influence on both the load distribution in the anchor as well as the ultimate resistance of the rock mass to pullout. The mapping considerations required to produce a DFN model for anchor pullout are described in this thesis and recommendations for incorporating DFN based models in anchor design are provided herein.

PREFACE

This thesis is original and independent work done by the author. The author was the lead author in the one published journal manuscript and two published conference papers based on the work for this thesis. In addition, the thesis supervisor co-authored all of these papers listed below.

The paper "*Numerical Simulation of Rock Cone Pullout and the Influence of Discrete Fracture Network Statistics on Foundation Anchor Capacity*", published in the proceedings of the 13th International ISRM Congress 2015 in Montreal, Quebec is based on Chapter 5 in this thesis.

The paper "*Design of Rock Foundation Anchorage Using Discrete Fracture Networks*", published in the inaugural proceedings of the 2014 International Discrete Fracture Network Engineering Conference in Vancouver, Canada is based on Chapter 8 in this thesis.

The paper "*A Discrete Fracture Network Approach for the Design of Rock Foundation Anchorage*", published in the Mining Technology Journal (in press) is based on Chapter 5, 6, and 8 in this thesis.

TABLE OF CONTENTS

List of Tables

List of Figures

List of Figures cont'[1]

List of Figures cont'[2]

ACKNOWLEDGEMENTS

"*The plan was simple. Surround myself with the best people I could find, give every bit of energy toward [the project], and let the results speak for themselves. Below is a list of these people. I am forever grateful for your efforts*". - Jeremy Jones, Deeper Project.

I would like to express my sincere gratitude to my supervisor Dr. Davide Elmo for sharing his extensive knowledge of Discrete Fracture Networks, brittle fracture mechanics and numerical simulations with me. In addition, I would like to thank my examining committee members Dr. Erik Eberhardt and Dr. Scott Dunbar for their useful review comments, both in the context of rock mechanics and engineering design.

A special thank you to my good friends and mentors at Golder Associates, particularly Dr. Paul Schlotfeldt, Mr. Richard Humphries, Dr. Jose (Joe) Carvalho and Dr. Edwin (Ted) Brown for the reviews, encouragement and guidance both my career and in the work presented in this thesis.

I would also like to thank the British Columbia Ministry of Transportation and Infrastructure, in particular Mr. Daryn Yonin and Mr. Terry Harbicht, for encouraging me to pursue my interest in the field of civil engineering rock mechanics and for guidance in engineering design.

Finally, I would like to thank my fiancé Chelsie for her love and understanding in the time it took for me to finish this thesis. I look forward to our life together and adventures that the future will bring us in the Kootenays and the mountains of the world.

"*If I have seen further it is by standing on the shoulders of giants*". – Isaac Newton

1 INTRODUCTION

1.1 Problem Statement

This study investigates the influence of fractures or joints on the stability and pullout resistance of rock foundation anchors in geo-mechanical simulations.

Rock mass pullout is an important consideration in the design of rock foundations, where tiedown anchors or micropiles transfer external loading from the structure to the surrounding rock mass. Pullout failure, as opposed to rock-grout bond failure, often governs the design of anchor lengths where foundation anchor groups are tightly spaced or "pullout cones" have considerable overlap. The current standard of practice for foundation design in Canada does not explicitly consider naturally occurring fractures in the design of anchors.

Engineers often use rock mass rating type correlations (RMR, Q, GSI), developed for other applications, to make simplifying assumptions for Type D (rock mass pullout failure) in design. However, it is contended that if the distribution of discontinuities in the rock mass is not homogenous the rock mass rating type correlations may not be valid, since many of these relationships assume that the rock mass behaviour is in fact homogenous and isotropic.

Part of the reason that no detailed correlation has been completed specific to the Type D mechanism is the difficulty in full scale "cone pullout" testing. Testing the cone pullout mechanism, as opposed to the rock-grout interface (Type C failure), requires a very large testing jack with widely spaced out-riggers which provide a reactionary force outside of the area of influence of rock mass dilation. This dilation occurs as a result of the complex, modulus dependant load transfer from the steel tendon to the grout and finally to the rock mass. For this reason, the standard of practice is to use very conservative estimates for rock mass strength, forgo in-situ testing, and often forgo confirmation of anchor designs in the field prior to installation of the final foundation anchors.

Many of the historic full scale pullout tests were completed in the 1970's and 1980's when numerical modelling codes were much less sophisticated. It is contended that the numerical modelling codes available today, calibrated with full scale testing, can be used to improve our understanding of the cone pullout mechanism. These codes can also be used incorporate the influence of rock mass heterogeneity in the design of anchors.

1.2 Research Objectives

To assist in better understanding the failure mechanism associated with Type D anchor pullout failure, this research introduces the influence of joints on simulated capacity, by combining discrete fracture networks (DFN) with geo-mechanical numerical simulations. At the scale of many rock anchor pullout problems, the strength and deformation properties of the rock mass are anisotropic, and can be controlled by a few persistent fractures and small "rock bridges". The distribution of joints or fractures can be quantified by mapping fracture orientations, intensity or volumetric fracture counts, fracture termination and distribution of fracture radius/lengths. The "cone" of deformation or dilation is highly dependent on the distribution of load along an anchor. This load transfer mechanism is heavily influenced by the modulus of elasticity of the grout compared to the modulus of elasticity of the surrounding rock mass, a variable that also depends on the frequency and distribution of fractures. Rock mass behaviour is also investigated in this thesis.

The primary research objectives of this thesis are:

1. To validate the suitability of a finite element code, with explicit representation of joints in the mesh domain, to model the rock cone pullout mechanism and dilation prior to failure;
2. To determine the influence of DFN statistics on modelled anchor capacity. Specifically, the influence of fracture intensity (P21), the interconnectedness of jointing and joint persistence, and joint orientation are investigated; and
3. To develop a methodology for incorporation of numerical models in design. Modelling iterations should be fast enough that this methodology can incorporate multiple Discrete Fracture Network (DFN) realizations for efficient integration with reliability based design methods.

In order to achieve these objectives several secondary objectives are addressed:

1. Establishment of a conceptual softening relationship for joints and the rock mass, checked against the standard design approach, and calibrated to historic testing;
2. The progressive nature of the cone pullout mechanism is also validated using a finite-discrete element code, and the influence of intact rock modelling parameters in this code is also investigated;
3. Difficulties with three dimensional analysis of the cone pullout problem are also investigated using Fracman and 3DEC; and
4. Further engineering applications for the combined DFN-numerical approach are outlined.

1.3 Thesis Organization

This thesis is divided into 9 chapters; following this introduction (Chapter 1) is a literature review (Chapter 2) and discussion on quantifying variability of naturally occurring fracture (Chapter 3). The final chapter (Chapter 9) summarizes the conclusions and recommendations. The five research chapters in between follow the organizational structure shown in Figure 1 below.

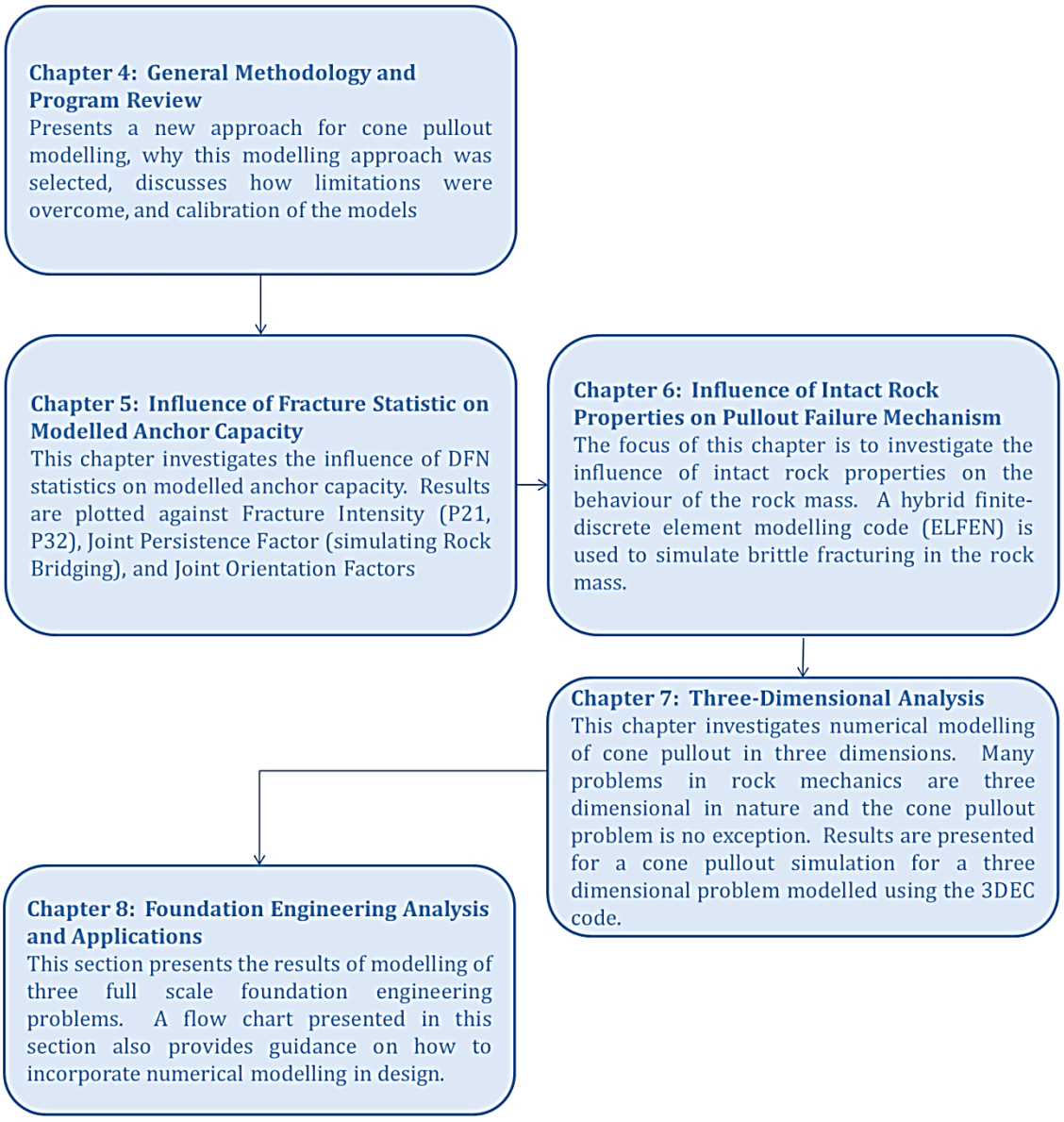

Figure 1 – A Flow Chart Indicating Thesis Structure of Main Research Chapters

2 LITERATURE REVIEW

2.1 Introduction

Chapter 2 provides a literature review describing the current state of practice of rock anchor design, a summary of available testing data where rock mass pull out was reported, and a general overview of the use of anchors in the rock mechanics stabilization of foundations. Specifically, this literature review focusses on the Type D (mobilization of the rock mass) failure mechanism which is described by Brown (2015).

The purpose of rock anchorage in design is to stabilize foundations where overturning moments or uplift forces result in tensile and shear forces in the rock mass. Brown (2015) notes that engineering applications of anchors include stabilizing sheet piles; anchorage of buildings, bridge and tower foundations; anchor marine structures or to prevent overturning, sliding and hydrostatic uplift of dam foundations. Of these applications, rock mass pullout in primarily a concern in fractured rock where structural design requires the installation of tightly spaced, heavily loaded anchors. Dam or bridge foundations typically have the highest load concentrations, specifically where retrofit or upgrade of the existing structure is required and new anchors are installed in the same footprint as existing tightly spaced anchors.

Bruce and Wolfhope (2012) describe the history and use of rock anchors in dam engineering dating back to 1934 where anchors were first reported for the stabilization of the Cheurfas Dam in Algeria. The first high capacity prestressed rock anchors installed in North America were reported in 1962 for the John Hollis Bankhead Lock and Dam in Alabama where the first 6 test anchors and 19 production anchors were installed. This project was completed by the U.S. Army Corps of Engineers who gained sufficient confidence from the installations during the project to recommend the use of anchors on half a dozen anchor projects over the next six years.

Prior to producing standards for anchors, anchorage technology was driven by post tensioning equipment suppliers employing the same standards assumed for the design of anchors for concrete structures such as towers and buildings. Bruce and Wolfhope note that the “geotechnical” inputs (including activities for drilling and grouting) were typically within the scope of drilling contractors that were specialized in site investigation, dam foundation grouting and tieback anchor installations. Early engineering and construction practices are documented further by Littlejohn

and Bruce (1977) who provide an overview of prestressed rock anchor design, construction and sizing. Since the first anchor project in 1962, anchors have been used successfully in North America on over 400 dams. A histogram showing the distribution of dams anchor per year is shown on Figure 2 and a sketch showing the number of dams anchored / number of large dams in Canada is provided by Bruce and Wolfhope as shown in Figure 3.

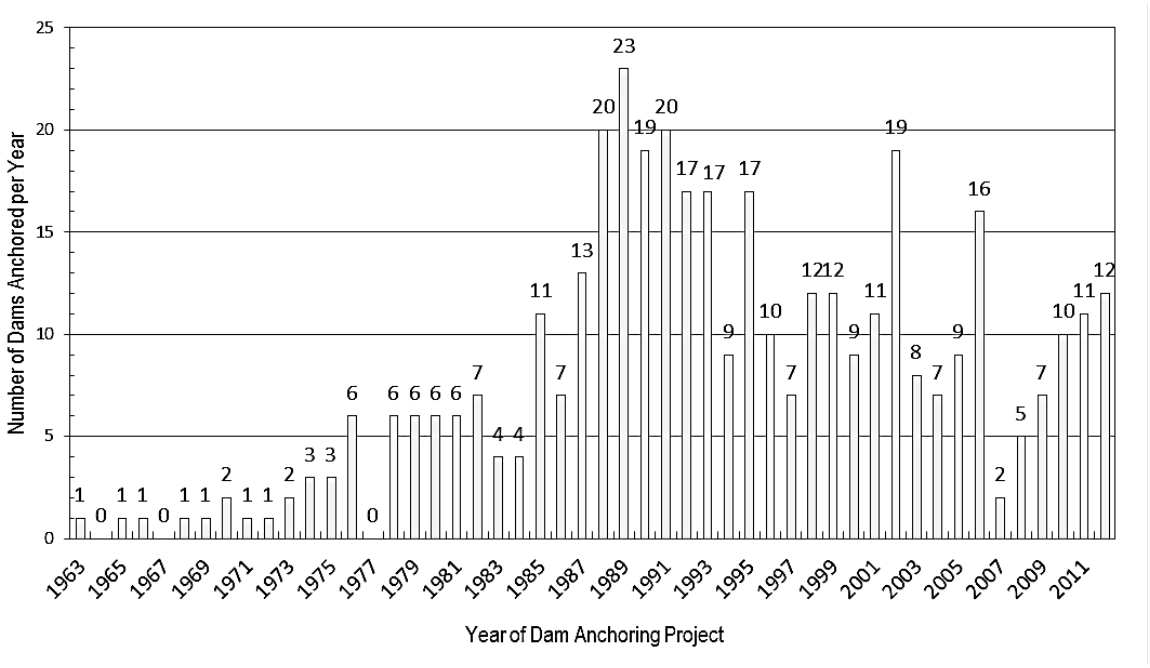

Figure 2 – A histogram of dams anchored per year; modified after Bruce and Wolfhope (2012)

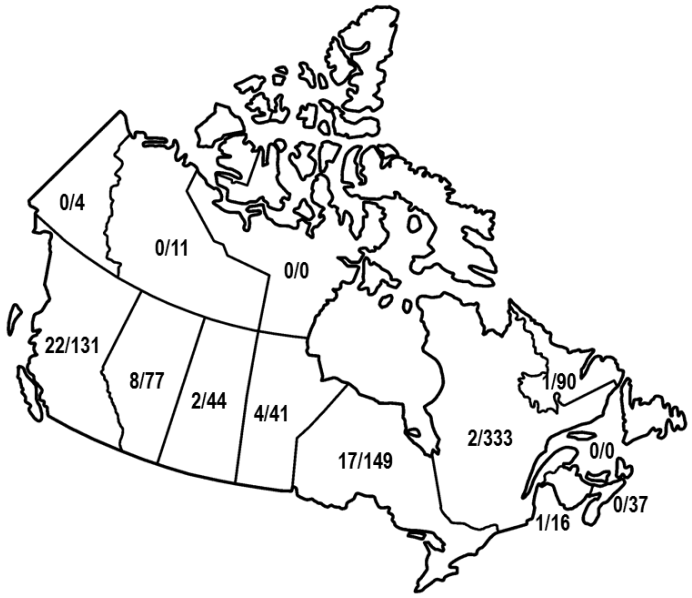

Figure 3 – A sketch indicating the number of dams anchored / number of large dams in Canada; modified after Bruce and Wolfhope (2012)

To allow for a sense of scale of the anchor problem to be developed, Hobst and Zajic (1977) describe the load distribution calculations required to incorporate pre-stressed anchors in dam design. In order to visualize how the anchor forces grow with increasing dam height the authors provide a graph, Figure 4, which plots the calculated anchorage force required for a specific dam height. A reduction in the required anchorage force is also decreased by reducing the downstream batter (λ), with the assumption that this value is between 0.8-0.25, that the coefficient of friction in the footing has a value of 0.75 and that the factor of safety in the stability calculation is 1.5. Hobst and Zajic also describe the cost savings associated with anchorage of gravity dams in bedrock, the first of which to be "*fully anchored into bedrock*" was the 20m high Ernestina Dam in Brasil which was completed in 1955. The dam foundation is embedded deep into rock so that the dam acts as a cantilever. The securing of the dam was further advanced by anchorage installed in the upstream heal of the dam, and which this design the volume of concrete was reduced from 22,000 m^3 to 7,300 m^3. The 45m high Catagunya Dam, completed in 1960 in Tasmania, also reported significant cost savings from anchorage into rock. A cross section through the spillway block of this dam is provided in Figure 4. As shown on this figure an anchoring force if about 5.25MN was required per meter of dam, which was transmitted to the rock mass by 7.5 cm diameter cables installed in drill holes and encapsulated with grout. The anchorage reportedly reduced the project construction costs by 50 percent.

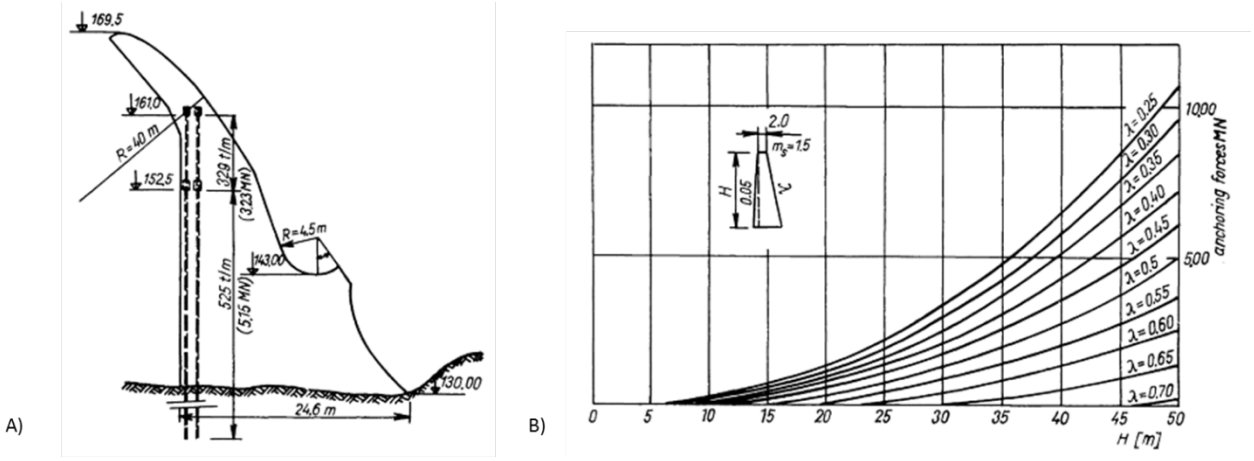

Figure 4 – A cross section through the spillway block of the historic Catagunya Dam in Tasmania with Anchor Forces shown (left); and chart indicating anchoring forces plotted against height for a given gradient (0.8>λ>0.25) for the downstream face of the dam (right);

Modified after Hobst and Zajic (1977)

Further to the anchorage design for new structures, Xu and Benmokrane (1996) reviewed a number of cases where post-tensioned or pre-stressed anchors were required for strengthening existing structures. The authors note that many old dams are in need of strengthening and rehab as a result of aging, deterioration, deficiencies in historic design and construction, and more stringent safety standards. It is the opinions of the authors that post-tensioned anchors are the most practical and cost-effective method of strengthening existing dams subjected to direct tension, sliding, overturning and seismic loading. This is partly due to the fact that the post-tensioning technique requires minimal demolition of the existing structure, has only minor impacts to the dam, and is relatively inexpensive compared to pouring the mass amounts of concrete that would be required to provide similar resistance.

The Xu and Benmokrane note that upgrades at various facilities may be required to:

- Increase spillway capacity and stability relating to a new design code for the probable maximum flood (PMF);
- Upgrading to a new design code for the design seismic accelerations or Maximum Credible Earthquake (MCE);
- Upgrading stability relating to structural considerations such as ageing or deterioration, or stabilizing concrete cracks;
- Raising dam height due to new design codes for the PMF;
- Raising dam height for greater storage or to remedy other deficiencies in design;
- Strengthening dam abutments or dam foundations, reinforcing shear keys.

The upgrades and strengthening requirements, to meet changes in safety standards or to improve the performance of an existing structure, often require that new anchorage is installed immediately adjacent to the anchorage installed during historic construction. Geometric constraints of these type of upgrades often require that anchors are closely spaced to develop the required design resistance.

A number of cases where additional anchors were required to rehabilitate structures include:

- Menjil Dam, Iran: the 106m high gravity dam was built in 1962 and in 1991 with two hundred and thirty five (235), 54 No. 15.2 tendons installed with a working anchor load of 8400kN to increase dam safety due to fissuring during the MCE. The minimum hole spacing

was reportedly 1.4m with a maximum total anchor length of 43m embedment with a bond length of 12m.

- Stewart Mountain, USA: the 30m high concrete buttress dam was upgraded in 1987 with thirty three (33), 18 No. 15.2 tendons installed with a working anchor load of 4680kN for seismic safety upgrades for the design MCE. The minimum hole spacing was reportedly 0.7m which required a maximum total anchor length of 38m embedment with a bond length of 5.6m.
- John Hart Dam, Canada: the 30m high concrete buttress dam was upgraded in 1987 with thirty three (33), 18 No. 15.2 tendons installed with a working anchor load of 4680kN for seismic safety upgrades for the design MCE. The minimum hole spacing was reportedly 0.7m which required a maximum total anchor length of 38m embedment with a bond length of 5.6m.
- Manly Dam Australia: the 19m high dam was built in 1882 and in 1981 46 x 24 No. 15.2 tendons were installed to an ultimate load of 3600kN to accommodate deficiency in the uplift design of the structure. The minimum hole spacing was reportedly 5m with a maximum total anchor length of 43m embedment into Sandstone with a bond length greater than 3m.
- Corra Linn Dan, Canada: the 14m high gravity dam was upgraded in 1992 with one hudred and fourteen (114), 15 No. 15.2 tendons installed with a working anchor load of 2350kN for seismic safety upgrades for the design MCE. The minimum hole spacing was reportedly 4.3m which required a maximum total anchor length of 30m embedment with a bond length of 6.0m.

More recently, there have been significant developments in the design and fabrication of re-stressable, corrosion protected, high capacity (>13.5 MN), re-stressable ground anchors. Seven Mile Dam in Canada was upgraded in 2003 using 92-stand cable anchors with an individual ultimate anchor capacity of 23MN. Testing on these anchors was completed to a test load of 19MN which is about 80% of the ultimate strength of the bar. The longest anchors on the project were 126.5m length (Sutton et al 2004). Sinclair and Rodd, 2011 describe the use of 91-strand cable anchors with larger strand thickness for upgrades at the Catagunya Dam. This project required the installation of ninety two strand anchors, installed with an ultimate anchor capacity of 25MN. This size of anchor is now being accepted as the "standard" choice for large tendons for dam upgrades in Australia, and the world record capacity of these anchors was pioneered on the Canning Dam circa

2000. The basics of permanent anchoring is still common with the intentions of the developments that took place in the early 1980's (Sinclair and Rodd, 2011). Since that time the tendon capacities have increased by over 400%. The current design approach produces anchors in the range of 30-50m for large dam upgrades. These anchored lengths are very long and these designs are based mostly on empirical relationships developed for other purposes. The current design approach is discussed in the next section.

2.2 Canadian Standard of Practice for Anchor Design

Significant advances have been made in the area of design and fabrication of strand anchors for the use in rock anchor design, however, advances have not been made in the understanding of how the rock mass is mobilized around high capacity anchors. The standard of practice appears to be unchanged over the past 40 years. This is likely due to the fact that no documented cases of "cone pullout" have been reported for a dam foundation. The current standard of practice for the design of anchors is suitably conservative, however, with tendon capacities increasing by 400% over the past forty years the current standard for assessing the Type D cone failure mechanism should be reviewed.

Much of the standard of practice for anchor design assumptions used today dates back to the 1970's. Bruce and Wolfhope (2012) note that in 1974 there was a recognized need to develop national standards for the anchorage of foundations. In response to this need, the Post-Tensioning Division of the Prestressed Concrete Institute (PCI) formed a technical committee that published a 32 page document, Tentative Recommendations for Prestressed Rock and Soil Anchors. After this document was produced, the Post-Tensioning Institute (PTI) was formed and successive editions of "Recommendations" were issued in 1980, 1986, 1996 and 2004. The current state of practice of tensioned tiedown anchor design is centered around recommendations prepared by the Post-Tensioning Institute in a publication titled PTI DC35.1-04: Recommendations for Pre-stressed Rock and Soil Anchors, Fourth Edition, 2004. These recommendations were produced under the review of a committee of engineers with backgrounds in geotechnical consulting, government agencies (such as Federal Highway Administration, U.S. Army Corps of Engineers), construction, and bolt manufacturing. However, the most recent editions focus on five design considerations which include materials, design, corrosion protection, construction and stressing/testing. In Section C.6.7.1 Rock Anchors some commentary is provided on analysis of rock mass pullout of anchors.

The current edition of the PTI (2004) states that for conventional rock anchors installed in competent rock:

"*The bond stresses are typically concentrated at the top of the bond length. The maximum strain in the tendon bond length occurs at the top of the tendon bond and may cause a local load redistribution within the rock or the displacement of a small cone of rock. When this occurs, the peak stress position moves down the tendon bond length. When selecting the elevation of the top of the bond length, the designer must consider the resistance to pullout of the rock mass, which also governs the anchor length. The shape of the volume of rock mobilized by the anchor depends on the orientation and frequency of jointing and bedding planes.*"

The PTI then continues on to provide average ultimate bond stress estimates for various rock types to be used in design against the Type C failure mechanism, of rock-grout bond pullout, but notes that the stress distribution along an anchor may not be uniform. No additional commentary is provided specific to the Type D, pullout cone mechanism, which leaves the design of the pullout failure mechanism up to the judgement of the design engineer.

A supplemental design reference is provided by the U.S. Army Corps of Engineers who produced a guideline for the engineering design of rock foundations in 1994 which describes the design of anchors (U.S. ACE Engineering Manual 1110-1-2908, 1994). This document describes the failure mechanism or potential failure paths for loaded foundations and provides a general approach to the design of foundations and anchorage. The current practice of the design of anchors noted in this document is provided in Section 2.3. In this document it is apparent that jointing and kinematic type failure mechanisms should be considered in the design of foundations, however, for the analysis of tensioned foundation anchors the Corps refers to the cone pullout method by Littlejohn and Bruce. As an opening statement to the anchorage section the Corps of Engineers notes that "*typically analysis of systems used to anchor mass concrete consists of one of two methods; procedures based upon classical theory of elasticity or procedures based upon empirical rules or trial and error based methods. The gap between the methods has been narrowed by research in recent years but has not significantly closed to allow purely theoretical analysis of anchor systems*". In particular, the Corps refers to the Type D pullout cone method where the dead weight of a pullout cone is calculated to resist anchor pullout with an assumed initiation point and breakout angle. The design of this pullout cone is noted to be dependent on rock quality, however, no guidance is given of which breakout angle is to be used in design.

Further to the reference provided by the Corps, the textbook prepared by Wyllie (1999) titled "Foundations on Rock" is used as a primary reference for Canadian rock engineering in the civil engineering rock mechanics industry. Similar to the reference provided by the Corps, Wyllie notes that a check is required to assess that the anchor will mobilize a sufficient volume of rock to support the applied load. The results of uplift tests described by Wyllie suggest that the mass of rock mobilized around the anchor is approximately conical, with the dimensions and shape of the cone being dependant on the structural geology of the site. Wyllie notes that the weight of the cone can be given from the simplifying assumption that the cone of rock mobilized can be approximated by an apex angle of 90 degrees and the position of the apex of the cone is at the midpoint of the apex, as shown in Figure 5. Wyllie notes that the weight of the cone can be calculated from these dimensions, but test results show that the maximum uplift load that is actually supported is as low as 7 and as high as 56 times the weight of the cone. The supporting testing to back up these numbers is provided in Section 2.2.2 in this thesis.

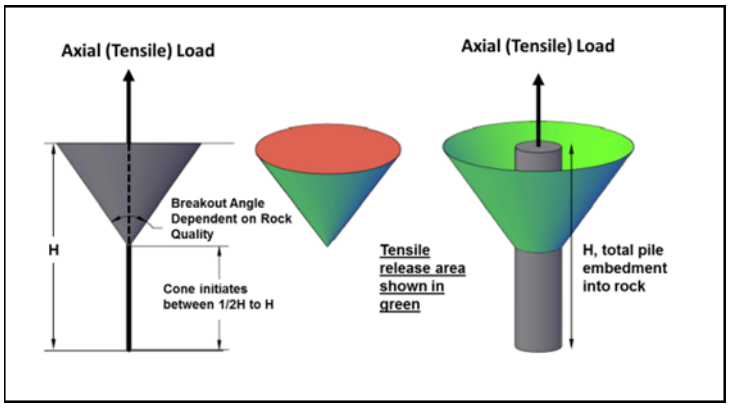

Figure 5 – A sketch showing the apex angle / breakout angle described by Wyllie for the design of anchors

The difference between the cone weight and the actual uplift capacity is that additional support is provided by the strength of the rock on the surface of the assumed cone surface. However, Wyllie notes that a precise design method for the capacity of uplift anchors is difficult to define. Littlejohn and Bruce (1977) suggest that the apex angle varies from 60 to 90 degrees, and Wyllie contends that in strong rock the apex angle can be as great as 120 degrees. The influence of structural geology on the theoretical shape of the pullout cone is provided in Figure 6. Wyllie hypothesizes that the most favourable case is that the structural geology is aligned at right angles to the anchor and the least favourable is where the structural is alignment parallel to the anchor. However, comments by Littlejohn and Bruce suggest that jointing perpendicular to the core axis may in fact

be unfavourable since "laminar" failure can occur as a result of opening up of these joints at shallow anchorage depths. This mechanism is described further in Section 2.2.2. of this thesis where the results of anchor testing are described in more detail. Due to the fact that laboratory testing data suggests that the dead weight cone assumption is conservative, tensile or shear strength is applied to this cone surface. Wyllie notes that the rock strength that operates on the surface of the cone can only be estimated because the combination of shear and tensile movements related to the geological structure is very complex. It is suggested by the author that it is not possible to simulate this behaviour in the laboratory and that the behaviour and strength of the cone is best determined by the results of full scale uplift tests. However where tests are not possible or economically feasible, Wyllie recommends using rock mass strength correlations such as the Hoek-Brown failure criterion. Due to the large apparatus required to develop a reactionary force outside of the zone of influence of the cone, most designers typically do not complete testing prior to design.

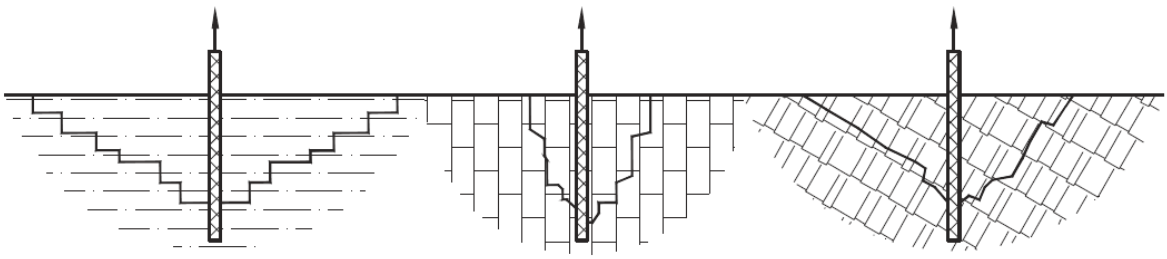

Figure 6 – Influence of Structural Geology on the Shape of Cones of Rock Mobilized by Uplift Anchors, modified after Wyllie, 1999

An example case study of the Canadian standard of practice of anchor / pile design is provided by Schlotfeldt et al. (2013) for the Kicking Horse Canyon New Park Bridge, specifically Pier 5. This structure was designed for live loading and wind loads which result in tensile loading on piles, induced by overturning moments. To complicate the design, unfavourable jointing was noted in the phyllite rock mass and the Pier 5 footing is perched on the edge of a very steep natural bluff. To facilitate the geotechnical component of the design, the compressive loads and uplift loads on the piles were provided by the bridge designer. These load are given as unfactored loads. Depending on the wind direction (typically upstream or downstream) and other live loading, a particular pile may have tensile loads of up to 3MN, as noted by Schlotfeldt et al. (2013), which required a combination of 65WR threadbar and 900mm rock socketed piles.

As described by Schlotfeldt, the design process firstly starts with assessment of the bond length for piles or anchors by assuming or calculating a rock-grout allowable bond stress. This allowable side wall shear stress for rock socketed piles is a key strength parameter for rock socketed pile design

and is a function of the uniaxial compressive strength (UCS) of the rock mass and the roughness of the sidewalls. The rock-grout interface capacity assumes that the stress distribution along the bar is uniform.

After the bond length checks have been completed a rock mass pullout check is required for the tensile design loads. As noted above, Littlejohn (1975 and 1993) and Wyllie (1999) state that the mass of rock mobilized around anchors and piles will be approximately conical in nature. At the Kicking Horse Bridge site the dimensions and shape of the potential 'pull out' cones are complex and are a function of the joint sets present in the rock mass. Possible cone truncations also result due to the edge effect and the potential overlapping cones from individual piles and the loading case considered, as shown in Figure 7 and Figure 8.

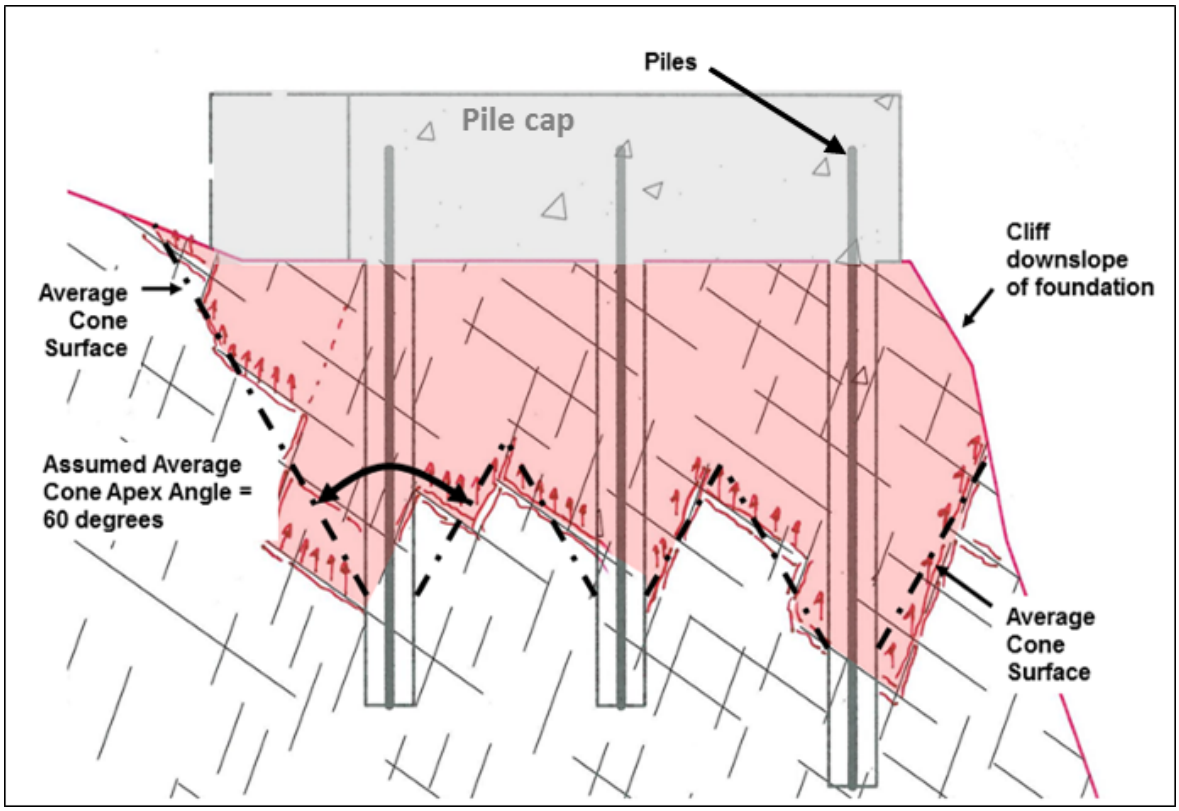

Figure 7 – Idealized group pullout cone geometry estimated based on potential failure along joints sets developed in the rock mass and pile lengths. Reprint from Schlotfeldt et al., (2013) with permission

For Pier 5, it was assumed that the apex of the pull out cone, or potential initiating failure point of the cone, is centered at about 0.5 to the full depth of the rock socket. The apex angle and shape of the cone, and therefore the rock cone surface area available to resist uplift, are affected by the orientation and number of major joint sets present in the rock mass. The pull out cone apex angle for Pier 5 piles is estimated to be close to 60 degrees. Based on the observed improvement in the rock quality with depth in the bored pile sockets for Pier 5, the tensile strength of the rock mass was estimated be around 200 kPa. Even with the worst case truncation for the downslope edge piles and truncation due to interference from adjacent piles, it was estimated that individual piles had an allowable uplift capacity of at least 7 MN (FOS = 3), which exceeds the required maximum uplift of -3.1 MN per pile. Group effect uplift was also considered to be more than adequate.

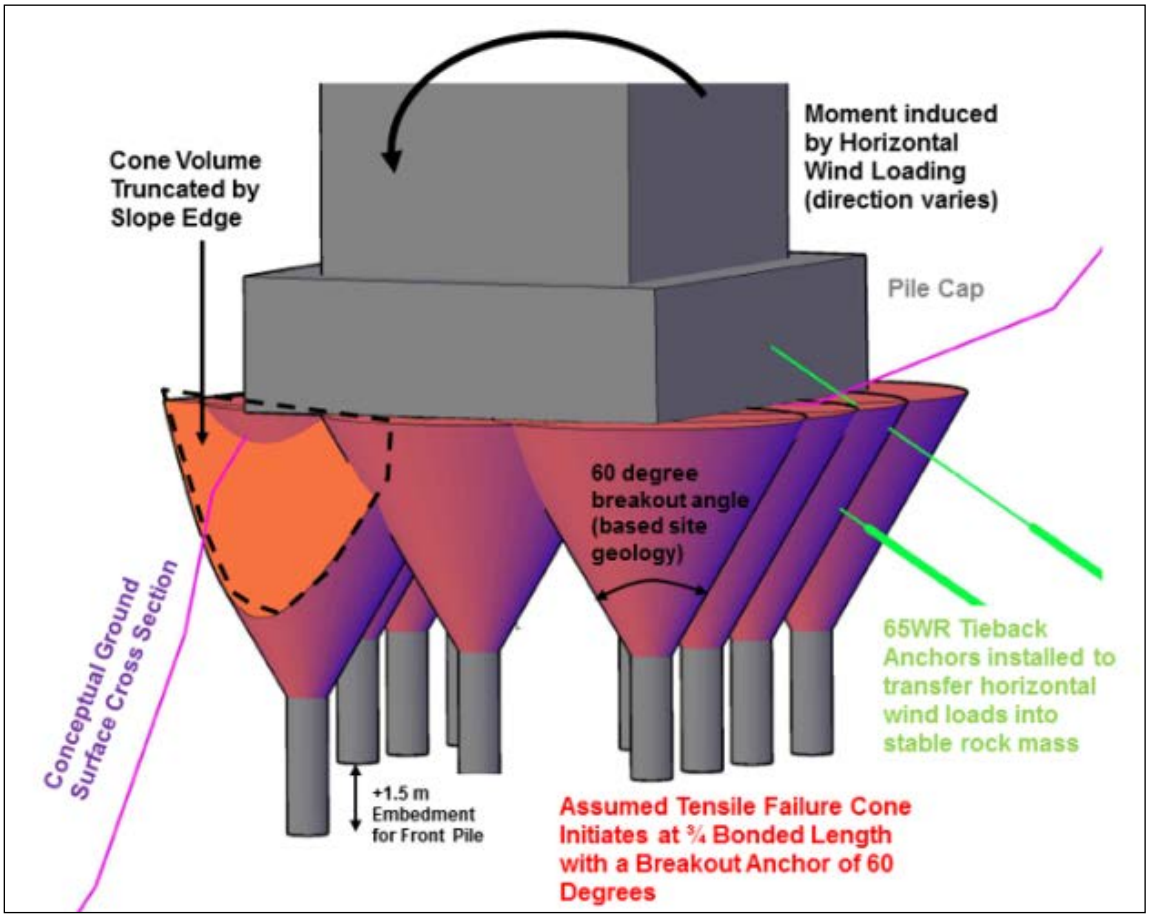

Figure 8 – Conceptual Pier 5 rock foundation design with idealized rock tensile pullout cones (breakout angle 60 degrees shown). Not all piles will act in tension at once, since uplift is as a result of wind loading resulting in a moment with the foundation in compression on one side and uplift or tension on the other side. Since the wind direction changes, each pile needs to be able sustain the maximum uplift. Reprint from Schlotfeldt et. al., 2013 with permission

Further to the bridge and dam examples provided above, anchors are a consideration for powerhouse foundations. Some Structural designer's proposed the use of both fully grouted dowels and post-tensioned anchors, required independently for resistance of foundation loads. The dowels are often required to resist hydrostatic uplift forces and longer anchors, designed with a free stressing length to extend below the embedment depth of the dowels, are required to resist overturning moments from emergency shutdown of the turbines. These anchor are often attached directly to the turbine foundation structures which means that the "pullout cones" formed by these anchors can have significant overlap. The spacing of the dowels is generally determined by the structural designer which provides the driving force across this group cone pullout area. An example screenshot it provided in Figure 9. For the project shown, the good rock exposures and the strong to very strong granitic rock observed on site allowed for some tensile strength to be considered along the outer surface of the pull out cone in the assessment of anchor lengths by the Geotechnical designer. Given that some designers consider only the dead weight of the pullout cone in the assessment, the design method employed on this project was not considered overly conservative. However, since only two well-developed joint sets were observed in the rock on the project site, it is very difficult to visualize a "cone" pulling out as a result of anchor forces since shearing of intact rock would be required in the direction perpendicular to the prominent conjugate joint set orientations. The project used a combination of the cone approach as well as the application of shear strength along the direction perpendicular to the prominent jointing using project specific block geometry in a limit equilibrium analysis. While this method is suitably conservative given the standard design practice, the "cone" overlap between the 100 four meter length dowels and 160 six meter length dowels required for hydrostatic uplift, combined with the envisaged pull out cones initiating below the 12-16m free-stressing length for the post-tensioned anchors was significant. As a result of this overlap, the use of post-tensioned anchors for resistance of turbine shutdown loads was not considered feasible for the project and the design of the Powerhouse foundation proceeded with the application of shear keys with careful blasting into bedrock and a large steel strut was also used to resist lateral loads.

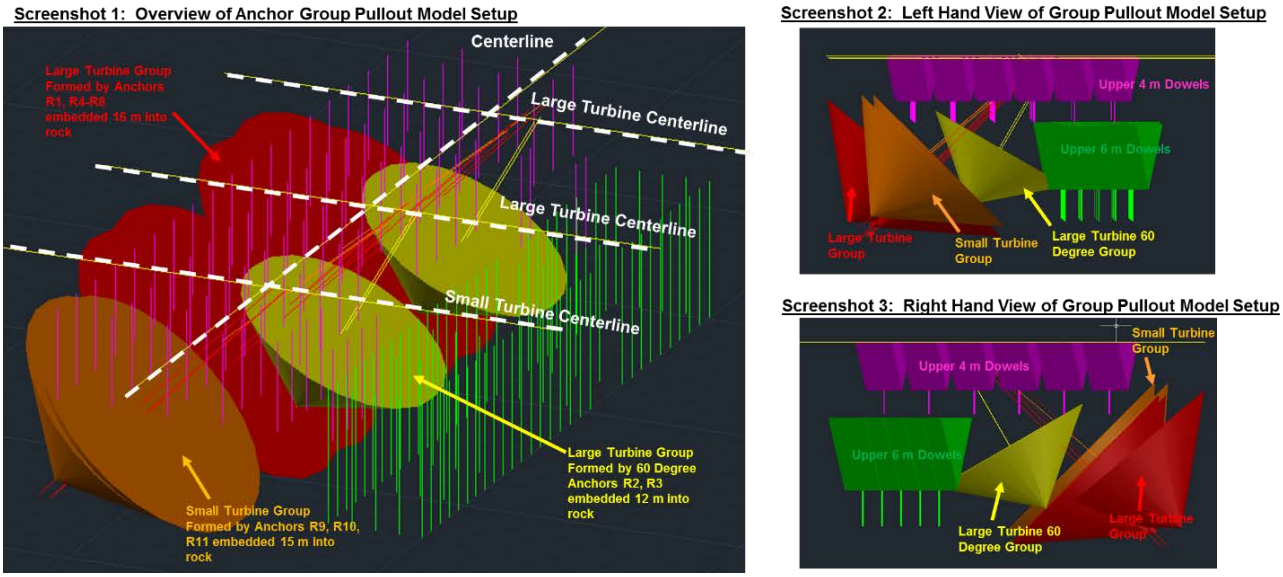

Figure 9– A graphical representation of anchor groups and pullout cones for a small powerhouse foundation

While a limit equilibrium approach was used on this project to try to reflect the difference in the direction of loading and the orientation of jointing at the site, the geotechnical designer could not stray too far from the standard of practice using the cone approach. It is contended that if numerical modelling was completed on this project, the nature of the strong to very strong granitic rock may have been better accommodated in the anchor design and a foundation concept using anchors to stabilize the turbines may have been feasible. In addition, the loads for this small powerhouse foundation were not considerable compared to the 25MN capacity cable anchors used to stabilize the abutments of large arch dams. Given that the recommended anchor lengths for these upgrades exceed 50m in length, it is also contended that the design length of anchors could be optimized using a new design approach.

Further to the typical cone approach and the Canadian standard of practice, Weerasinghe and Littlejohn (1997) discuss a hybrid anchor failure mechanism that they suggest may be applicable for "weak, fissile" mudstone. This mechanism, observed for a fully grouted dowel, included a small amount of local mounding/surface disturbance due to displacement of a central cone, active 'cone' failure and this surface rock mass deformation and cracking is combined with bond failure at the distal half of the rock anchor. The hybrid mechanism observed by Weerasinghe and Littlejohn (1997), and shown in Figure 10, may be applicable for many weak, structureless rock types. However, if persistent discontinuities are present in the rock mass the distribution of tensile cracking may be influenced by joints and the influence of loading may extend further from the

anchor. In a technical review of rock anchorage practice Weerasinghe and Adams (1997) noted that "where a failure plane or major discontinuity exists, the free length of the anchorage must extend beyond this feature thus locating the fixed anchor length in competent rock mass". Furthermore, in a discussion session following the Weerasinghe and Littlejohn (1997) presentation, Littlejohn/Weerasinghe noted that "shear planes are irregular and local features of the rock can influence the point where the cone is generated". This suggests that, although structural features were not noted in the failure mechanism presented by Weerasinghe and Littlejohn (1997) for the rock type discussed, the authors recognized that naturally occurring joints or fractures in the rock mass may have an influence on the behaviour of rock anchorage. Designers generally consider jointing in the shape of cone generated, however, consideration of jointing in the behaviour of rock mass deformation and to the degree that Weerasinghe and Littlejohn describe has yet to make it into engineering practice. A typical example of the cone pullout standard of practice is described in Section 2.2.2. and the behaviour of the rock mass to loading is also described in Section 2.3.2.

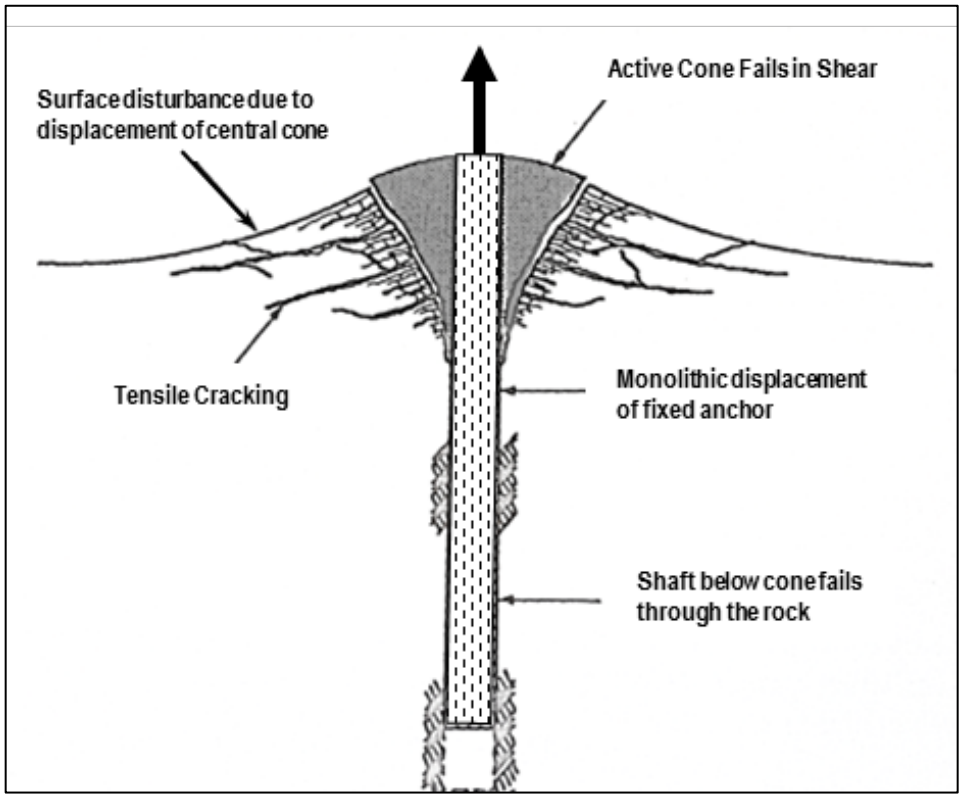

Figure 10 – Alternate pullout mechanism modified after Weerasinghe and Littlejohn (1997)

2.3 Full Scale Anchor Pullout Testing

The Canadian standard of practice does not provide anchor specific references to empirical relationships for calculation of the resistance to the Type D rock mass failure mechanism. Testing data is limited and many references to testing are anecdotal since most of the testing data has the caveat that the results and conclusions are site specific. However, a review of the available testing data has produced a number of interesting conclusions which are presented below.

In 1977 when the paper by Littlejohn and Bruce titled "Rock Anchors: State of the Art" was written, the authors note that there is a "*dearth of data on anchor failures in the rock mass*". The authors continue on to describe a case presented by Saliman and Schaefer (1968) where four tests were carried out on "deformed re-inforcement bars" grouted into 70mm diameter holes to a depth of 1.52m in sedimentary rock. In all test cases, failure occurred when a "block of rock and grout" pulled out and the propagation of cracking to the rock surface gave an indication of the "cone of influence". This pullout "cone" was defined by a zone of propagation of cracking on the rock surface and the shape of cracking is provided in Figure 11. Assuming a bulk density of 2Mg/m^3 for the rock, back analysis of the failure loads indicates very conservative results which include safety factors ranging from 7-23 for an assumed 90 degree breakout angle initiating at the midpoint or lower factors of 0.9 to 2.9 if the cone initiates the base of the four respective anchors tested (Saliman and Schaefer 1968).

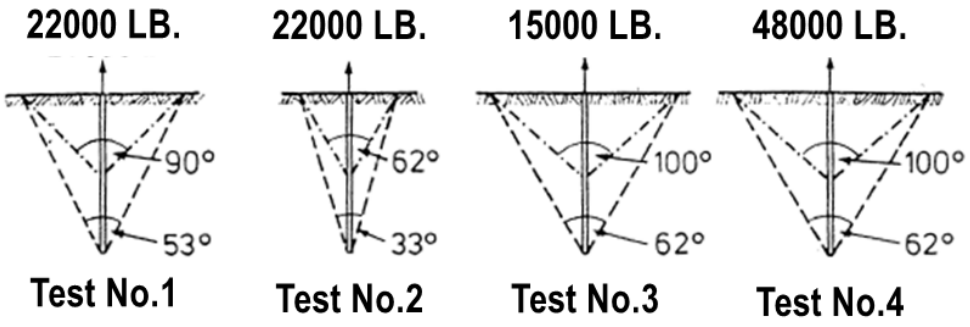

Figure 11 – A summary of four breakout angle from anchor tests. Modified after Saliman and Schaefer 1968

Around the same period, Brown (1970) completed testing on shallow anchors installed in "laminated dolomite" and the shape of the pull-out zone could not be observed at the maximum test load. However, the extensive area over which the rock surface was uplifted around certain anchors suggested failure along a horizontal bedding plane. Littlejohn and Bruce suggest that the mode of failure described by Brown, although possibly restricted only to shallow anchors, has led to the staggering of closely spaced anchors to avoid dilation along discontinuities at depth. In unfavourable conditions, for example where rock bedding planes occur normal to the anchor axis, the purpose of staggered anchor lengths in practice today is to reduce the intensity of stress across such planes at the level of the fixed anchors.

At the Design Methods in Rock Mechanics conference hosted by the University of Minnesota in 1975 (Fairhurst & Crouch, 1977), a general discussion session on 'pullout cones' followed a presentation by Littlejohn and Bruce. An experience with anchor testing in jointed and bedded quartzitic sandstone was noted by a member of the audience to produce one rock mass failure of a 2 m embedment anchor at a load of 2200kN. This failure was described to occur on joint surfaces of "classically poor orientation" and it was noted that a "shear strength" may be applicable for back analysis of this failure (over and on top of the dead weight of the wedge). In a subsequent research Bruce (1976) noted that rock anchors of 1.5 to 2 m embedment were observed to fail through the rock mass at loads ranging from 1000kN to 2000kN (higher than the dead weight assumption).

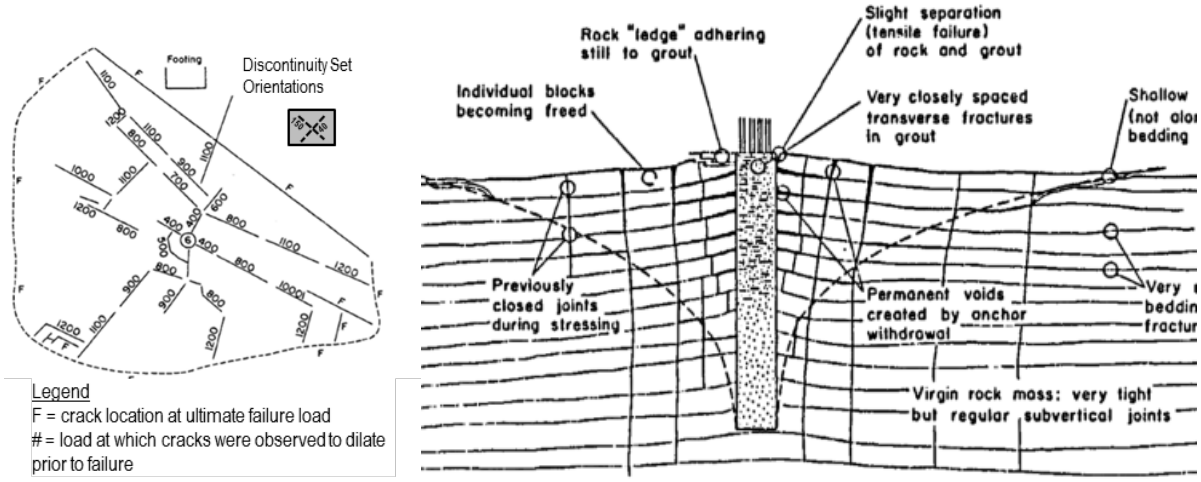

Figure 12 – Plan view of a full scale pullout test on top, and Section view of a full scale pullout failure mechanism on bottom. Modified after Bruce (1976)

Based on observations such as these, many design engineers have adopted the approach of considering some tensile or shear strength along the outer surface of the cone pullout surface. This commentary indicates that structurally controlled failure of the rock mass surrounding an anchor has been a consideration for some time, and that the shape of the cone may actually be irregular and anisotropic. However, most of the pull out cone references noted above are anecdotal and don't provide data as to the structural orientation or length of the pre-existing joints in the rock mass, the load at which these joints dilated prior to failure or information on the distribution and onset of tensile cracking in the rock mass prior to failure. As a side note, this thesis contends that these are all important considerations in the numerical simulation of rock anchors.

Following publications in the mid-1970's, Bruce (1976) completed full scale pullout testing on a number of anchors ranging in length from 1.5m to 2m. Figure 11 provides a plan view of a test completed by Bruce in "slabby sandstone". The numbers on the traces in the plan view indicate the anchor loads (inkN) at which various fractures dilated prior to failure.

It is apparent from this figure that the fracturing around a rock anchor may be controlled by the structural geology and jointing in the vicinity of the test. Furthermore, Bruce described inelastic rock mass deformations, associated with loosening and permanent voids developing, as the rock mass is progressively loosened with increased loading, as shown in the right sketch in Figure 12. Bruce (1976) noted observations from this figure indicate that the degree of cracking changes with, and that the assumption of "intact cone lifting out" is only a rough approximation. Bruce (1976) also noted that "*although the zone of loosened rock is approximately conical, it is not intact, and it does not lift up as an intact mass. The true failure mechanism is a complicated combination of shear along joint planes, movement of discrete blocks, and more detailed analysis is not possible*". Dados (1985) completed a series of ten field pullout tests on vertically cemented rock anchors installed in "unweathered granite", with "moderately" spaced sub-horizontal jointing. The testing results indicated that as the pullout load increases the rock bulges upward to a distance roughly equal to the anchor depth. The author also described the simultaneous formation of tension cracks along the joints and separation of blocks along the sub-horizontal jointing observed on site. Dados suggested an empirical relationship for the site which suggested that "*the pullout capacity of a certain anchor in a certain discontinuous rock can be estimated based on empirical values from past experience of the probable total anchor deflection at failure*". Observations from this author are consistent with Bruce (1976) that the rock mass dilates or deforms in a progressive manner prior

to ultimate failure or "cone pullout". Further to the development of pullout cone theory from historic testing on rock, some of the understanding of cone breakout also comes from observations made in the testing of short anchors embedded in concrete. Ballarini et. al. (1986) note that when a bolt fails through pullout of the concrete, the resistance can be assessed by calculating the resultant of tensile stresses equal to the maximum concrete tensile strength, directed perpendicular to the surface area of the truncated cone. The angle between the horizontal and the cone values from 25 degrees for anchors of shallow embedment to 45 degrees for anchors of deep embedment. Alternatively, a second criteria was noted which considers that the failure is the resultant of the tensile stresses equal to the maximum concrete tensile strength, directed parallel to the direction of applied load. Ballarini et. al. noted that testing by other authors (specifically a study in 1983 by the National Bureau of Standards) has revealed that the onset of cracking occurs at about 30-40% of the ultimate load which ends the elastic response of samples tested. The results of the NBS study indicated that stress concentration, crack initiation and crack growth play an important role in determining the pull out response of concrete. Additional studies by Krenchel and Shah (1985) confirmed that crack initiation in concrete pullout tests occurs about about 30% of the maximum load, and at loads of up to 65% of the peak load cracking seems to be concentrated near the corners of the pullout "disk" (or cone). It was noted that crack growth at 65% of the peak load, confirmed by the use of acoustic emissions, was approximately 15-20 degrees from horizontal (with the anchor load being applied in the vertical direction). For loads near the peak load, secondary cracks form 25-45 degrees from the horizontal until the peak load is reached. The study by Ballarini et. al. was commissioned to confirm these observations with testing and development of a numerical model for crack growth. The study concluded that the tensile capacity of an anchor is dependent on the fracture toughness which leads to plastic deformation of the rock mass. Similar to the testing completed in the laboratory on concrete, Wolfrum et. al 2007 completed laboratory testing on very short anchors embedded in intact rock samples of sandstone, limestone, granite and mortar. Since the tests were completed on intact samples without natural fractures, these should be viewed in the similar context as that of the testing completed in concrete. The very short anchors were embedded less than 0.2m into the rock samples and some of the tests on these intact samples produced failure at loads up to 80kN. This suggests that intact rock may have a significant contribution to the pullout resistance of anchors.

A new wave of full scale testing of the rock mass began in the 90's with Carter (1995) completing testing in sandstone using a full scale apparatus on a 1.5m embedment anchor. Pre-failure deformation was noted in the sandstone with a radius of dilation of about 1.5m radius for the 1.5m anchor depth. Although global failure was not observed in this test, irrecoverable dilation or plastic deformation was observed around an anchor load of 200kN. If lessons are drawn from the work by Ballerini it is possible that the onset of tensile crack growth may occur at loads of 30% of the maximum failure load in concrete pullout testing completed on concrete. Carter noted that at 200kN, the maximum ground movement adjacent to the anchor had reached 4mm upward displacement within a zone about 20-50cm from the anchor radiating outwards to about 2mm upward movement recorded about 1m from the bar. For practical purposes this amount of deformation may indicate "failure" since steel threadbar broke shortly after this deformation was observed. Carter concluded that while no disruptive failure of the rock mass developed in the test due to failure of the steel, plastic deformation developed in the rock mass during the 5th and 6th loading steps between 200kN and 250kN which suggests a factor of safety between 4 to 6 using the dead weight assumption for cone development with a 1m radius initiating at the base of the 1.5m anchor (60 degree breakout angle).

The testing completed by Carter was consistent with the results of Saliman and Shaefer (1968) and Ismael (1981) which suggest that the dead weight cone approach is conservative, however, Carter (1995) concluded while the testing was very valuable for assessing the response of the rock mass at the site, the absolute results are not widely applicable beyond the site. Carter noted that although nearly all of the tests that have been reported in the literature suggest that basing ultimate capacity on dead cone weight is conservative, not enough information is yet available to formulate an effective alternative. Carter also concludes that "*obviously, more site testing of cone failure mechanisms is essential if current design approaches are to be rationally improved*." Since the work of Carter, attempts have been made to correlate the behaviour of the rock mass to RQD and RMR (Kim and Lee, 2005). The work by these authors presents the results of full scale testing performed on 54 passive anchors at several sites across Korea. Various rock types were testing ranging from "highly weathered shale" to "sound gneiss". In many tests rock failure was reached and the ultimate loads were recorded along with observations on the shape and extent of the failure surface.

Kim and Lee conclude that the uplift resistance of anchors generally increases with RQD, however the authors do not provide additional details on the structural geology of the site or the length or

persistence of joints. The results by the authors indicate that deformation is generally observed prior to failure of the bar. The work by Kim and Lee identified that jointing (albeit RQD) has an influence on the capacity of a rock anchor. However, this type of classification (while quantitative) does not provide evidence that the discrete location of joints have an influence on the capacity and behavior of rock anchors.

Most recently, Thomas-Lepine (2014) completed testing of approximately 50 bolts embedded 0.5-1.5m into rock. The author identified that the discrete location of fractures in the rock mass have an influence on the failure mechanism of the anchor. Thomas-Lepine notes that where fractures formed a removable block within the area of anchorage the failure mechanism was defined as "liberation of a block". Alternatively, where fractures are present in the general area of the anchor the mechanism was noted to be "generalized cracking" which suggests that a discrete block was not mobilized around the area of anchorage. It is of particular interest to this study that Thomas-Lepine identified that the presence of jointing in the rock mass has an influence on the pullout behavior of the rock surrounding an anchor. In addition, the load tests were completed from the boom of an excavator and therefore the reaction force was outside of the zone of stress influence, which is a common problem for test setup. Thomas-Lepine, identified two failure mechanisms for anchor pullout including "liberation of a block" and "generalized cracking", and photos of these failure mechanisms is presented in this research. The work by this author also identified that variation exists in the rock mass across a site.

3 USING THE DISCRETE FRACTURE NETWORK APPROACH IN ENGINEERING DESIGN

3.1 General

The literature review identified that joints in the rock mass have an influence on the stability of anchors. It is also contended that the discrete location of joints and proximity of joint to the anchor in a numerical model have an influence on stability. The rock bridges between these non-persistent joints are also anticipated to have an influence on anchor capacity, as intact rock cohesion or tensile strength provides a significant measure of strength. By understanding the statistical distribution of fracture patterns in the rock mass, joints and bridges of rock between joints can be represented explicitly using Discrete Fracture Networks.

However, before modelling work can be completed, the input parameters for Discrete Fracture Networks (DFNs) need to be understood. This Chapter (Chapter 3) provides a summary of mapping considerations for development of DFN's and how these models are are incorporated in geo-mechanical anchor simulations. The Discrete Fracture Network approach has been adopted since this method can accommodate uncertainty in the discrete locations of fractures within a model.

The DFN approach offers the opportunity to maximise the use of fracture data collected from mapping of rock exposures and boreholes, including direct physical mapping and indirect data collection by remote sensing techniques (e.g. digital photogrammetry and laser scanning techniques). The synthesis of a DFN model requires collecting and characterising information about i) fracture intensity, ii) fracture orientation, iii) fracture length and fracture terminations (Elmo et. al. 2015). The International Society of Rock Mechanics (ISRM) guidelines for the quantitative description of discontinuities include most, if not all, of the main parameters required to generate a DFN model. However, there are important differences engineers should be aware of. Elmo (2015) and Panton et. al. (2015) describe many differences between ISRM methods and requirements for DFN modelling and these are summarized in Section 3.2.

3.2 Mapping Requirements

The quality of the DFN model depends directly on the quality of the field data, therefore there is an ever greater demand to review the process of collecting fracture data in the specific context of DFN modelling. For instance, fracture size (also referred to as fracture length) is an important parameter in DFN modelling. Measurements of fracture length can be obtained by mapping 2D rock exposures, using conventional (scanline or window mapping) or remote sensing techniques (e.g.

photogrammetry and/or LiDAR); however, this parameter is either seldom available at the pre-feasibility stage due to a lack of exposures (Elmo et. al, 2015). An extra layer of complexity is given by the fact that the fracture radius used an input parameter in most DFN codes is not the same as the fracture length mapped on an exposed surface, see Figure 13. Fracture trace length is an explicit measure of the trace that a fracture or fault makes with a geological surface or mining exposure, while fracture radius is the radius of a circle of equivalent area to a polygonal fracture. The definition of fracture radius also requires geotechnical engineers to be familiar with truncation and censoring biases: values below a certain fracture length are typically omitted when mapping (truncation) or relatively larger values cannot be measured because of the limited extent of the rock exposure (censoring). Note that when using remote sensing techniques to process fracture length, this is generally assumed to coincide with the diameter of a disc inscribing the mapped feature; using the radius of the disc inscribing the fracture in the processed image or point cloud in lieu of the fracture radius in a DFN context would be erroneous, as censoring bias would be neglected in the process. The truncation bias plays also a major role in defining the correct fracture intensity for DFN analysis, as the probability density function for fracture size would be bounded by a minimum (estimated at the borehole scale) and a maximum (estimated at the mapping scale), but it would not be possible to define the full extent of the distribution. Therefore, the mapped intensity would reflect the extent of the size distribution available.

Fracture termination is another parameter that is generally overlooked when collecting data for rock engineering problems. It directly relates to fracture connectivity, which is an important parameter in the context of stability and failure through intact rock bridges. Fracture termination could provide useful insights on the structural character of the rock mass, as well as could be used as a calibration tool by comparing mapped terminations on exposed surfaces with those generated in equivalent surfaces within the DFN model. Elmo et al. (2015) provides further insights on to what extent discontinuities can be sampled and which limitations are inherently introduced in the analysis by the sampling methods being adopted represents important aspects that should drive the collection of discontinuities data for DFN analysis.

For the specific case of anchorage design, it is argued that if mapping data were available for the location where the anchorage were to be installed, then the location of relatively large structural feature would have to be included deterministically within the DFN model. The stochastic features would then represent relatively smaller fractures not observed outcropping where the anchorage is to be installed.

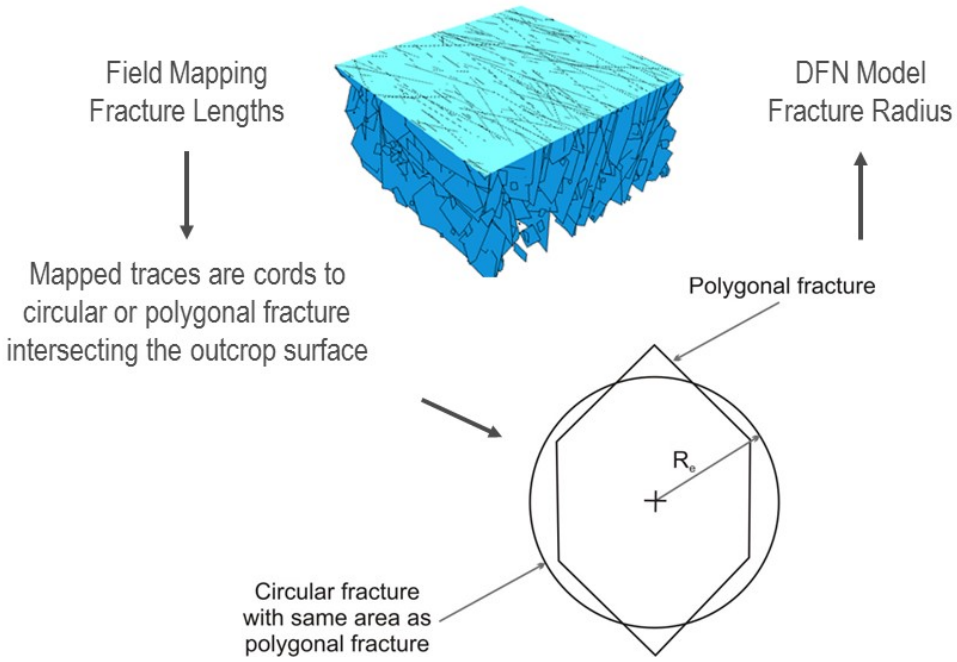

Figure 13– Distribution of mapped fracture traces (data source) versus distribution of fracture radius

3.3 Incorporation of DFN's in Numerical Models

The use of Golder Associates' FracMan code and the incorporation of pseudo-random Monte Carlo type simulations allows for discrete fracture networks to be generated stochastically based on mapping statistics. This type of analysis can be incorporated in limit states design if the designer has a good understanding of the geological constraints of the problem. It is contended that at the scale of anchor pullout the discrete location of joints may have a significant influence on the capacity of a rock anchor. Furthermore, it is contended that the failure mechanism of an anchor also changes with spacing variation and variation in the length of discontinuities. For example, in more fractured or blocky rock masses the capacity of an anchor will likely be governed by the frictional properties of joints. Conversely, in rock masses with widely spaced discontinuities strength will be developed by intact rock bridges governed by the length or persistence of fractures. In addition, the orientation of discontinuities is also an important consideration in anchor design.

For this research, DFN's developed in the FracMan are used to represent jointing in a synthetic rock mass. Cross sections are cut perpendicular to the prominent joint set orientations in the DFN and numerical simulations in Phase2 by RocScience are carried out to assess the variation in pullout

strengths. Figure 14 illustrates multiple DFN domains that may be applicable across a foundation and Figure 15 shows the two dimensional cross sections cut from this model for use in geomechanical simulations. It is well understood that the cone pullout problem is 3D in nature and this is investigated in Chapter 7. However, it is contended that if cross sections are cut perpendicular to the controlling joint sets the failure mechanism associated with pullout can be assessed in a much more efficient (quicker) manner. Furthermore, it is considered essential that the tensile fracture processes between joints can be simulated in the numerical model. This requires a very fine mesh between fractures (in some cases 1 cm element length) and most 3D models cannot accommodate this scale of meshing over a large area. For this reason, 2D models were considered in the following chapter. Using numerical simulations and discrete fracture networks, the variability across a foundation can be assessed and these capacities can be used to validate the performance requirements for a foundation design.

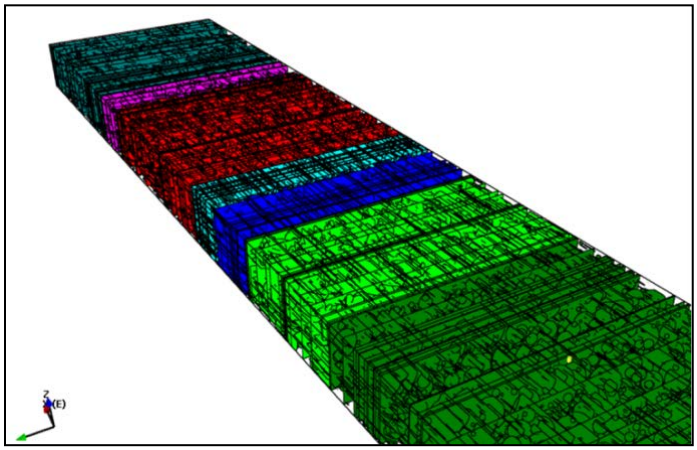

Figure 14–An example of development of 3D DFN for a large foundation surface

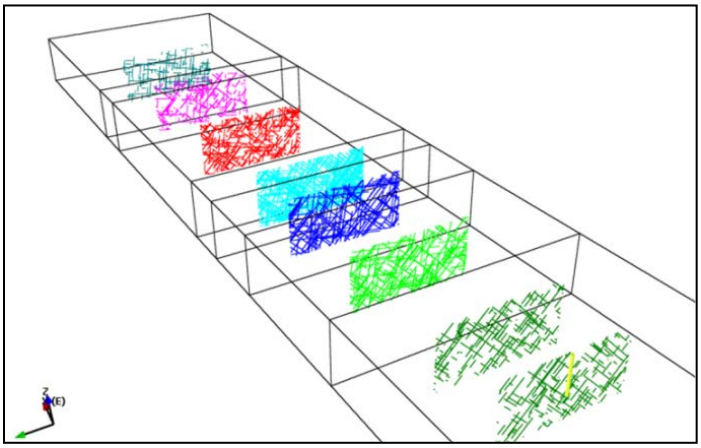

Figure 15–An example of development of 2D cross sections for use in geo-mechanical modelling

4 MODELLING AND CALIBRATION OF IN-ELASTIC YIELDING IN JOINTED ROCK

4.1 Introduction

Chapter 4 discusses the failure mechanism envisaged for the rock mass surrounding an anchor and how the numerical models presented in later sections are calibrated.

The observations from full scale testing by others indicate that the rock mass pullout failure mechanism may be influenced by the presence of discontinuities or natural fractures in the rock mass. Furthermore, historical work both in structural testing on concrete and rock with natural fractures indicate that damage or plastic deformation may occur at loads as little as 20-30% of the ultimate failure load when pullout is observed and that the failure of the rock mass may be dependent on the fracture propagation properties of the rock mass.

Brittle fracture associated with discontinuities and imperfections in the rock mass have been investigated by many authors. Hoek notes that discontinuities affect the response of the intact rock by reducing its strength and inducing non-linearity and anisotropy in the stress-strain response (Hoek, 1983; Hoek et al. 2002). Hoek also notes that discontinuities add kinematic constraints on the deformation and failure modes of structures in rock (Hoek et al., 1995; Hoek, 2006) and cause stress and displacement redistributions to deviate from linear elastic, homogenous conditions (Hammah et al., 2007). Wong and Einstein (2008) assessed the influence of pre-existing cracks on the cracking and coalescence behaviour in tests on "laboratory moulded gypsum" and "Carrara marble" samples containing two artificial, parallel pre-existing flaws. High speed video was used in this study to identify nine different crack types which formed based on different flaw inclination angles, flaw lengths, length of intact rock between flaws, and the rock bridging angle between flaws. Wong and Einstein noted that comparing the historic results of tests completed on samples with single flaws with their 2008 study, the presence of neighbouring flaws in the stress field was found to have a significant influence on the initiation of shear cracks.

Further studies on cracking and coalescence behaviour was assessed by Morgan et al. (2013) who completed similar UCS testing on the "Barre granite" with artificial neighbouring flaws. The study confirmed the results by Wong and Einstein that neighbouring cracks have an influence on cracking behaviour and indicated that damage or preliminary indications of failure, noted by the authors as "white patching" of grains, between flaws occurs at loading steps as low as 20-30% of the ultimate failure load of the sample. From these observations it can be concluded that the brittle failure of rock is progressive and occurs throughout loading steps leading up to ultimate failure. In addition,

pre-existing joints and fractures seem to have an influence on the formation of cracks both during tensile and shear loading, as described by Bruce (1976).

A numerical code that allows for the location of discontinuities in the simulated rock mass to influence the propagation of brittle fracture in the model is an important consideration in modelling the Type D pull out mechanism. Figure 16 compares the failure mechanism observed in a continuum model to that of a continuum model with joints inputted in the mesh domain (also known as a discontinuum model). Each model was loaded incrementally in stages until tensile fracturing connected with the surface inducing "failure" in the model. The upper portion of the figure shows the continuum model without joints. In this model, tensile fracturing or yielding induced by stress concentrations is firstly observed within the rock immediately adjacent to the anchor (bond failure) prior to global failure. In contrast, in the continuum model with joints inputted in the mesh domain tensile fracturing is firstly observed as 'wing cracks' at the joint ends or discontinuities in the model. With progressive loading, these cracks are observed to coalesce between the existing fractures until the breakage of "rock bridges" or intact rock induces failure of a removable wedge. The development of pre-failure yielded elements and the interaction of these elements with the pre-existing jointing in the model is an important component of modelling the cone pullout mechanism.

The continuum model with joints inputted in the mesh domain also allows for deformation to occur in a heterogeneous manner depending on the discrete location of joints in the model. The classic equivalent continuum homogenization approach, without joints, is typically limited by the fact that slip, rotations and separation as well as scale effects induced by discontinuities cannot be explicitly captured (Hammah et al., 2008). The addition of joints in the anchor simulation produces a "cone" of influence closer in magnitude to that observed in the limited field tests. In these types of models the discrete locations, intensity and orientation of discontinuities play an important role in the dilation and ultimately the failure of the rock mass.

It is contended that jointing, dilation and brittle fracturing processes between joints need to be simulated. The magnitude and shape of rock mass deformation is dependent on the modelling approach (continuum vs. discontinuum), constitutive model (elastic vs. elasto-plastic), post-peak failure response (ductile vs. brittle) and the geometry of a discontinuity network. A continuum model produces deformations that are homogenous and isotropic in nature. Consideration of joints in the model is important since pre-existing or naturally occurring fractures not only have the

ability to influence the location of fracture initiation in the rock mass, but these features also have the ability to influence stress rotations through sliding and the normal force applied along joints. For these reasons, a discontinuum method was chosen for the assessment of cone pullout.

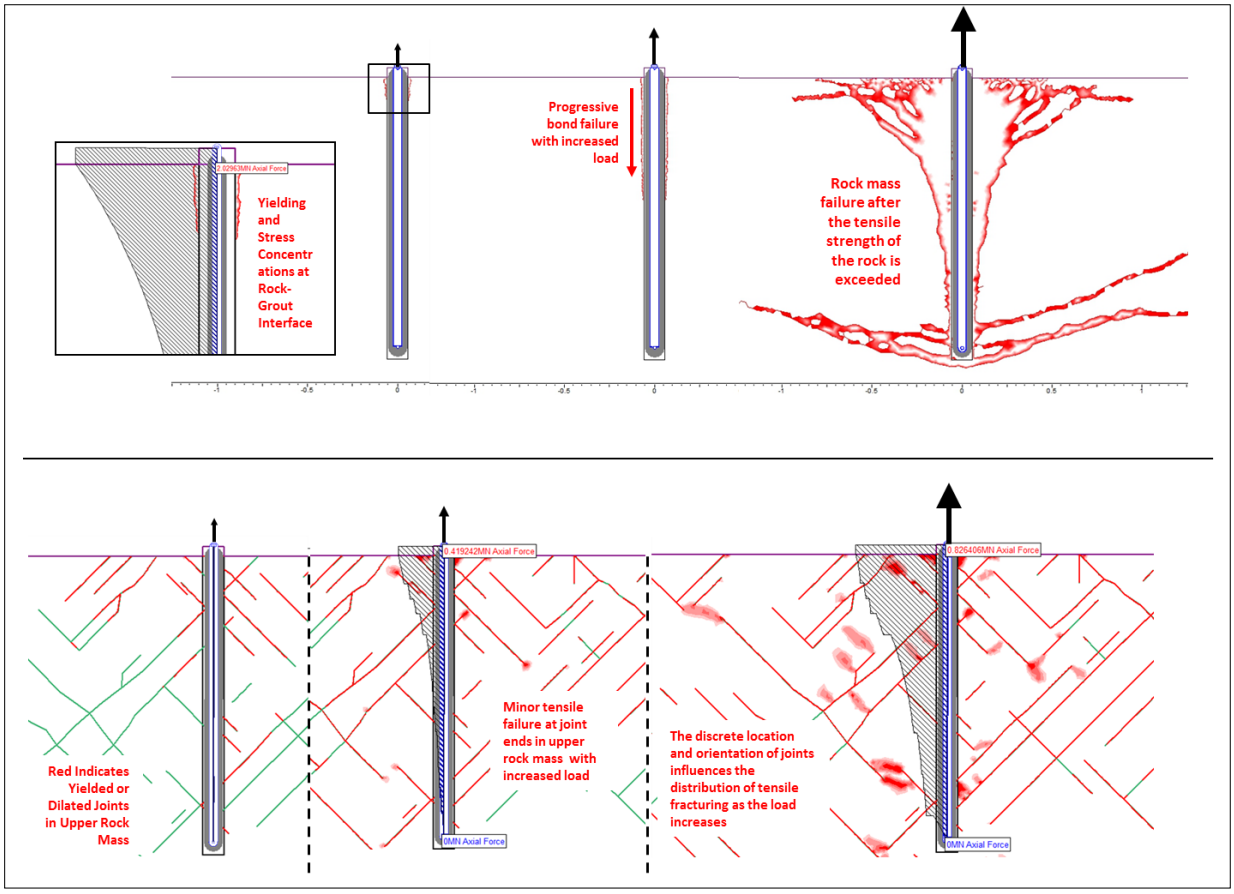

Figure 16 – A comparison of the tensile fracturing in a continuum model (with and without joints)

4.2 Calibration of Numerical Models

4.2.1. Developing a Sense of Scale from the Canadian Standard of Practice

Prior to calibration of numerical models the designed capacity of rock anchors must first be understood. A sense of scale for the anchor problem can be developed for anchors embedded 1.5m to 2.0m into rock by assessing the resistance to pullout using the traditional approach to anchor design and the standard of practice. As noted in Section 2, Canadian engineering practice has adopted the "pullout cone" approach summarized by Wyllie for the analysis of anchor lengths. This method has produced successful designs over many years of rock engineering in the civil

engineering industry. Due to the conservative nature of the "dead weight" pull out assumption Wyllie (1999) recommends that additional rock mass strength is applied to the outer surface of the envisaged pullout cone to resist failure, as noted in Section 2.0. Figure 17 provides allowable anchor capacities developed using this method with the assumption that a 90 degree cone breakout initiates at the base of the anchor. The variation in tensile strength of the rock mass is compared to the allowable anchor capacity using the Wyllie method.

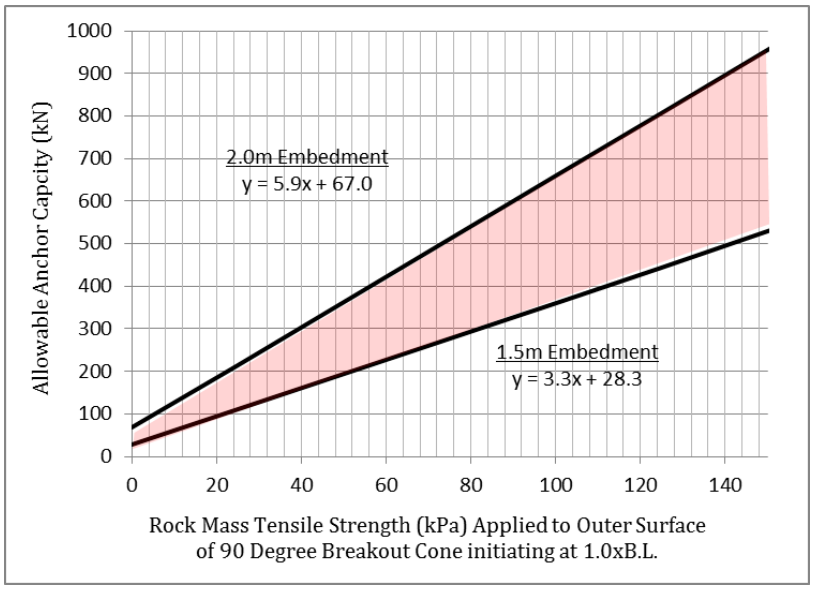

Figure 17 – Theoretical Allowable Anchor Capacity vs. Rock Mass Strength Estimates calculated using the method recommended by Wyllie (1999)

By assuming a tensile strength = 0, the allowable capacity is governed only by the weight of the inverted cone of rock. Using this "dead weight" assumption, allowable anchor capacities are calculated to be 28kN and 67kN for the respective anchor lengths of 1.5m and 2.0m assuming a unit weight of rock is 24kN/m^3. If a modest strength is applied to the outer surface of the inverted cone, allowable anchor capacities for the same anchor lengths are calculated to be 200kN to 360kN for an applied equivalent cone strength of 50kPa and 360kN to 660kN for an equivalent strength of 100kPa. Calculations of uplift resistance in a range of applications, some authorities seek to allow for the tensile or shear strength of the rock mass (Brown, 2015), generally through the use of assumed values of rock mass tensile strength, shear strength or cohesion (Hobst & Zajíc, 1977; Anon, 1996; Kim & Cho, 2012).

Further to the work by Wyllie (1999), Hobst and Zajíc (1977) give a number of alternative solutions in terms of the rock mass shear strength. Kim and Cho (2012) suggest that the tensile resistance on the failure surface of the rock cone, f_r, is given by:

$$f_r = \sigma_{trm} \pi D_c^2 \tan(\vartheta_c/2) / \cos(\vartheta_c/2)$$

where σ_{tr} is the tensile strength of the rock mass and D_c is the depth of the rock cone, initiating at 0.5 bond length for a breakout angle, θ_c.

Assuming that the stress is applied in pure tension, the tensile strength of the rock mass can be calculated using the Hoek-Brown failure criteria (Hoek-Brown, 2002):

$$\sigma_{trm} = -s\sigma_{ci}/m_b$$

The constants m_b and s are functions of the Geological Strength Index (GSI) of the rock mass, a disturbance factor used to account for blast damage or relaxation, and m_i which is an intact rock material constant which is related to the tensile and shear behaviour of the rock. σ_{ci} is the unconfined compressive strength of intact rock developed from UCS testing.

Based on the results of direct tension testing (as opposed to indirect tensile tests such as the Brazillian test), Langford et al. (2014) note that the intact rock estimates used in the rock mass tensile strength calculations may in fact have a tensile strength cut off and a ratio may be required to factor the m_i constant for use in design. The authors note that "*one outstanding question that is not addressed by this analysis is how the rockmass tensile strength can be determined. While the intact Hoek-Brown strength curve can be transformed based on the estimate of rockmass quality (e.g. GSI), these equations do not account for a tension cutoff. Further research is needed to ensure this process can be used with the GSI system to provide accurate estimates of the rockmass tensile strength for use in numerical models*". In a different paper, Hoek et al. (2013) notes that a fundamental assumption of rock mass rating criteria, such as GSI, used in equivalent continuum models is that the discontinuities are sufficiently closely spaced such that the rock mass can be considered homogenous and isotropic. At the scale of the rockmass pullout problem it is contended that discontinuities may have an influence on the stability of the anchor and the rock mass may not behave in a homogenous and isotropic manner. For this reason many of the design assumptions used to calculate anchor lengths cannot be used to calibrate the parameters for this study. Much of the state of practice is based on anecdotal references to historic tests, not anchor specific empirical relationships.

In response to the use of empirical relationships using tensile strength, Brown (2015) notes: "*of course, this approach begs the question of the exact physical meaning of the assumed parameter, σ_{trm}, and how it might best be estimated. An alternative approach is to use a rock mass shear strength, rather than a tensile strength, back-calculated from the results of pull-out tests, assuming a theoretical failure cone of the type being discussed here*".

4.2.2. Model Setup and Calibration of Phase2 Finite Element Code

Based on commentary by both Hoek (2013) and Brown (2015) respectively, and due to the fact that crack propagation is influenced by the presence of joints, equivalent continuum properties that assume that the rock mass is homogenous and isotropic in nature should not be selected for the analysis of the cone pullout mechanism. The finite element code selected should be able to model joints in the mesh domain, and intact rock properties to be used in between joints. The use of intact rock properties requires that all of the stability controlling joints in the rock mass are added to the model, since the simulated "rock mass strength" is developed from both the frictional properties of the joints and the contribution of intact rock between joints. This approach is introduced and tested by Elmo (2006) and Elmo et al. (2011). The authors contend that using a synthetic rock mass approach, with a representative distribution of fractures and intact rock, allows for the anisotropic and inhomogeneous spatial distribution of jointing in the model to influence the deformational behaviour and failure mechanisms observed in response to loading. Furthermore, the opportunity for elements to fail in both tension and shear should be provided in the model both by a shear strength envelope and a tensile strength cut off. Phase2 Version 7.0 and Version 8.0 both allow for joints to be inserted in the mesh domain and for yielding to occur in both tension and shear. This program was selected for analysis of the cone pullout mechanism since modelling iterations can be completed for multiple DFN realizations in a relatively short timeframe, compared to other models. It should be recognized that the Phase2 finite element code is limited to small strain deformations, however, since pre-failure deformations are anticipated to be on the order of 5-10mm this model is considered suitable for modelling the onset of global anchor failure.

For the strength estimates of intact rock and joints, strength estimates can be developed from the results of laboratory testing. Since cone pullout data is available for the rock mass pullout testing described by Bruce (1976), the intact rock properties noted for this rock mass were inferred based on the description of the rock by the author. Intact rock mohr coulomb friction angle and cohesion

were assumed to be 52 degrees and 3.4 MPa respectively. During the first stages of rock mass mobilization, the parameters assumed in the model are revised to reflect mobilization of friction (to a maximum friction angle of 58 degrees) and softening of cohesion during the first stages of tensile failure. After the initial stages of dilation, the frictional properties of the rock mass are softened to the base friction angle of the natural joints in the rock mass. The properties of joints were developed using a base friction angle of 30 degrees factored based on a Joint Roughness Coefficient, JRC value of 8, and the low normal force across the failure plane. This correlation was completed with methods presented by Barton and Choubey (1977) and Barton and Bandis (1993). For R3-R4 sidewall strength, an assumed JRC value of 8, and an assumed "i" angle of 5 degrees, calculates a peak friction angle of 52 degrees. No cohesion was applied along the surfaces of joints in the model since it was assumed that the intact rock bridges between the non-persistent fractures in the model would provide the effective cohesion in the rock mass. When these rock bridges (represented by "intact rock" in the model) had shear to a residual state a nominal cohesion of 0.2MPa was given to the failed elements.

While it may be argued that calibration of complex softening relationship is very difficult, and not practical for design outside of academia, it is contended that full scale pull out cone data can be used to calibrate the parameters in the first DFN realization of a numerical model. The results from testing by Bruce (1976) indicate that failure of an anchor through the rock mass generally occurs at between 5mm-10mm at the surface. This deformation in the upper rock mass can be used as an indication to calibrate the modulus of the rock mass at the ultimate failure load. In Phase2 by RocScience the load must be distributed to the rock mass by means of multiple loading stages. For this assessment 25 loading stages were assumed and the model was noted to fail when tensile fractures (or yielded mesh elements in the model) were observed to form a consistent path at the surface. At this time, the model generally fails due to lack of convergence. The ultimate load is increased until lack of convergence is achieved at between 5-10mm displacement. After the ultimate load has been calibrated to a full scale pullout test, the softening behaviour can be set. Assumed parameters are provided in Table 1 and addictional DFN realizations can be run using different joint spacings and orientations.

As described in the previous section, inelastic rock mass deformation can be simulated by allowing for tensile cracking and slippage along joints. Bruce (1976) noted that inelastic anchor displacement can be observed both along the rock-grout interface and by "*inelastic deformations in the rock mass while the rock grout interface remains intact*". Figure 18 indicates the axial stress

distribution along a full scale pullout test completed by Bruce. The plan view sketch on the right indicates the load at which various fractures in the rock mass surrounding the anchor dilated prior to failure during testing. This data is important since it can be used to calibrate the deformation behaviour at various points in the rock mass at different load increments. The test result provided in the upper right of Figure 18 was completed to ultimate failure of the 1.5m embedment anchor at a load of 1200kN, however, crack initiation was observed at 400kN in this test. While the test in lower figures observed the onset cracking of the rock mass at 900kN but the 2.25m embedment anchor did fail through the rock mass at the 1800kN test load. It should be recognized that rock mass dilation at the surface manifested as opening of cracks sub-parallel to the dominant structural orientations at the site in both tests as shown on the figures.

Table 1 - Strength parameters used to model anchor pullout

Parameter	Type	Property Ranges		
		Initial	**Peak**	**Residual**
ϕ'_{intact}	Strain Dependent (mobilize friction)	52 deg	58 deg	30 deg
ϕ'_{joint}	Strain Dependent (shearing asperities)	50 deg	-	30 deg
c'_{intact}	Strain Dependent (softening cohesion)	3.4MPa	-	0.2MPa
c'_{joint}	No joint cohesion	-	-	-
$\sigma'_{t\ (intact)}$	Constant	1MPa	-	No post failure tensile strength
E_{intact}	Constant	15000MPa	-	-
$E_{rockmass}$	Constant	1500MPa	-	-

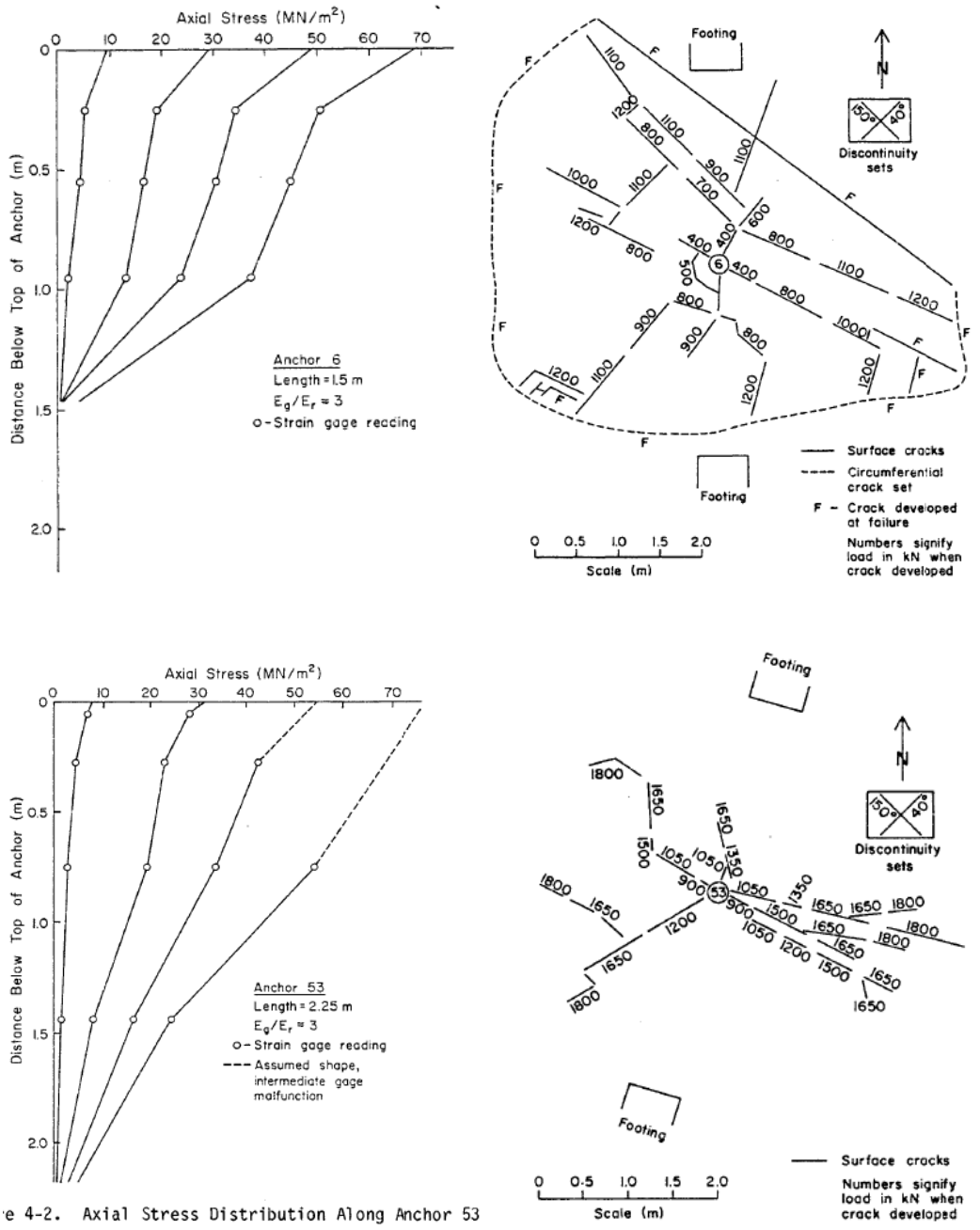

e 4-2. Axial Stress Distribution Along Anchor 53

Figure 18 – Axial Stress distribution along Anchor 6 (upper left) and a plan view sketch indicating the load at which various fractures in the rock mass surrounding this anchor dilated prior to failure during testing (upper right). Axial Stress distribution along Anchor 53 (lower left) and a plan view sketch indicating the load at which various fractures in the rock mass surrounding this anchor dilated during testing. Modified after Bruce (1976)

Further to the development of dilation and strain softening in the rock mass, the load transfer is also an important component of observing the pullout failure in the mode. The progressive "cone" of deformation or extent of dilation in a numerical model is highly dependent on the load transfer mechanism from the anchor to the anchor grout and finally to the rock mass. Bruce et al. (1991) carried out testing on pre-stressed dam foundation anchors to better understand the load transfer mechanism at the rock-grout interface. This study indicated that, at the time, the state of practice of the design of rock anchors was to consider a uniform bond stress distribution along the length of the anchor. The authors note that there are experimental results and numerical simulations that suggest that the distribution of load along an anchor is heavily influenced by the modulus of elasticity of the grout compared to the modulus of elasticity of the surrounding rock mass (Ec/Erm). Based on the studies noted in this research, if the modulus ratio is less than 1 (i.e. the rock mass is stiffer than the grout), shear stress is concentrated at the anchor head and stress is dissipated rapidly along the bond length with depth. These results indicate that the more competent rock mass with a low concrete:rock ratio concentrates load at the proximal end of the grout column and the load is dissipated quickly at depth. If an anchor is installed in intact rock loads may be concentrated at the anchor head, however, if jointing in the rock mass may facilitate dilation this will in turn transfer load deeper into the rock. This is due to the fact that jointing decreases the rock mass stiffness and deformation surrounding the anchor.

Bolts have been implemented in various numerical methods such as the Finite Element Method (FEM) (Goodman et al. 1968) and block methods (Cundall, 1971). In Phase2 by RocScience the tieback bolt model was selected since this bolt model allows for a free stressing length to be applied in the model, if required. The bolts in the model pass through elements in the mesh and are modelled by a series of one dimensional elements. The equilibrium equation for the bond length considers the shear force due to relative movement between the bolts and the rock mass described by Farmer (1975) and Hyett et al. (1996). The stiffness of steel in the model was assumed to be 200GPa and the bond shear stiffness was adjusted to achieve the stress distribution noted in Figure 18. After one calibration model was developed, the shear stiffness of the bond was left constant for the remaining numerical simulations. Where the models in this thesis differ from other numerical bolt simulations is that, in addition to the one dimensional bolt element, a grout material type is also added to the mesh domain. This allows for the bolt element to be represented by both the one dimensional steel bolt element and the two dimensional 114mm diameter grout filled drill hole in the model. The representative area in the model allows the rock mass to deform in a more realistic manner as load is firstly transferred through the 30GPA elastic concrete medium in the model

before the rock feels the load. Since this study does not consider combined bond and rock mass failures the interface between the grout and the rock was assumed to be a material boundary with no frictional properties. However, where high stress concentrations exist along this boundary, brittle failure can occur in the mesh immediately adjacent to the material boundary which represents bond shear failure as shown in Figure 16 above.

For this research, a fully grouted dowel of 1.5m embedment was chosen for the numerical simulations since full scale testing data is available for anchors of this type. Figure 19 shows two stages of loading from an elasto-plastic finite element model with a discrete joint network in the mesh domain. These models simulate pullout of an unconfined, fully grouted dowel and the jointing in the upper rock mass allows for dilation prior to failure. As described above, this dilation is important since it reduces the confinement of the lower mass and provided that the dead weight of the dilated rock is not greater than the anchor load, this in turn allows for higher load to be transferred deeper into the rock. The intact modulus and rock mass modulus are calibrated to simulate rock mass dilation. In addition, the frictional and stiffness properties of the joints and tensile strength and residual softening envelope of the rock mass also influence the deformation behavior of the rock. The discrete locations of joints should be considered in calibration. If no joints are included in the upper rock mass in the model, the rock mass will effectively behave in a stiffer manner and it is expected that this will concentrate the loading to the upper portion of the rock mass which may change the failure mechanism for the anchor. This is illustrated in the next section.

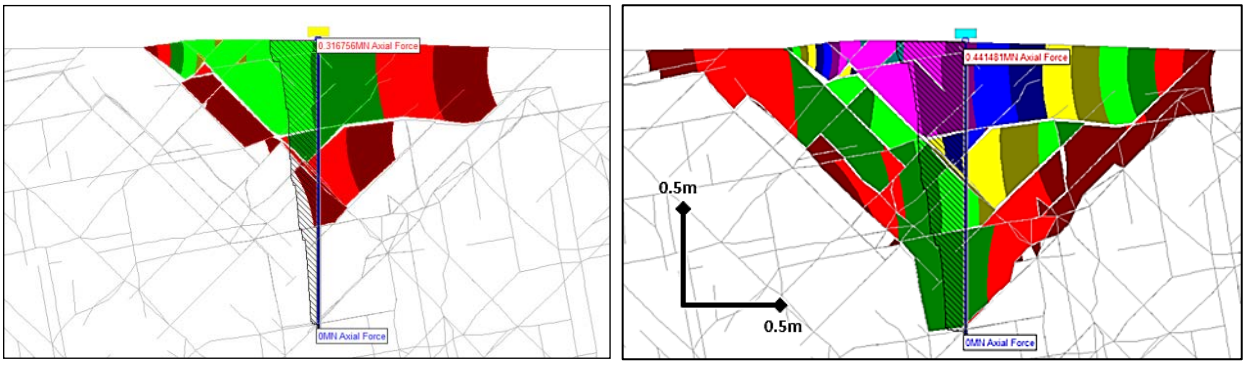

Figure 19 - Dilation of upper rock mass at 0.32 MN load (left); and 0.44 MN load (right) for two different loading stages of the same finite element model – minimum deformation 1mm, maximum 5mm shown in purple

5 INFLUENCE OF FRACTURES ON MODELLED ANCHOR CAPACITY

5.1 Introduction

Chapter 5 uses the calibrated strength parameters from the last chapter to assess the variation of anchor pullout loads for different fracture networks. A 1.5m embedment, fully grouted dowel was selected for analysis in this section. This anchor length was not chosen due to it's importance or significance in engineering practice, it was rather chosen since published failures have been documented at this scale of anchorage so it provided a convenient starting point for the assessment. Analysis and numerical simulation of more complex engineering problems are provided in Chapter 8. The fracture statistics in this sections are varied and assessed using the combined DFN-numerical approach discussed in Chapter 3. As previously described, the integrated finite element – DFN approach allows for a more realistic representation of rock mass behaviour since failure can occur in tension and shear, both along pre-existing joints in the model rock mass or through breakage of intact rock or rock bridges between joints. Modelling brittle fracture allows for the inhomogeneous and anisotropic nature of failure noted by Bruce (1976) and others to be reflected in the observed results.

Models with different fracture radius and fracture orientation can be obtained by generation of a DFN model in the Fracman code. In Fracman, each random iteration results in different statistically valid spatial model, and with the proximity of persistent or large fracture in the model to the anchor it is contended that the variability in the rock mass can be assessed. This variability is investigation in Section 5.2. Where large variations of uncertainty in strength could be represented by a higher value of the anisotropy index Ai or the coefficient of predictibilty Cp, which could correspond to the use of a higher factor of safety in design for a given set of fracture statistics (Elmo and Stead, 2009 ; Wiles 2006), The variation between DFN realizations represents uncertainty associated with the spatial variability of joints across a foundation. Furthermore, the results presented in Section 5.3 and 5.4 were obtained by scaling or rotating fractures 10 DFN realizations in order to assess the general influence of joint continuity or persistence and the influence of rock mass structure on failure. Since fractures are scaled or rotated not regenerated the variability in the rock mass is from these adjustments to fracture length or orientation not due to the spatial proximity of joints originating from the same realization, since the joint remains in the same location. The same strength and softening criteria described in Chapter 4 was assumed for all models run and the variation in the simulated pullout capacity is solely due to the influence of fractures in the model. It is contended that if the numerical model presented is combined with DFN modelling, some of the

aleatory uncertainty presented in the variability of jointing across the site and dilation can be observed prior to the failure of the rock mass. In addition the influence of fracture damage and confinement are also discussed below.

5.2 Variation in Anchor Capacity for Similar DFN Statistics

The addition of fracture networks to the mesh domain introduces variability into numerical simulations. This variability allows for the rock mass stiffness to change spatially in a model which in turn influences dilation and unloading of the lower rock mass near the distal end of an anchor. It is contended that this load transfer mechanism can influence the capacity of a rock anchor.

To measure the variation in joint spacing and continuity, the capacity of the anchor is plotted against the 2D or 3D areal fracture intensity (P21 or P32 respectively). Dershowitz (1984) introduced several expressions for characterizing fractured rock, most importantly P32, for measurement of fracture connectivity. Fracture connectivity indicates the extent in which fracture patterns in the rock mass intersect. The intersection of fracture pattern networks or joint sets is important with regard to flow or instabilities in the rock mass, which depends on fracture intensity. For the rock cone pullout mechanism, it is contended that fracture connectivity may influence the stability of a rock around the anchor, hence P21 which is a function of P32, should also have an influence on the stability of an anchor. However, where joints are non-persistent and moderately connected it is envisaged that the discrete location of the fractures in the model, and the proximity of intersection of these fractures with respect to the loaded anchor, also create variability in strength.

To prove that that the discrete location and orientation of joints in a numerical model have an influence on anchor strength, 21 numerical simulations were carried out using the same strength properties but different fracture network realizations (with the same statistics). Figure 20 summarizes the variation in failure load observed in the models for the four joint set fracture network. This chart plots the fracture intensity (P21) against the anchor capacity and the P21 for each cross section cut from the DFN varied between about 3-6 for a four joint set fracture network. In 2D, the joint trace lengths in the simulations ranged between 0.5 m and 3 m following an exponential distribution with a mean trace length of 0.7 m. Rock bridging length (along the plane of the joint traces of similar sets) ranged from about 0.3 to 0.6. As shown the pullout capacity for these models ranged from 0.35 to 1.6 MN.

For these 21 simulations, the average result (0.95 MN) is provided in the screenshot of Pullout Simulation 3 in Figure 20a. It is evident that the failure volume of Simulation 3 is much higher than that of Simulation 8, which provides the lower bound (0.35 MN) anchor capacity. This low capacity is a result of two joints forming slender release surfaces immediately adjacent to the anchor. Simulation 3 requires more breakage of intact rock which also significantly increases the rock mass resistance to pullout.

The variation in capacities observed illustrates the importance of running a number of numerical simulations to assess the various failure mechanisms possible for the rock mass surrounding an anchor. In addition, engineering judgement is important in determining whether the failure mechanism for the lower bound estimates for strength are reasonable.

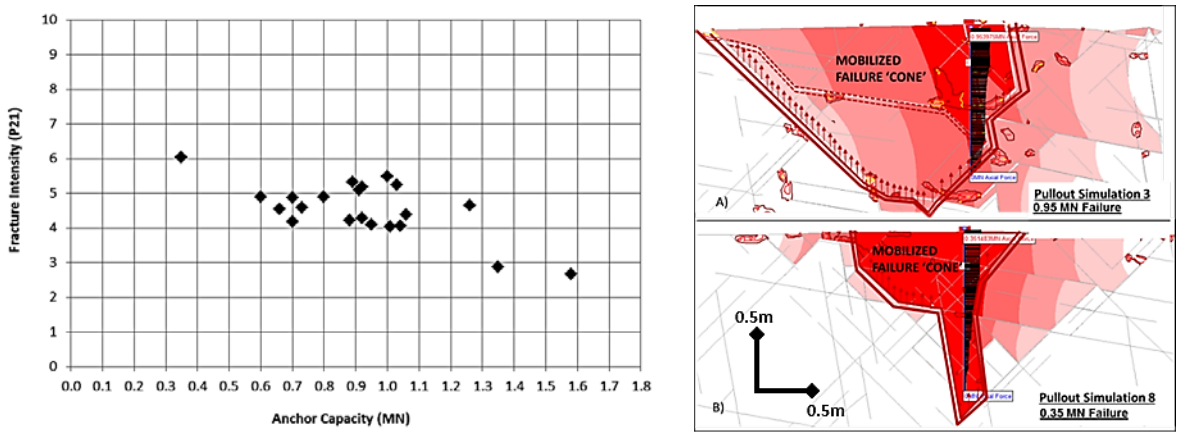

Figure 20- Fracture Intensity vs. Anchor Capacity plots for fracture networks in the 3<P21<6 Range, and, a comparison of two model realizations for fractures networks in the 3<P21<6 Range (right)

– minimum deformation 1mm, maximum 5mm shown in red in Figure

5.3 Influence of Joint Persistence

In general, there is a slight upward trend in the data presented in Figure 20 with the nominal increase in P21 across the model. It is expected that where greater variation in P21 exists this trend will become more pronounced. To complement the observation that the discrete location of joints in numerical simulations effect anchor capacity, an investigation into the influence of joint persistence and intensity was completed by scaling the fracture traces for a number of realizations generated in Fracman.

A scaling factor or "Persistence Factor" of 1.0, 0.9 and 0.5 was applied to generate the results indicated in Figure 21.

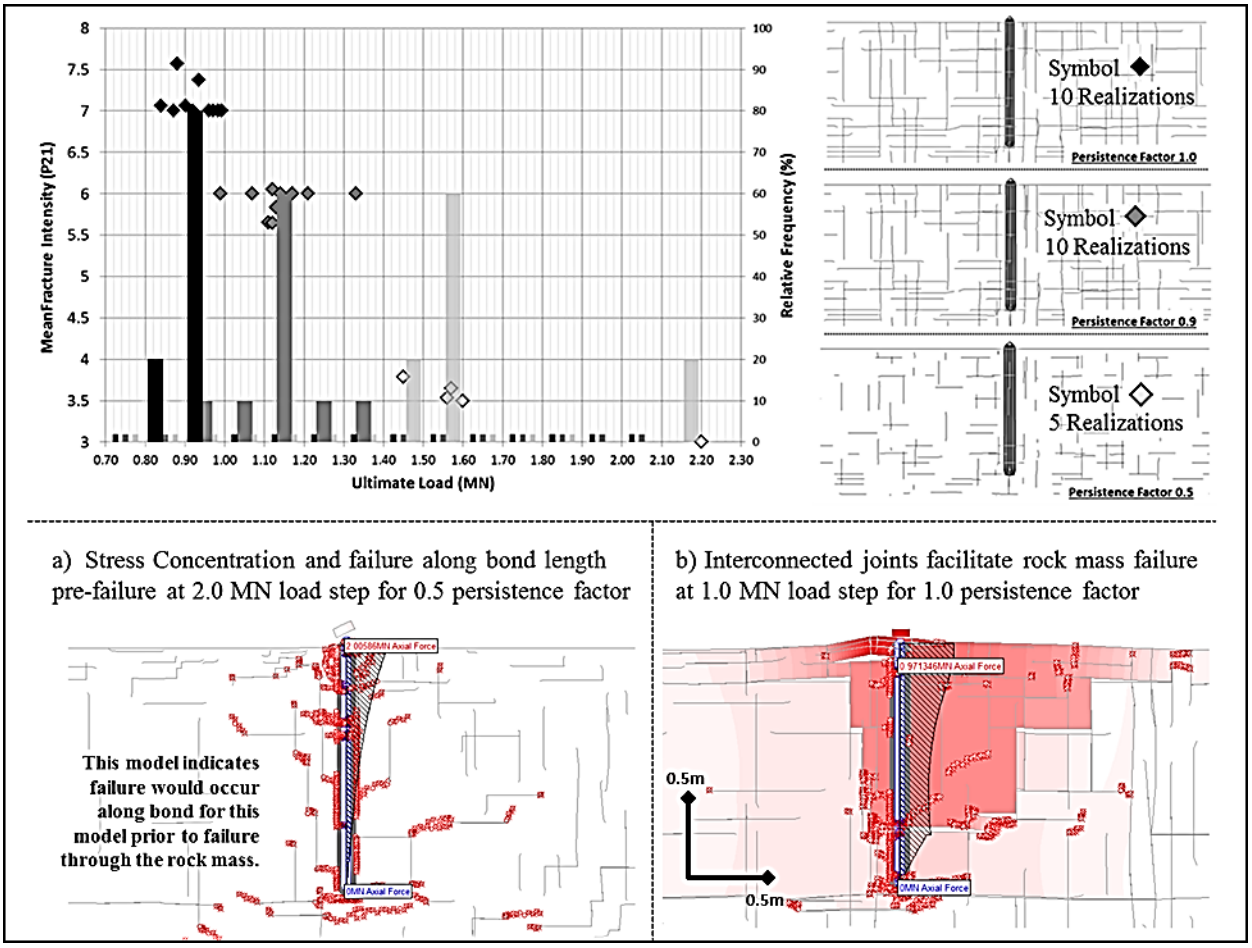

Figure 21 - Fracture Intensity vs. Ultimate Load plots for 1.0, 0.8 and 0.5 Persistence Factors, bars indicate the relative frequency of each load bin while symbolic points indicate the mean fracture intensity for a given DFN realization. The different colored symbols correspond to the Persistence factor provided in the right legend.

This figure also provides a legend illustrating the influence of the persistence factor visually. As the persistence of the joints (and joint lengths) decrease the percentage of intact rock increases and more breakage of intact rock is required for Mode D rock mass pullout failure. For example, in more fractured or blocky rock masses the capacity of an anchor will likely be governed by the frictional properties and confinement of interconnected unfavourably orientated joints. Conversely, in rock masses with widely spaced, poorly connected discontinuities strength will be developed by the strength of intact rock bridges. This is evident in the bottom left screenshot on Figure 21a where, for a realization with a 0.5 Persistence Factor applied, a 2.0 MN load does not produce a global rock mass failure and shear stress and failure is concentrated along the bond length of the anchor. For this persistence factor, global failure was observed between 1.4 MN-2.2 MN depending on fracture

network realization. In contrast, with a 1.0 Persistence Factor applied, a 1.0 MN load produced the dilation noted by the red contours on the bottom right figure. For this factor failure was observed through the rock mass as a load between 0.8 MN and 1.0 MN depending on the fracture network realization. This dilation and failure is due to the interconnectedness of joints in the model and the reduced requirement for breakage of intact rock between joints. For the 0.5 persistence failure it is evident that failure of the steel tendon or the rock-grout interface will occur long before the rock mass.

5.4 Influence of Joint Orientation

Further to the investigation of joint persistence, a number of model iterations were run to assess the influence of joint orientation on anchor capacity. Each fracture realization was adjusted by a "Joint Orientation Factor", indicating a rotation of the fracture network (in it's entirety) about the faceplate of the anchor. The results indicate a higher mean anchor capacity for the subvertical-subhorizontal dipping fracture network compared to joint networks with a rotation applied. The anchor capacity variation for the +0, +20, and +45 orientation factors ranged from 0.8-1.0 MN, 0.65-1.0 MN, and 0.55-1.2 MN, respectively. These simulations seem to suggest that subvertical conjugate jointing is more favorable for resisting pullout, possibly due to clamping of asperities and joints from overburden pressures. Alternatively, the discontinuities oriented at 45 degrees may provide lower strengths since these are roughly in alignment with the hypothetical cone pullout surface. It should be recognized that the finite element continuum mesh formulation may also have an influence on the accuracy of the results, since while the onset of failure is analyzed with joints, the models are still limits to small strain formulation.

Extensive full scale testing is required to validate this observation before bold conclusions can be made about the influence of joint orientation of the stability of anchors. It should also be noted that where either subvertical joints or subvertical joints are more persistent than the other, and the nature of the joint set is not truly a conjugate, the results of the models may differ from those presented.

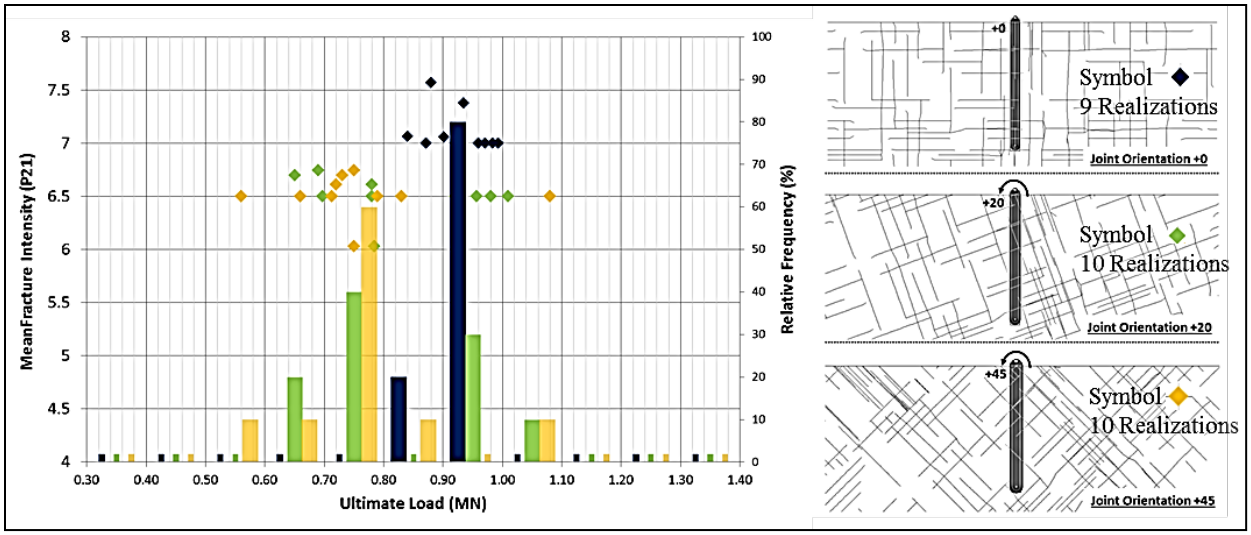

Figure 22 - Fracture Intensity vs. Ultimate Load plots for +0, +20 and +45 Orientation Factors

Furthermore, Barton and Quadros (2015) provide a discussion of rock mass anisotropy in a special issue of the Rock Mechanics and Rock Engineering journal. An important consideration not considered in these models is the geological origin and structural geology of the rock mass. Geological origins may provide distinctive bedding cycles in sedimentary rocks, distinctive flows in basalt, foliation in gneisses, schistocity in schists and faults through all the above. Igneous dykes and sills also have origin specific jointing patterns and weathered horizons. Each regime may influence the modulus, strength and permeability of the rock mass – hence creating anisotropy in the rock mass being modelled. It is well understood and appreciated by the author of this thesis that the rock mass is not simply a discrete fracture network system generated in a box, however, the box approach is taken to assess how different DFN statistics influence the simulated anchor capacity. In reality, if there are known discrete, stability controlling features in the rock mass, these features should be inserted deterministically into a DFN model and the proximity of the features to the anchor should be maintained. A statistically valid DFN could be generated around this feature so that the intersection of other joints in the rock mass that form unfavourable orientations within the zone of influence of the anchor load could be assessed.

The influence of single features is described in Section 5.2 and may result in the fairly significant variability in the moderate dipping DFN orientation's (+20, +45) compared to the variability within the sub vertical joint set. The typical value for the +45 joint orientation factor is between 0.7-0.8MN while the upper and lower limits are 0.56MN and 1.08MN respectively. A comparison of the two DFN realizations are presented in Figure 23 and Figure 24. The first figure provides a screenshot of

the displacement contours at the lower bound failure load of 0.56MN. In this model, interconnected jointing is present immediately adjacent to the anchor. This stepped failure path, formed by conjugate jointing in the model, does not require breakage of intact rock to connect the distal end of the anchor with the surface. In addition, a number of persistent features exist near the base of the anchor which form a release surface which connects a wedge with the surface. However, in order to fail the anchor, a counter-clockwise rotation of the wedge is required to allow for dilation of the stepped failure plane on the right hand side of the anchor in the model. Freedom for rotation and dilation is provided by the persistent jointing on the left and side of the model which facilitates movement by allowing sliding to the left. This effect assists the rock mass in deforming as if it were a removable wedge governed by its self-weight, hence, the low anchor capacity. At failure, the dilation in the rock mass exceeds 5mm in this model iteration at the lower bound load of 0.56MN.

In contrast, Figure 24 provides the pre-failure deformation from a different realization a load 1.02MN, near twice that of Figure 23. It is apparent in this model that the joints are not interconnected and dilation is only observed in the upper rock mass where a removable block is present. In contrast, Figure 25 provides an example of same DFN iteration with a +0 joint orientation. At the same load at Figure 24 the +45 orientation factor (with the same joints distribution but rotated) has failed at the load of 1.02MN. This is higher than the typical value of 0.7MN-0.8MN observed for this joint orientation factor. This is likely due to the fact that intact rock is required to be broken to facilitate failure. It is interesting to note that the discrete realization of the joint network presented in Figure 24 produced the highest failure load of all simulations. When compared to the same realization, but with a +0 orientation factor, failure occurs at the same load as that presented in Figure 24. This is due to the fact that dilation can occur by opening the sub-horizontal beds that are perpendicular to the applied load. Interestingly to note is this is the failure mechanism noted by Brown (1970) which may have lead to staggering of anchor lengths in this type of geological setting for anchor groups designed today. Upward dilation allows for cracking and damage in the rock mass parallel to bedding which may lead to anchor failure. Tensile cracking and the influence of damage is described in the next section.

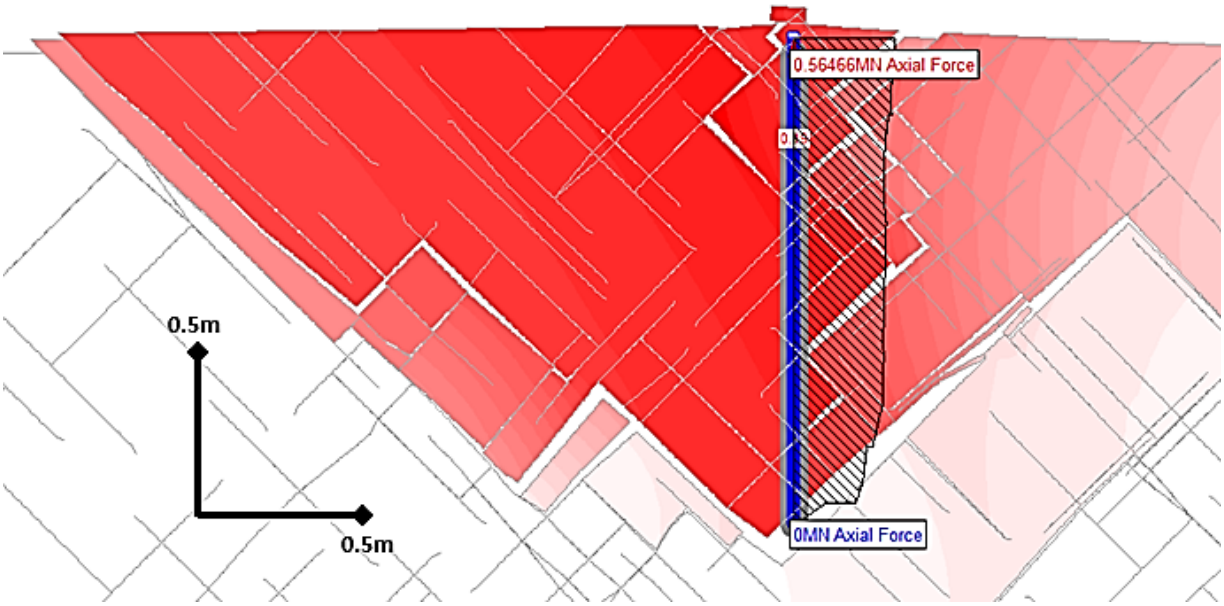

Figure 23 – Lower bound failure realization indicating greater than 5mm displacement at Load = 0.56MN

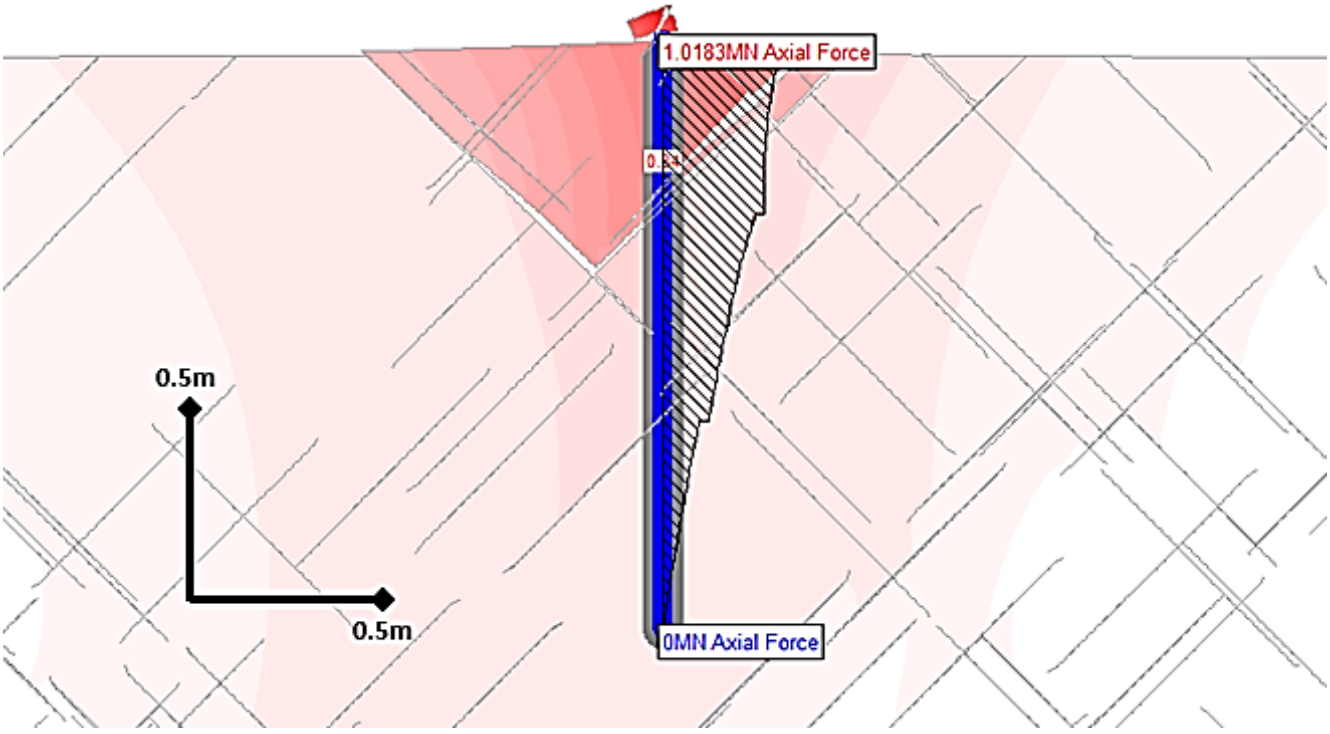

Figure 24 – Upper bound failure realization indicating less than 1mm displacement at Load = 1.02MN

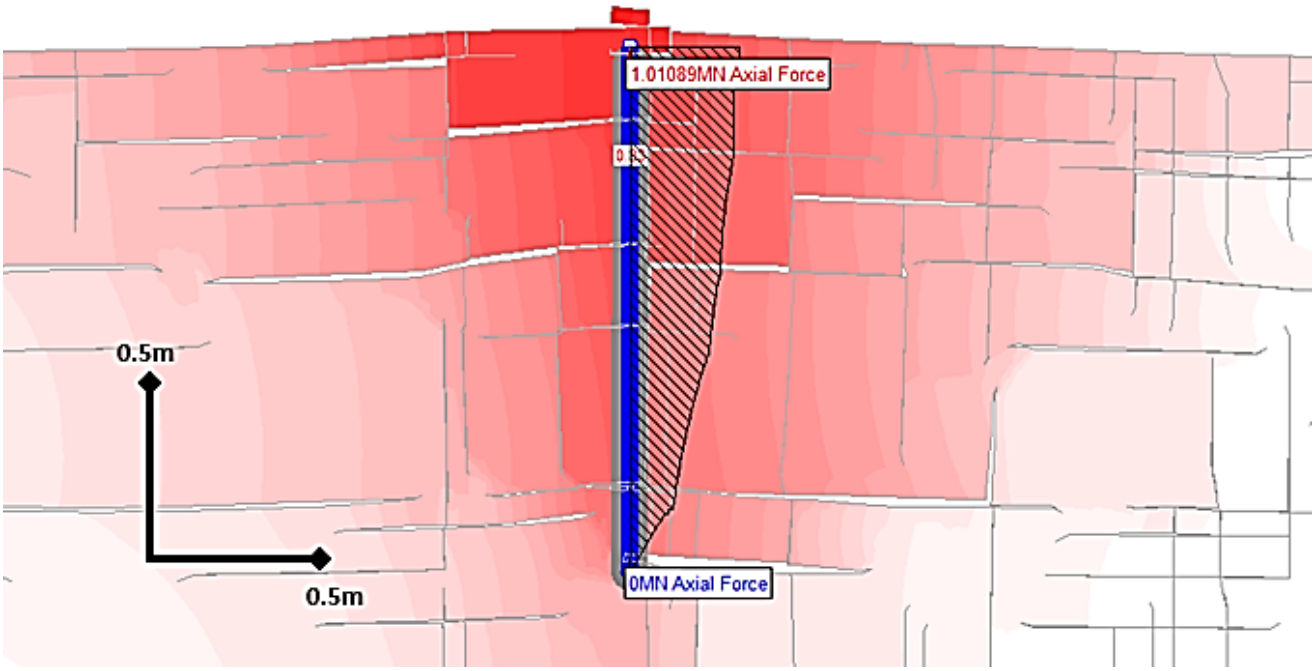

Figure 25 – A revised joint orientation factor = +0 produces failure with greater than 5mm displacement at Load = 1.02MN for the same fracture network realization as the upper bound failure realization with a +45 factor

5.4 Quantifying Rock Mass Damage (D21)

It was identified in the previous section that while the results of tests on moderately dipping conjugate joint sets seem to indicate that, in general, the ultimate load capacity of an anchor is slightly lower than that of a subvertical-subhorizontal conjugate set. However, some of the model outliers from the moderately jointed sets (+20, +45 orientation factors) actually have higher calculated capacities compared to that of the subvertical set. This may be due to the fact that dilation can occur by opening of subhorizontal bedding planes which may facilitate cracking while this may not be possible for other DFN realizations, such as that shown in Figure 24. While infrequent, these results are still consequential and cannot be ignored. Outliers exists since the fractures in the model are poorly connected and that intact rock breakout may govern the stability of the anchors with high capacities. This is also reflected in Section 5.2 where the influence of joint persistent was analyzed. To study the influence of rock mass damage further, an additional 25 DFN realizations were generated in Phase2 for a fracture network. The fracture network was generated in Phase2 this time to facilitate a quicker production of the 25 realizations produced with the same joint sets.

After each model iteration was run in Phase2, the fracture traces were then inserted back into Fracman for detailed analysis of fracture statistics. In addition, the location of yielded elements (both tensile and shear failure) was traces in Phase2 and the fracture traces were also imported into Fracman for analysis. Figure 26 provides a comparison of the imported pre-existing fracture traces for one fracture network realization, as shown in the left screenshot, to the imported pre-existing fracture traces and the "damage" or induced fracture traces which are provided in red in the left screenshot.

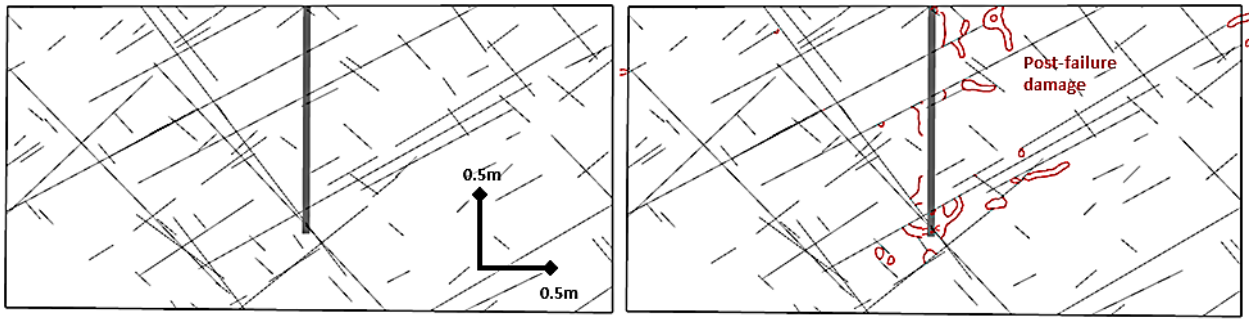

Figure 26 – A sketch comparing pre-existing fractures to induced fractures in DFN Realization 1

After the models had been run the P21, P20 and damage were calculated for each of the 25 fracture network realizations generated. A number of authors have assessed the degree of damage or intensity of induced fractures in a numerical model by calculating an intensity of damage factor. This damage factor can be calculated in a similar fashion to that of P21 but instead of assessing the density or intensity of pre-existing fracture in the rock mass, the length of new fractures or damage can be assessed for a given area. For blast damage, Tuckey (2012) described this factor is B21and loading induced damage in numerical models has been described by a number of other authors in two dimensional space as D21 (Preston 2014, Gao 2013, Hamdi et. Al. 2014, Stead & Eberhardt 2013), and in three dimensional space as D32 (Havaej et al., 2014, Zhang 2014). D21 has been subdivided into a shear and tensile component in some assessments, however, due to the complex and combined failure nature of the cone pullout problem post-yielded elements are considered in the same damage class for the purposes of this work. The D21 values for the 25 joint set realizations analysed are presented in Figure 27.

In general, where load required to achieve failure in the model increases, the amount of damage observed likewise increases. This is due to the fact that there is greater resistance provided by intact rock and breakage of rock bridges is required for pre-failure dilation and ultimate failure. Figure 28 illustrates total displacement contours for a DFN realization where greater than 5mm

dilation observed at failure for lower bound failure load = 0.7MN. In comparison, Figure 29 illustrates total displacement contours for a DFN realization where the same dilation observed at a much higher failure load = 1.2MN. A comparison of the damage required to mobilize each block is provided in Figure 30 and this progressive damage sequence is discussed in more detail below.

A comparison of upper bound (right) and lower bound (left) yielding behaviour is presented in Figure 30 for the two different DFN realization, where the displacement contours at failure are also shown in Figure 28 and Figure 29. The red lines in Figure 30 indicate combined shear and tensile failure induced by loading. The failure of the right hand set of screenshots is shown to be progressive and ultimate failure load of 1.2MN is only achieved after tensile cracks coalesce between joints and allow for dilation to occur to the base of the anchor. The left hand load progression indicates how much less breakage of intact rock is required to mobilize the anchor since pre-exist fractures form a removable wedge. Some minor cracking of intact rock is required to mobilize the wedge, however, this cracking is much less significant due to the presence of the unfavourably orientated, persistent fractures intersecting the base of the wedge.

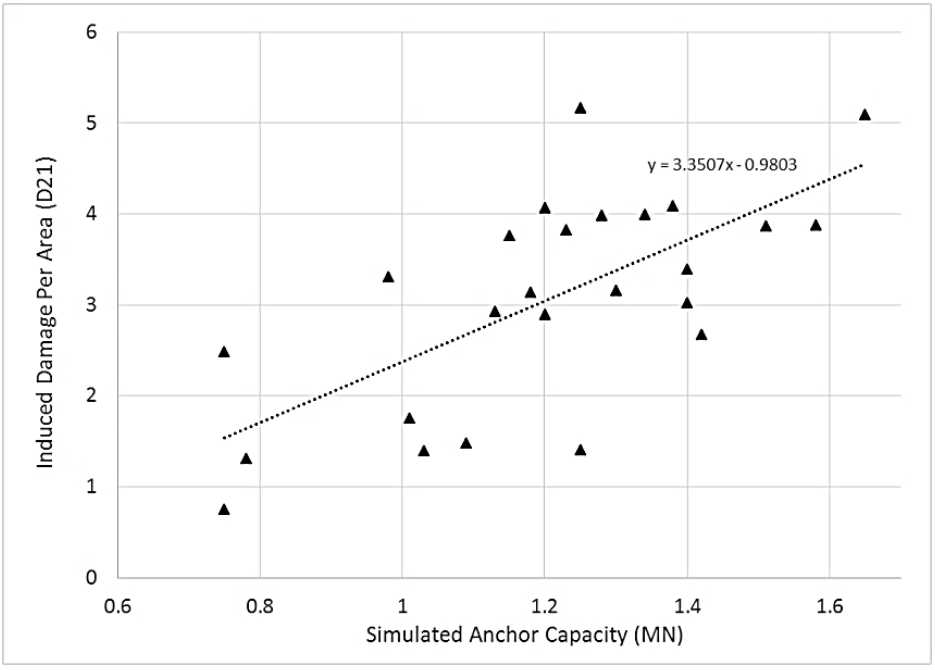

Figure 27 – Induced Damage Intensity vs. Ultimate Load plots for 25 DFN Realizations

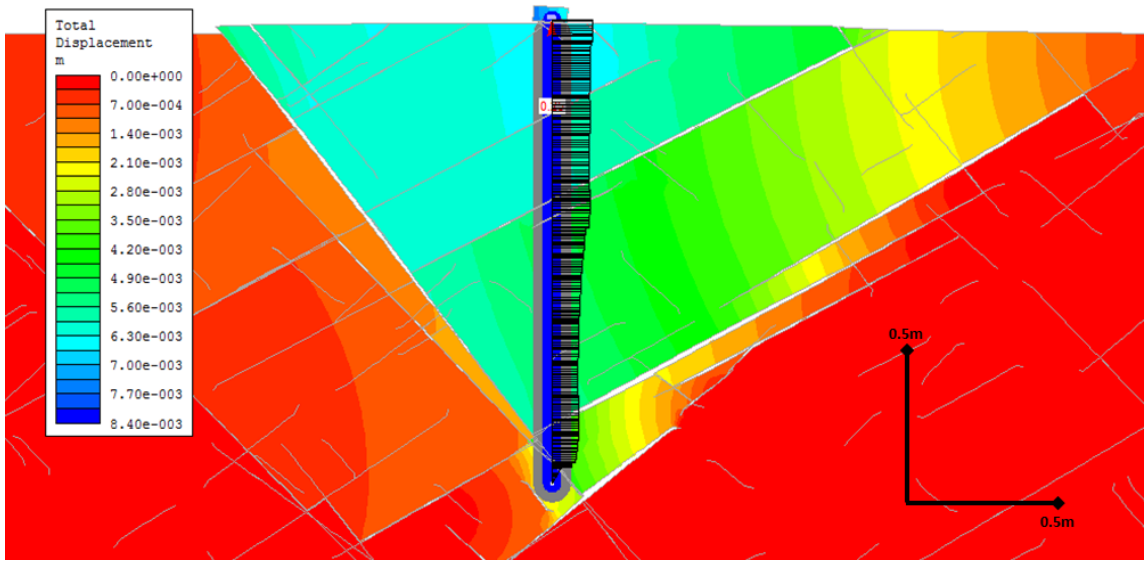

Figure 28 – Greater than 5mm dilation observed at failure for lower bound failure load = 0.7MN

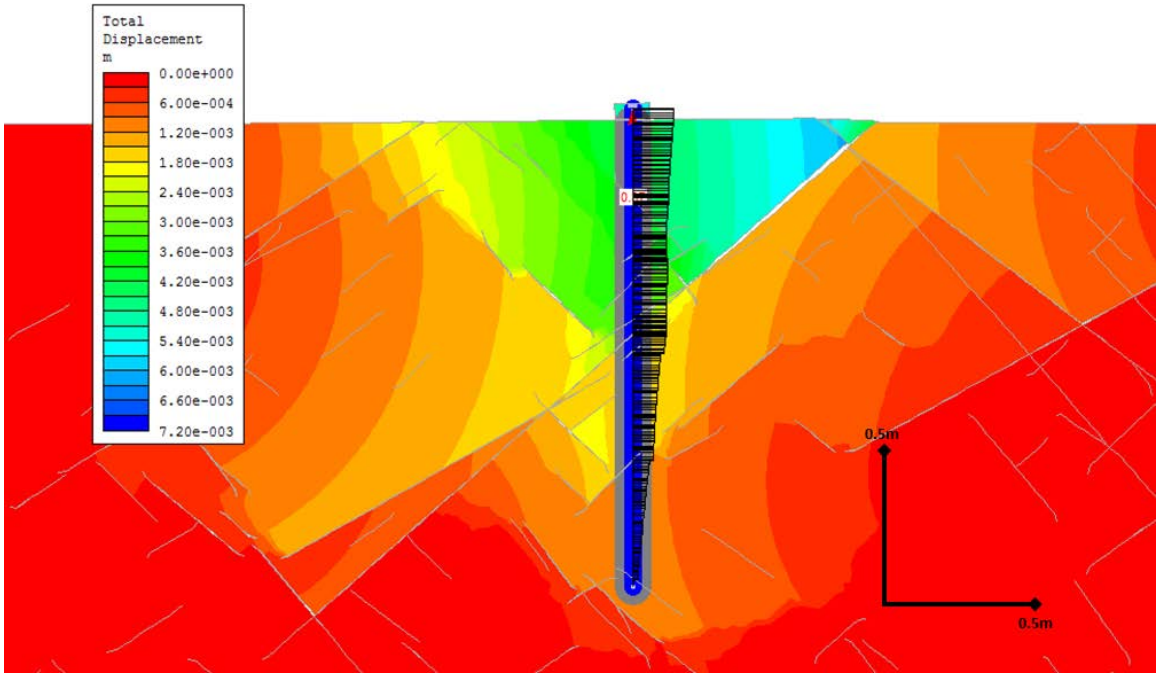

Figure 29 – Greater than 5mm dilation observed at failure for upper bound failure load = 1.2MN

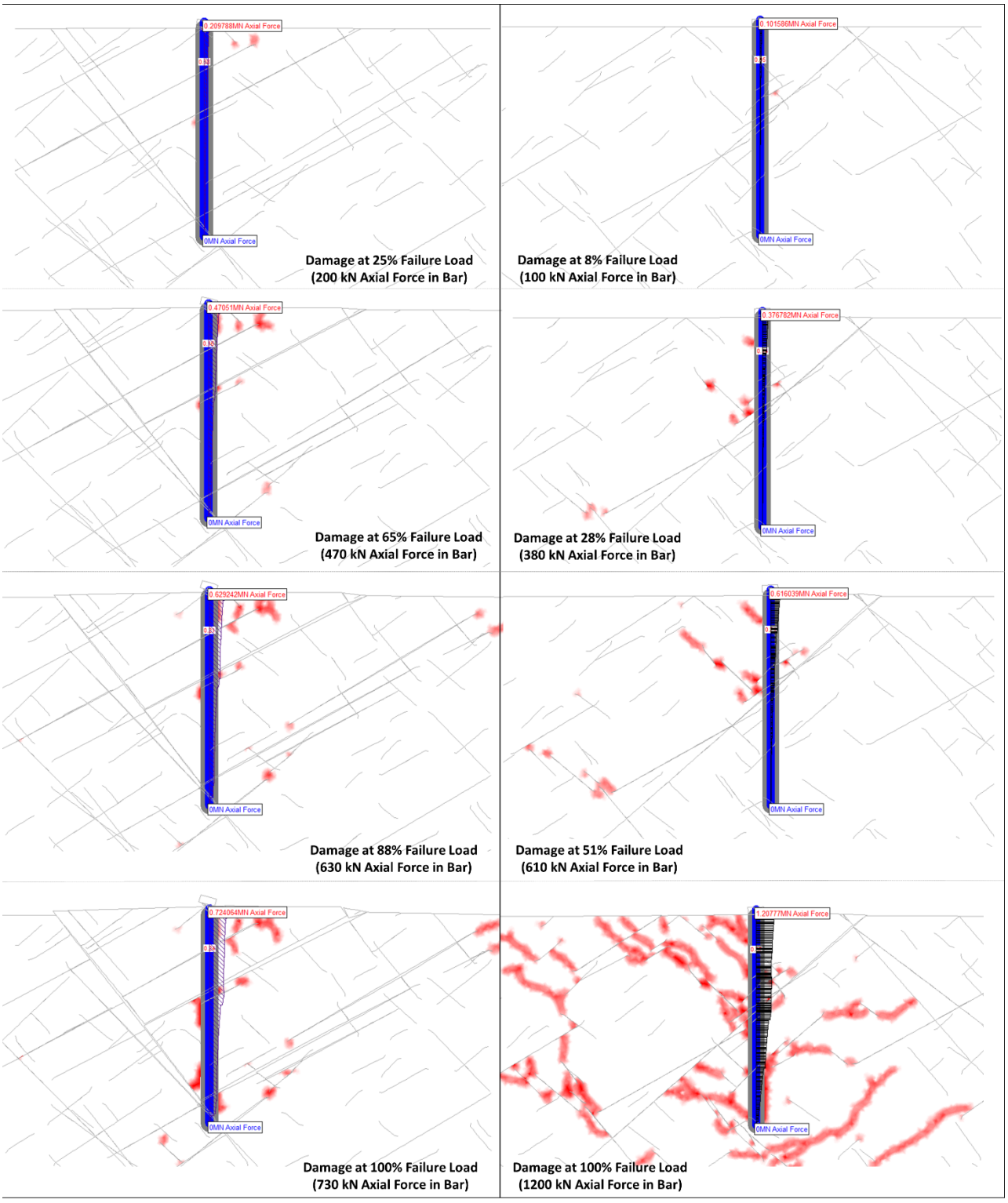

Figure 30 – Comparison of upper bound (right) and lower bound (left) yielding observed in two different DFN realizations. The red lines indicate combined shear and tensile failure induced by loading. The upper bound failure is progressive and ultimate failure is only achieved after tensile cracks allow for dilation to occur to the base of the anchor. The left hand load progression indicates how much less breakage of intact rock is required to mobilize the anchor since pre-exist fractures form a removable wedge.

5.4 Influence of Confinement on Pullout Capacity and Dilation

The previous sections have illustrated that jointing in the rock mass has a significant influence on the calculated capacity of a rock anchor, however, if confinement is applied at the rock surface, dilation may not occur in the upper rock mass which may make the influence of these fractures less significant. This concept is explored further in this section where confinement is applied to the rock mass as a result of closely spaced outriggers from an anchor test apparatus. The model setup for this section is provided in Figure 31 where the Phase2 model is compared with a historic ISRM test setup recommended for evaluating the resistance of the rock mass to pullout. In this model, the anchor load (T) is applied in the same staged manner as the previous section, however, as T increases with loading stages the reaction force (R) is applied to a 0.3m footing located about 0.3m from the anchor. In reality, this anchor load is not applied as a uniform distributed load of infinite length, however, for this simple model the plane strain assumption has been assumed. The reaction force increases at each footing at a factor of half of the anchor load since these footings provide the resistance to the pull from the jack on the top of the anchor. It is considered essential that the reaction frame and footing are installed outside of the area of stress influence of the anchor, however, in current practice this is not often the case. To illustrate this point, Figure 32 provides the current recommended test setup from the American Society for Testing and Materials (ASTM) designation 4435-84 which is designed to "*measure the working and ultimate capacities of a rock bolt anchor*". This test setup has reaction anchors which are inside the probably zone of influence for dilation and rock mass pullout.

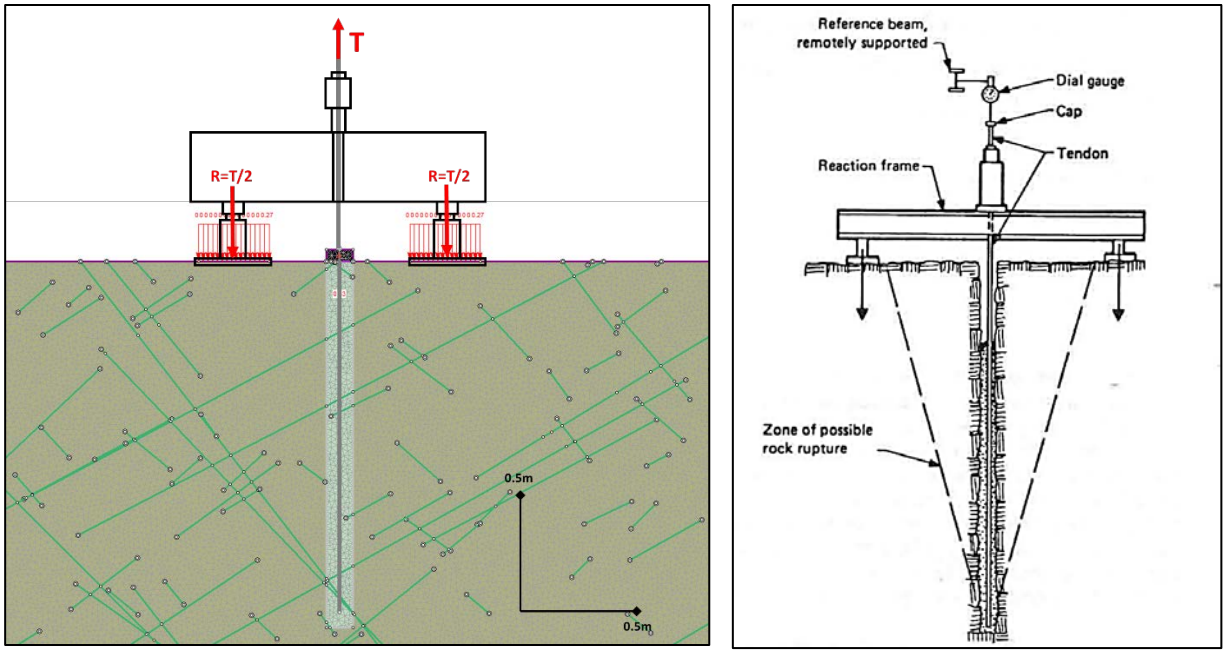

Figure 31 – Model setup for typical rock anchor pull test on left (Test force=T, Reactionary Forces=R) compared to historic ISRM recommendation for rock anchor pullout apparatus set up on right, modified after Carter (1995)

Figure 32 not shown due to copyright permissions,
Figure shows testing arrangement with reaction anchors installed within the area of the probable "pullout cone"

Figure 32 – ASTM 4435-84 Anchor Test Setup Recommendation (see ASTM 4435-84)

As mentioned above, an important component of testing the resistance of the rock mass to pullout is having a reaction frame with footings or reaction plates of adequate spacing to limit the influence of the loads from these anchors on the rock mass foundation. The arrangement presented in Figure 31 models the influence of the confining loads from the reaction plates within the zone of influence of rock mass dilation. The distributed loads and reaction frame are also provided in Figure 33 where rock mass dilation is shown as contours at an anchor test load T=0.73MN. The observed displacement in this model is less than 1mm at this test load. When compared to the model simulation in Figure 34 it is apparent that the confining pressures at the reaction plates have a significant influence on the failure behaviour of the rock mass. In the unconfined model, failure and displacements are observed to exceed 5mm at the rock surface. In addition, the fracturing behaviour required to produce ultimate failure of both models is very different. Figure 35 illustrates the development of progressive yielding in the confined model to a load of 1.25MN where failure was observed. When comparing this model to the damage in the same rock mass in unconfined conditions it is apparent that the current practice of anchor testing may be influencing

the failure mechanism observed. In addition, the influence of confinement observed in these models may have implications on the design of post-tensioned anchors where a free stressing length is used to transfer the loads deeper into the rock mass. While the concept is interesting, full scale testing on anchors with a free stressing length is required to validate these claims.

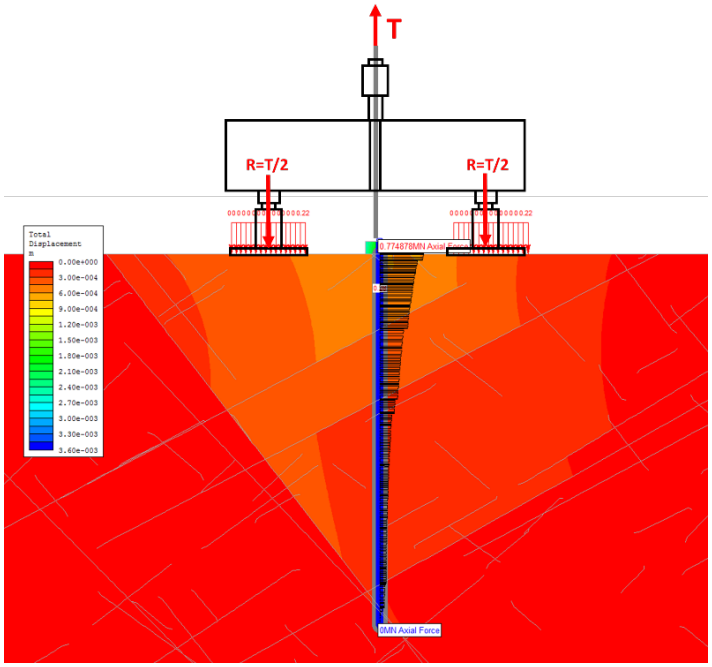

Figure 33 – Idealized pullout test arrangement provides reaction force inside the area of influence of rock mass dilation; The maximum dilation in the rock mass at failure is less than 1mm in the model for the test load, T of 730kN, where failure occurred in unconfined model presented in the next figure.

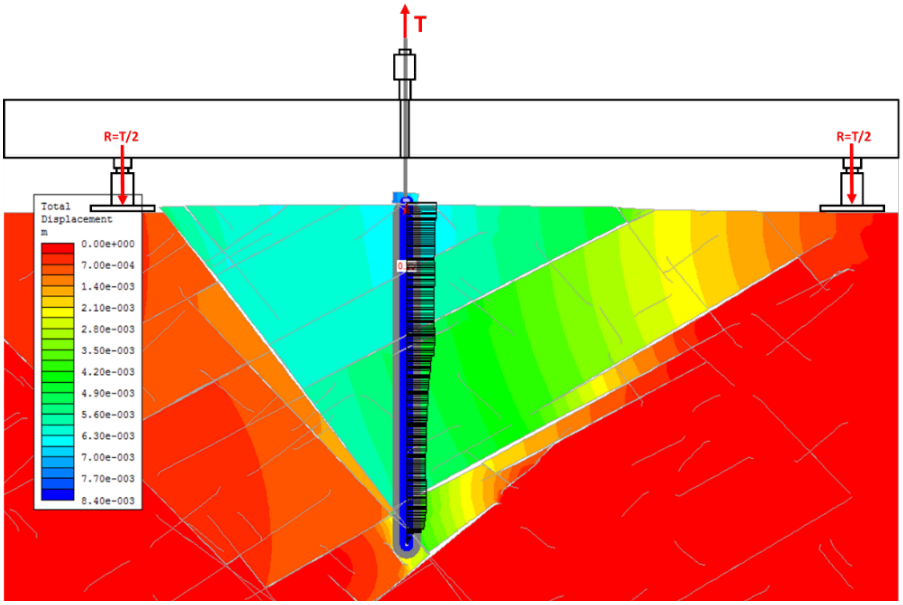

Figure 34 – Idealized pullout test arrangement provides reaction force well outside of area of influence of rock mass dilation indicated by color contours in the Phase2 realization shown; The maximum dilation calculated in for the rock mass in the model at failure is greater than 5mm for the maximum test load, T of 730kN

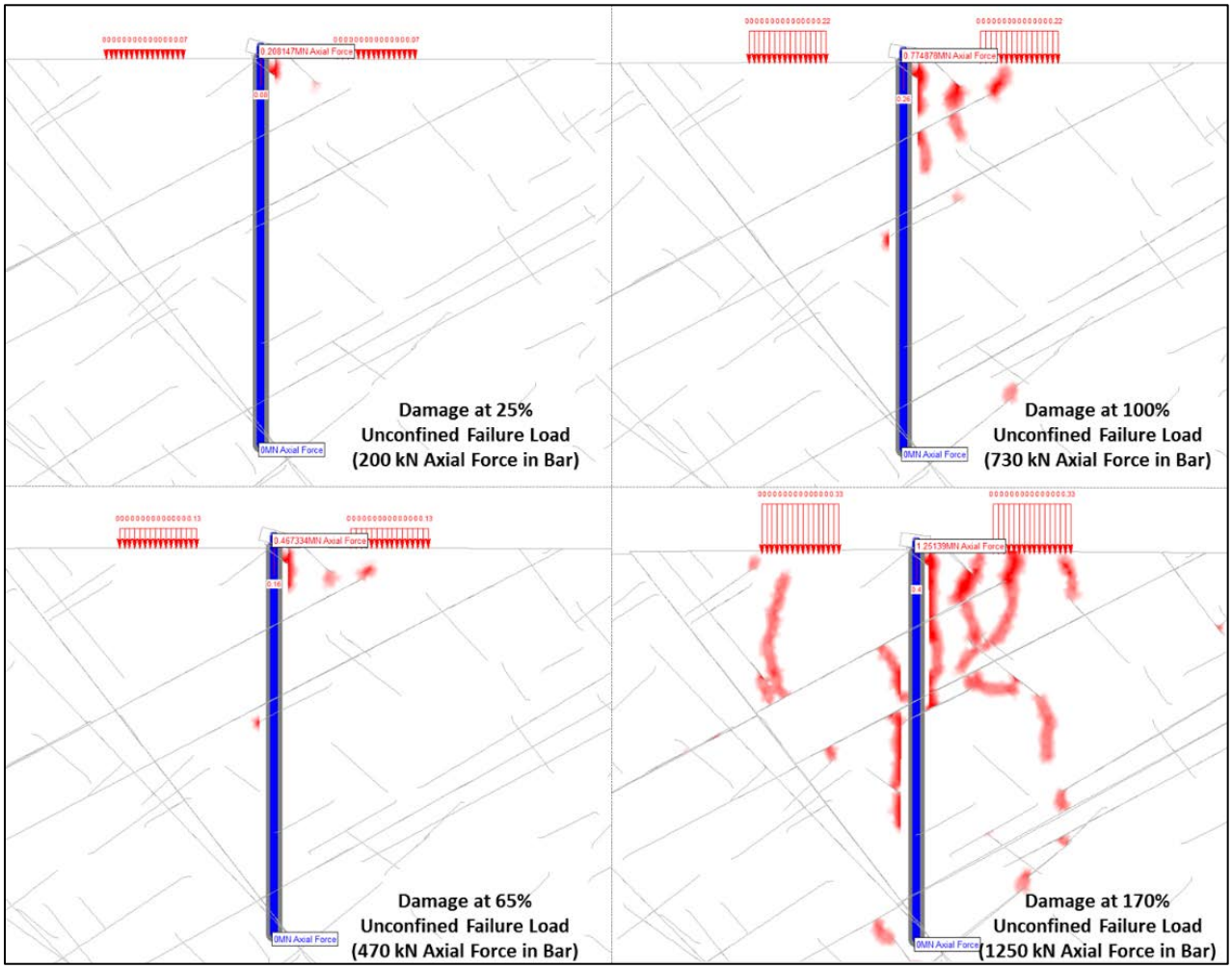

Figure 35 – A Phase2 model showing 4 different loading for the confined test model. It is apparent in this model tensile / shear fracture propagation is influenced by the reaction load from the test setup

5.5 Concluding Remarks and Discussion

The influence of joints was investigated in Chapter 5 using the numerical simulations and it is apparent that the interconnectedness and proximity of jointing in the simulations has an influence on the modelled capacity of the rock anchor.

For these simulations, the same calibrated strength parameters and softening relationship were used for all model iterations. Had the finite element method been employed without joints, the same modelled capacity would have been calculated for each model iteration. Instead, Discrete Fracture Networks (DFN's) were used to model the variability inherent in the rock mass. For each

DFN realization, variation in anchor capacity was observed with the proximity of persistent discontinuities to the anchor and the upper rock mass of the model simulation.

Furthermore, general trends in the persistence and orientations of joints were observed. A fairly pronounced trend was observed using a persistence factor to scale the joint lengths in the model simulations. Where joints were more persistent and interconnected, the simulations indicated, in general, a lower modelled capacity.

In addition, the influence of joint orientation was also investigated and the model iterations with conjugate subvertical jointing were observed to have a slightly higher modelled capacity with less variability than the model iterations with conjugate with shallow to moderate dip angles. While this is an interesting observation, the influence of joint orientation should be assessed using full scale field tests before any significant conclusions can be made based on model simulations. It should be recognized that the purpose of this section is not to present design tables relating P21 fracture intensity or joint orientation to modelled capacity. Rather the purpose of these analysis was to illustrate the important consideration of jointing in the design of anchors. It is recognized by the authors that additional testing is required to validate the anchor pullout failure mechanism.

It is contended that if anchor tests are complete on 1.5m-2m length anchors, these results can be used to calibrate the intact rock strength and fracture propagation properties in numerical simulations. After these properties have been calibrated, it is envisaged that numerical simulation of more complex and relevant engineering problems can be assessed using these calibrated rock mass parameters. Based on the results presented in this Chapter, it is considered of upmost importance that the calibration of anchor pullout simulations use the discrete location, length and orientation of joints observed in the field tests in the model simulations. This is based on the observation that the modelled anchor capacity is influenced by the proximity of persistent joints in the upper rock mass of the anchor. During field pullout testing, the dilation of the rock mass and the naturally occurring joints should be measured as testing is completed. This will allow for both the strength and deformational properties of the rock mass to be assessed. If cyclic load stages are applied to the anchor, both the elastic and in-elastic response of the rock mass could be assessed as the anchor is loaded and then unloaded progressively to higher loads.

The distribution and number of yielded elements was also observed in the model simulations. It is contended that the in-elastic response of the rock mass described above is a consequence of tensile and shear failure of the rock mass surrounding the anchor. The exact distribution of shear and tensile failure is deemed by current engineering practice to be too complex to quantify, and for this reason yielding in the rock mass observed in the models was noted as simply damage or induced fracturing (D21). The models in this Chapter indicate that simulations that require more damage to failure have a higher simulated capacity. This is likely due to the fact that D21 damage is lower where the interconnectedness of fractures requires less breakage of intact rock bridges to mobilize a failure "cone". It is contended that acoustic emissions could be used during field tests on anchors to determine the load at which damage is induced in the rock mass surrounding an anchor and the spatial distribution of damage as the anchor is loaded.

Furthermore, it was also identified that the confinement provided the testing jack may have an influence on rock mass damage, therefore it is considered of upmost importance that the footings used to provide jack reaction are placed with outriggers well outside the zone of influence of rock mass dilation. With future testing it is anticipated that the distribution of shear and tensile fracturing can be assessed and it is possible that this distribution may dependent on the ratio of shear strength to tensile strength of the rock and the Hoek-Brown intact rock, m_i, coefficient for different rock types.

6 FEM-DEM SIMULATION OF FRACTURE PROPAGATION IN INTACT ROCK

6.1 Introduction

The previous Chapters introduced the influence jointing and damage on simulated anchor capacity. It was concluded in Chapter 5 that future research in the field of anchor design should include full scale testing to calibrate rock mass dilation and damage, by mapping the distribution of dilated fractures at a 1:1 scale during loading and assessing the onset of damage using acoustic emissions. To illustrate how fracture processes may manifest in the rock mass, this Chapter (Chapter 6) investigates how a changes the elastic modulus and fracture energy parameters may have an influence on damage and the failure mechanism observed in numerical anchor simulations in massive rock.

This assessment was completed by using the hybrid finite-discrete element model (FEM-DEM) ELFEN by Rockfield. A FEM-DEM model was chosen since this type of model more accurately reflects the behavior of fracture propagation using fracture energy, not an assumed user-developed softening relationship. Extensive calibration was not completed in this assessment since anchor testing data in intact rock is very limited, however, fracture energy correlations from other rock mechanics applications was used to develop the properties in the sensitivity assessment. Modelling in ELFEN is a secondary objective of this thesis but the results presented proved to be very interesting.

6.2 Hybrid Finite-Discrete Element Method (FEM-DEM) Model Characteristics and ELFEN Model Setup

6.2.1 Description of ELFEN Model and Mechanical Properties of Rock

The continuum in ELFEN is based on an explicit finite element code and material softening in the continuum domain is governed by a Mohr-Coulomb elasto-plastic model. The material properties used in the setup of the anchor simulation in the intact rock domain include a peak friction angle of 60 degrees, a cohesion of 3MPa, and a dilation angle of 5 degrees. To illustrate the influence of other parameters in the model, the mohr-coulomb parameters were left constant for all model simulations.

A number of different model iterations were run, as shown in Table 2, and one of the parameters that was adjusted was the intact rock Young's moduli (E), which varied from 1.5GPa to 50GPa in the simulations. The unit weight of the rock and poissons ratio are assumed to be 24kN/m^3 and 0.2

respectively. Using these parameters, strain is obtained through both standard elasto-plastic deformation in the continuum model as well as through the incorporation of fracture mechanics principles governing quasi-brittle extensional failure (Klerck et. al. 2000). Softening develops in the model by coupling the Mohr-Coulomb inputs with damage or strength reduction with the Rotating Crack (Rankine) model. This constitutive model produces dilation as a result of inelastic deformation as the model moves from an elastic state in the continuum model to as discontinuum model as new tensile fractures form as a result of breaking the mesh in the model, as shown in Figure 36, either by intra-element crack insertion or inter-element crack formation.

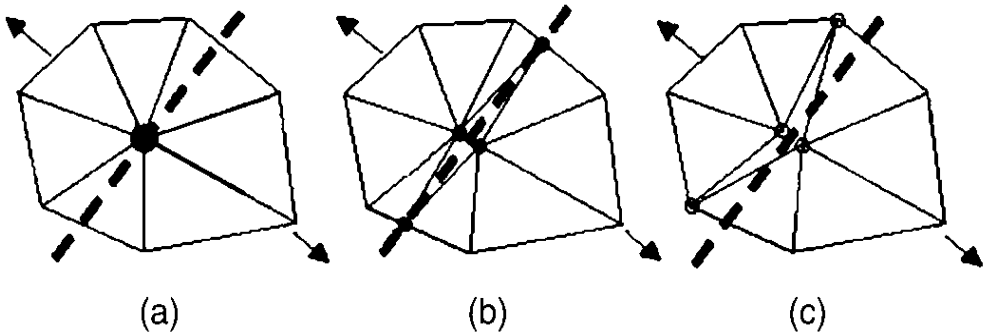

Figure 36 – Fracture Scheme in ELFEN. (a) Initial state before fracturing, (b) intra-element crack insertion, and (c) inter-element crack insertion; Modified after Klerck (2000)

The Rotating Crack (Rankine) failure parameters include tensile strength and the fracture energy parameter (G_f) which is a function of mode I fracture toughness (K_{IC}) a term that is related to the tensile strength by $\sigma_t=6.88K_{IC}$ (Elmo, 2006; Zhang, 2012; Hamdi, 2015). The fracture energy is calculated as $G_f = K_{IC}^2/E$. To assess the influence of fracture parameters, twelve model iterations were run and the properties used for generation of microcracks or damage in the models are provided in Table 2. It should be noted that the fracture energy parameter for model iteration 1, 2, and 5b were assumed and not calculated in order to evaluate the influence of variation in this parameter on the anchor pullout mechanism.

The purpose of varying the Rankine failure parameters is to assess the influence of these parameters on the failure mechanism observed in the models. This was completed without the inclusion of joints in the mesh domain to simplify interpretation, however, in reality jointing using a combined DFN approach should be considered in design. The Mohr-Coulomb failure parameters were only varied in Model 13 and Model 14.

Table 2. Mechanical properties used in ELFEN to assess the influence of the Rotating Crack failure parameters on the behavior of loaded anchors in massive rock

	Young's Modulus, E (GPa)	Intact Rock Mohr-Coulomb Failure Parameters (Constant)		Rotating Crack / Rankine Failure Parameters (Varied)	
		Internal Friction Angle, ϕ_i'(deg)	Internal cohesion, c_i (MPa)	Fracture Energy, G_f (J/m^2)	Tensile Strength, σ_t (MPa)
1	15	60	3	1.0*	1.0
2	1.5	60	3	1.0*	1.0
3	15	60	3	1.4	1.0
4	1.5	60	3	1.4	1.0
5a	1.5	60	3	1.3	3.0
5b	1.5	60	3	3.8*	3.0
6	50	60	3	3.8	3.0
7	30	60	3	6.3	3.0
8	20	60	3	4.2	3.0
9	10	60	3	2.1	1.0
10	5	60	3	1.1	0.5
11	3	60	3	0.6	0.3
13	5	60	1.2	1.1	0.5
14	3	60	0.8	0.6	0.3

*Arbitrary fracture energy parameters selected – i.e. does not follow $G_f = K_{IC}^2/E$ (Elmo, 2006; Zhang, 2012; Hamdi, 2015)

6.2.2 Mechanical Properties of Grout, Steel and Load Setup

For the assessment of rock mass pullout a #18 threadbar with a diameter of 1 ¾ inch (57mm) was assumed to be installed in a 114mm grouted drillhole. For confinement, the threadbar was capped at the surface with a rigid bearing plate to prevent "necking" of the bolt at the surface. The general arrangement of material types in the model is provided in Figure 37. The grout and the steel material types were assumed to be elastic with respective elastic moduli of 200GPA and 30GPA. It should be noted that the yield strength of 'Grade 75' (517/690MPa) steel is 1425kN for the #18 bar, if higher grade steel. The maximum anchor load in the models is 1425kN, therefore no plastic deformation is expected in the bar. If 'Grade 150' steel is used, the design load in the model is less than 0.8 times the yield strength of the bar. However, this does not consider the Von Mises influence of combined shear and tension that may develop in the bar due to stress rotations in the rock mass. For simplicity, the elastic assumption is assumed since the scope of the assessment is cone pullout.

Debonding at the concrete-rock interface is modelled by assuming cracking will be concentrated in the edge of the mesh within the intact rock domain. This was assumed since no roughness was applied along the interface between the concrete and the intact rock and the fractures that develop in the model are considered more representative than that of a smooth joint model with strain softening occurring along an interface with no roughness.

The loading in the model is applied at the top of the anchor bar over a period of 3.5 seconds. A nominal upward vertical stress is applied in the model at load step T=1.5sec and the load is increased until 1425kN/m is achieved at the top of the bar at T=5.0 sec. The progressive initiation and development of fractures at various loading steps is recorded as well as the ultimate failure of the rock mass.

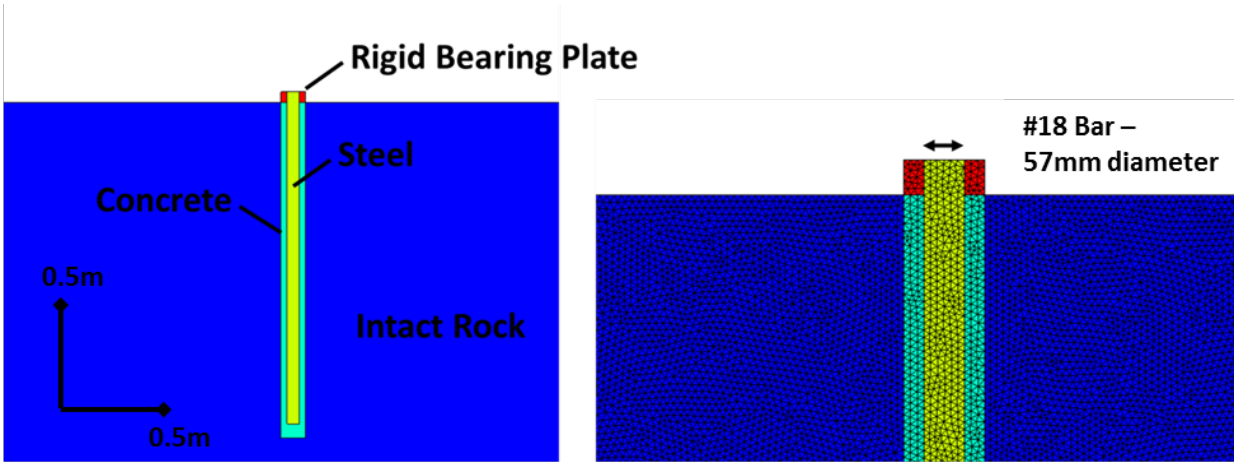

Figure 37– ELFEN screenshots showing material properties and mesh size used in FEM-DEM simulations

6.3 Load Transfer Mechanism (Elastic and In-Elastic Rock Mass Deformation)

After model setup was complete, the load transfer mechanism within the steel was assessed. Bruce et al. (1991) note that there are experimental results and numerical simulations that suggest that the distribution of load along an anchor is heavily influenced by the modulus of elasticity of the grout compared to the modulus of elasticity of the surrounding rock mass (Ec/Erm). Based on the studies noted in this research, if the modulus ratio is less than 1 (i.e. the rock mass is stiffer than the grout), shear stress is concentrated at the anchor head and stress is dissipated rapidly along the bond length with depth. These results indicate that the more competent rock mass with a low concrete:rock ratio concentrates load at the proximal end of the grout column and the load is dissipated quickly at depth.

This concept is shown in the three ELFEN model iterations provided in Figure 38 for Intact Rock Moduli, E = 5GPa, 15GPa, 50GPa. This model indicates how stress is evenly distributed throughout the anchor length in the 5GPa and 15GPa models, however, when the Young's Modulus of the rock is increased to 50GPa the stress is concentrated near the top of the anchor.

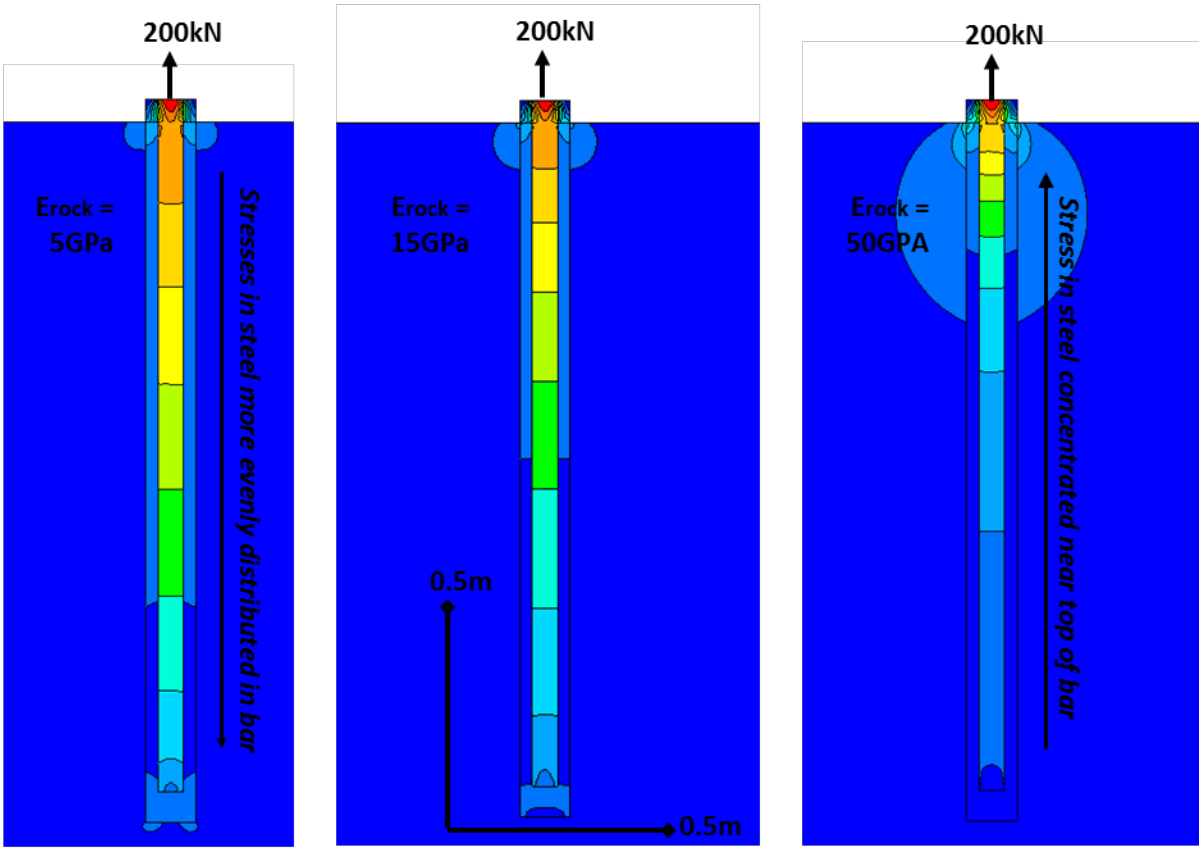

Figure 38– Principal Stress, σ_1, distribution during Elastic loading at Load Step T=2.0sec for Three Different Intact Rock Moduli, E = 5 GPa (left), 15GPa (middle), 50GPa (right);

It should be recognized that in-elastic deformation in the rock may result in changes to the stress distribution in the anchor bar. This is shown in Figure 39 where local de-bonding is noted at the distal end of the anchor. The right hand screenshot shows the development of shear stress in the bar due to this local stress concentration. Below the zone of in-elastic deformation, the stress is evenly distributed in the bar since deformation in the lower rock mass remains uniform and elastic. Figure 40 shows a different model with extensive cracking and in-elastic deformation. This model indicates the Maximum Principal Stress, σ_1, concentration (left) and stress re-distribution following in-elastic deformation and cracking (right). It should be noted that the steel thread bar in the model is elastic and in reality a plasticity cut off should be developed in the constitutive

relationship of the steel. This was not completed since hybrid failure mechanisms (Combined Mode 1 + 4) are not considered part of the scope of this study. In-elastic rock mass failure is discussed in the next section.

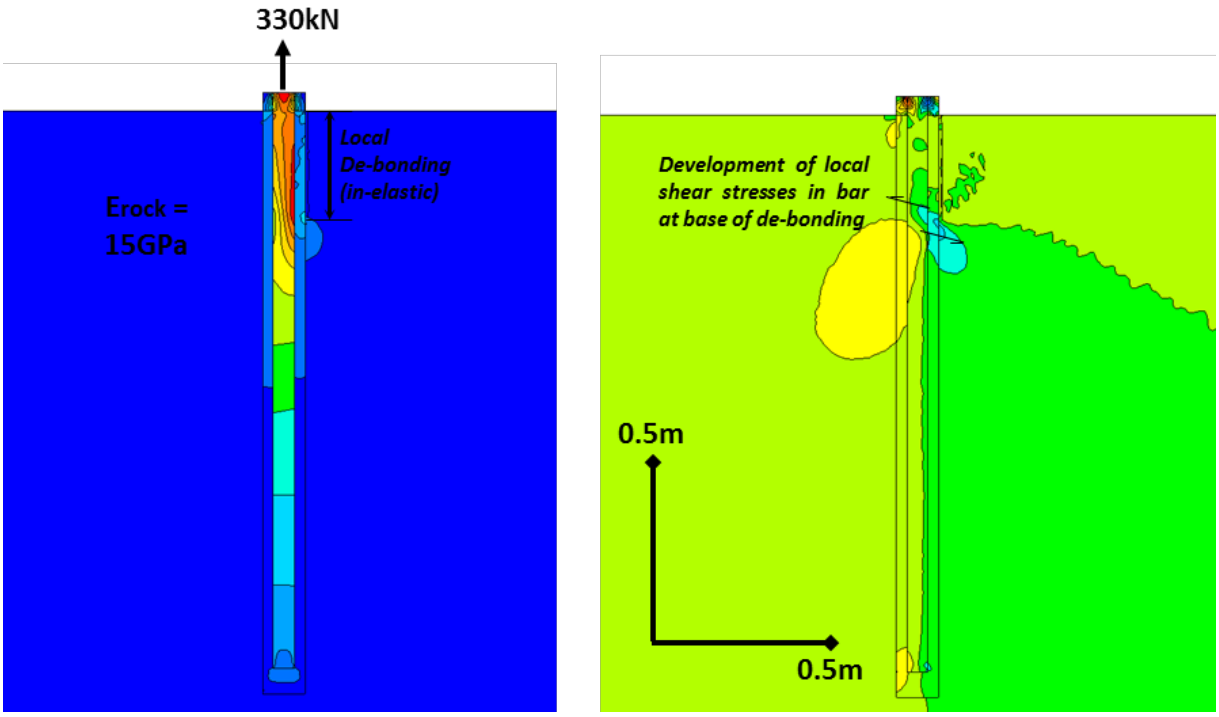

Figure 39– Principal Stress (left), σ_1, and Shear Stress (right), τ, distribution at 330kN Load Step; Model illustrates how de-bonding and in-elastic deformation may influence yielding in Steel Bar

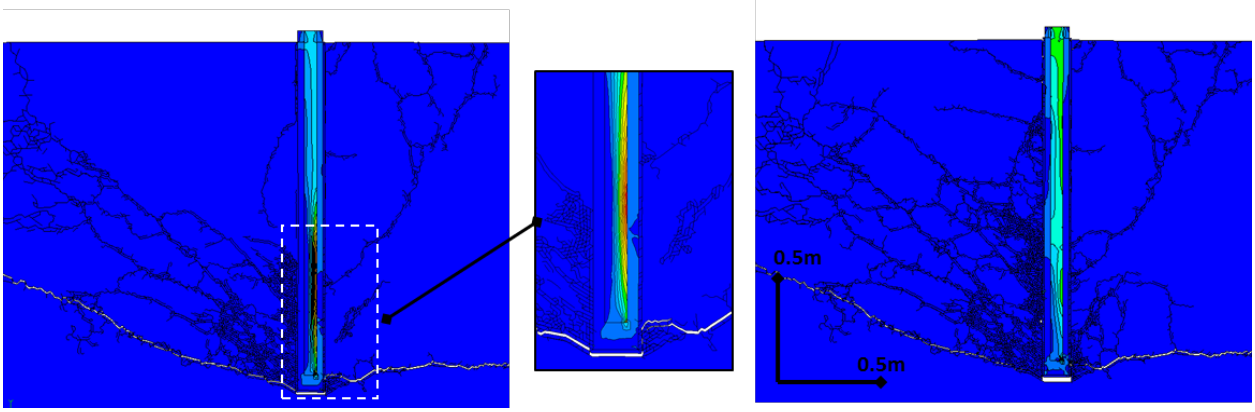

Figure 40– A different model indicating Principal Stress, σ_1, concentration (left) and stress re-distribution following in-elastic deformation and cracking. It should be noted that the steel thread bar in the model is elastic and in reality a plasticity cut off should be developed in the constitutive relationship of the steel. This was not completed since hybrid failure mechanisms (Combined Mode 1 + 4) are not considered part of the scope of this study.

6.4 Results – Crack Initiation, Propagation and Observed Failure Mechanism

The results of the fourteen (14) models presented in Table 2 are analyzed in this section. This included analysis of crack initiation, crack propagation and the dominant failure mechanism for the anchor.

In general crack initiation was observed at 24-44% Ultimate Failure Load in models, with outliers observed at 19%, 49% and 64% where cracks initiated in the rock at the base of the anchor at approximately the same load as the upper bond. With the exception of these outliers, cracking was first observed at the proximal end of the rock-grout interface before damage was observed in the surrounding rock mass. Table 3 presents the results of the 14 model simulations completed for the project. Figure 41 provides a sketch of the idealized failure mechanisms noted in this table. Type 1 and Type 2 failure modes were not possible in models since the steel and grout are modelled as elastic materials, and in general, cracking was observed to be a combination of 5 remaining failure mechanisms provided on this figure.

Crack initiation was analyzed for these five failure mechanisms which can be described as follows:

1) Mode 3 Failure at the Rock Grout Interface; requires initiation of tensile fractures at the proximal end of the bond length.

2) Mode 4.0 Cone Failure Initiating at the Base of the Anchor; requires initiation of tensile fractures at the distal end of the bond length, breakout angle is approximately 90 degrees

3) Mode 4.1 Shallow Cone Failure Initiating at the Base of the Anchor; requires initiation of shallow tensile fractures at the distal end of the bond length, typically fractures are too shallow to reach the surface but this mechanism leads to in-elastic deformation and eventually failure.

4) Mode 4.2 Cone Failure Initiating in the Upper Rock Mass; similar to Mode 4.0 failure, however, this mechanism requires cracks to initiate in upper 2/3 of bond length. This mechanism is described by Weerasinghe and Littlejohn (1997).

5) Model 4.3 Generalized Cracking Failure; cracking occurs along multiple failure surfaces within the area of anticipated 90 degree breakout angle.

The first two models were run with an elastic modulus of 15 GPa and 1.5GP respectively, and both models were run with arbitrary tensile strength and fracture energy estimates of 1.0. Model iteration 1 (15GPa) represents a reasonably low modulus for intact rock strength of a rock mass containing no natural discontinuities.

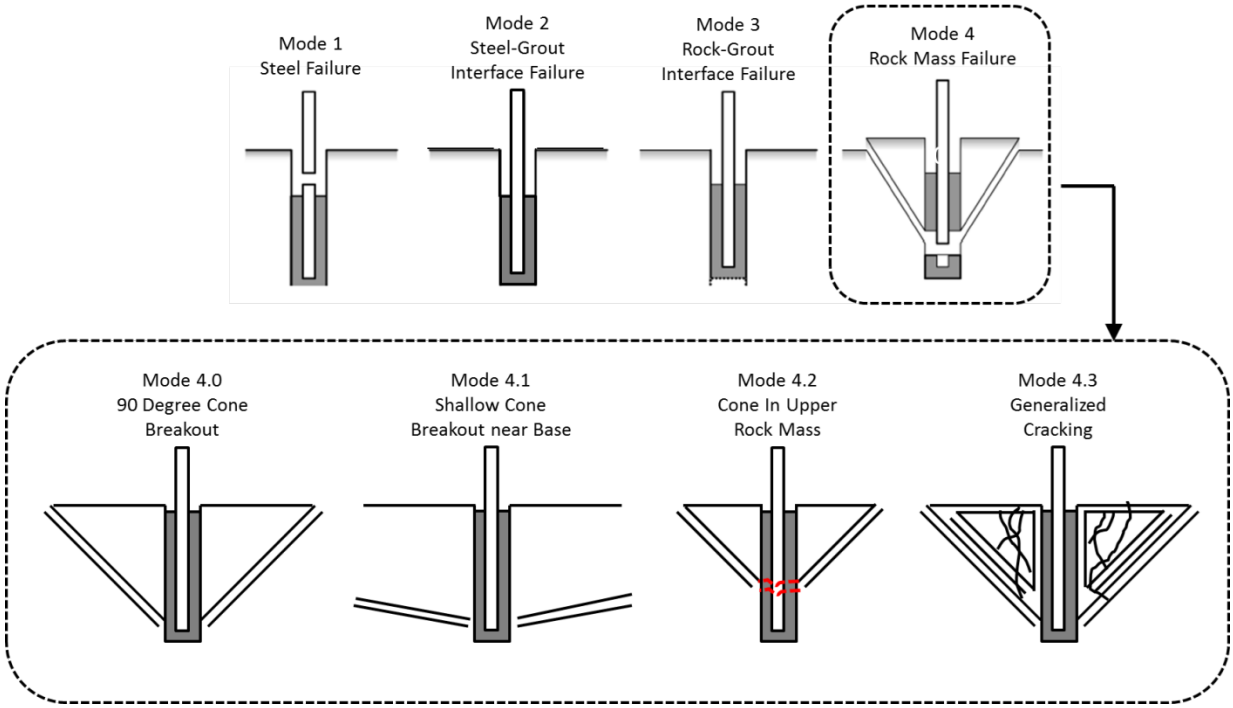

Figure 41– Various failure modes for classification of the cone failure pullout mechanism (Modified after Kim and Lee, 2005 - with Mode 4.0 to 4.3 added)

Figure 42 illustrates how a number of combined failure modes result in in-elastic failure of the rock mass. For Model Simulation 1 described above, in-elastic failure in the model begins with cracking at the proximal end of the rock-grout interface (Mode 3) at approximately 290kN. As this failure mechanism develops with de-bonding, Mode 4.1 tensile failure initiates at the base of the anchor and Mode 4.2 fractures start to develop cone failure in the upper rock mass. As failure develops this series of cracks coalesces, resulting in deformation, however, these cracks do not reach the surface. As the bond fails to the distal end of the anchor, cracks start to initiate at the base of the anchor, but at this time these cracks propagate closer to a breakout angle of 90 degrees (Mode 4.0) failure. These coalescing cracks develop greater than 5mm deformation and cone breakout to the surface at about 1170kN load. Failure develops as slippage along the bond length as well as cracking in the rock mass. The dominant failure mode is noted as Combined 3+4.0 failure since these two failure modes ultimately facilitated failure of the anchor. The cracking observed at failure is shown in Figure 42.

The combined failure mode for Model 1 can be compared to the progressive failure mode observed for Model 2 where model loading steps at 500kN, 780kN, and 1100kN for a model with a much lower Young's Modulus.

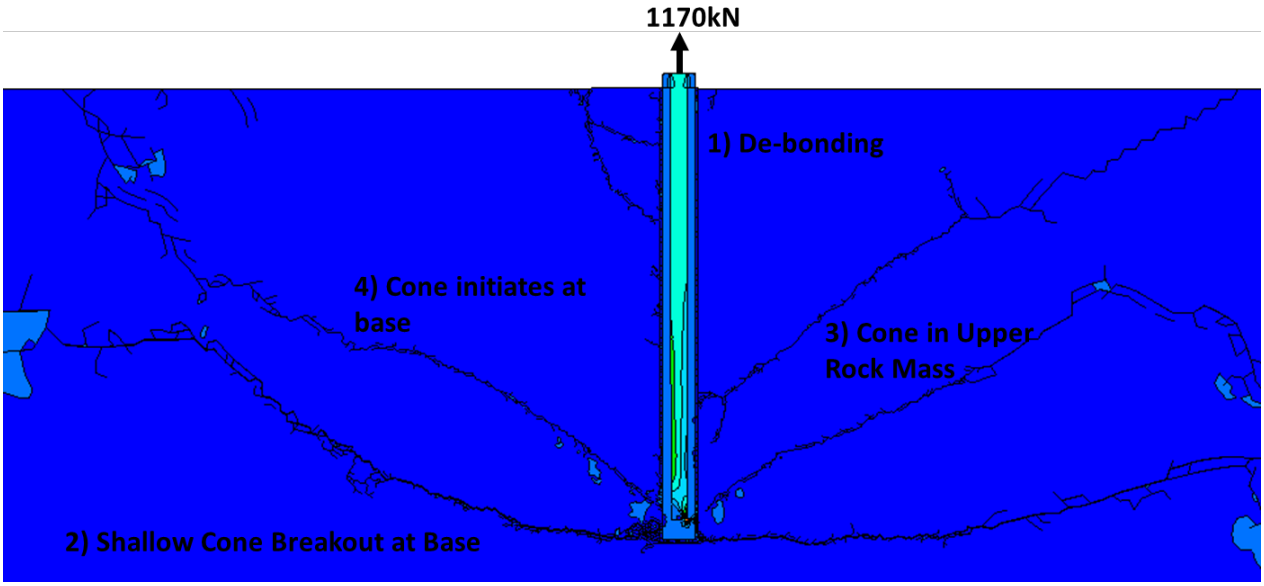

Figure 42– Principal Stress (upper), σ_1 , at 1170kN Load Step of Model 1; Model illustrates how various failure modes may develop independently in E=15GPa rock

The modulus used in Model 2 is considered very low, however, a value this low may be acceptable for very weak rock or to represent a jointed rock mass. In this model, elastic deformation occurs to a load of approximately 500kN. At this load, Mode 3 and Mode 4.1 cracks simultaneously develop along the bond and at the distal end of the anchor respectively. At a load of about 780kN a cone develops in the upper rock mass (Mode 4.2) and the shape of this cone is very similar to the failure mechanism observed by Weerasinghe and Littlejohn (1997). At this load, the upper rock mass has experienced greater than 5mm deformation and the failed bond and upper cone have formed a path of damage that extends to the surface, however, the anchor has not yet pulled out of the ground. This result begs the question as to what is the limit state of failure of an anchor. For the purposes of this assessment, failure is noted at 780kN, however, if load is continued to be applied to the anchor dilation continues and generalized cracking (Mode 4.3) failure is observed to initiate at a load of 1100kN where global failure of the rock mass is observed. These first two models (Model 1 and Model 2) were run with arbitrary fracture energy and tensile strength values both set to 1.0 respectively. The remaining models were run with the energy parameters calculated using the of mode I fracture toughness (K_{IC}) a term that is related to the tensile strength by $\sigma_t=6.88K_{IC}$ (Elmo,

2006; Zhang, 2012; Hamdi, 2015). These results are also summarized in Table 3 and described below.

Table 3. Observed Failure Mechanisms in ELFEN models

	Initiation of De-bonding, - Mode 3 - Failure (kN)	Initiation of Mode 4 Rock Mass Failure (kN)				Failure Load and Mechanism	
		90 Deg Cone Breakout at Base, - Mode 4.0 -	Shallow Cone Breakout Near Base - Mode 4.1 -	Cone in Upper Rock Mass - Mode 4.2 -	Generalized / Secondary Cracking - Mode 4.3 -	Dominant Mechanism	Load (kN)
1	285	1036	532	456		Combined Mode 3+4.0	1174
2	500	974*	500	777	974*	Combined Mode 3 + 4.2 + 4.3	777
3	326	979	497	570		Combined Mode 3+4.0	979
4	599	1425*	599		1425*	Combined Mode 3+ Mode 4.1	1220**
5a	247	-	247		1140	Combined Mode 3+ Mode 4.3	1288
5b	1244	1066	-			Minor Mode 3 + Mode 4.0 Cracking at 1100kN	No Failure Observed in Model
6	428	-	-	1209		Minor Mode 3 + Mode 4.2 Cracking at 1100kN	No Failure Observed in Model
7	569	1385	-	-	-	Minor Mode 3 + Mode 4.0 Cracking at 1100kN	No Failure Observed in Model
8	746	1316	-	-	-	Minor Mode 3 + Mode 4.0 Cracking at 1100kN	No Failure Observed in Model
9	390	-	532	570	1066*	Combined Mode 4.1 + 4.2	998**
10	299	-	320	355	718*	Combined Mode 3+4.1+4.2	678
11	228	-	228	249	674*	Combined Mode 3+4.1+4.2	649
13	299	707	320	374	-	Combined Mode 3+4.0+4.2	775
14	228	1036	247	355	-	Combined Mode 3+4.0	617

**Mechanism was observed after 5mm displacement in upper rock mass*

***Dominant mechanism is noted at 5mm displacement in upper rock mass; This mechanism achieved at 5mm displacement without discrete cracks connecting with surface (including Mode 3.0, bond failure cracks) since deformation is driven in part by the low modulus of elasticity of the rock;*

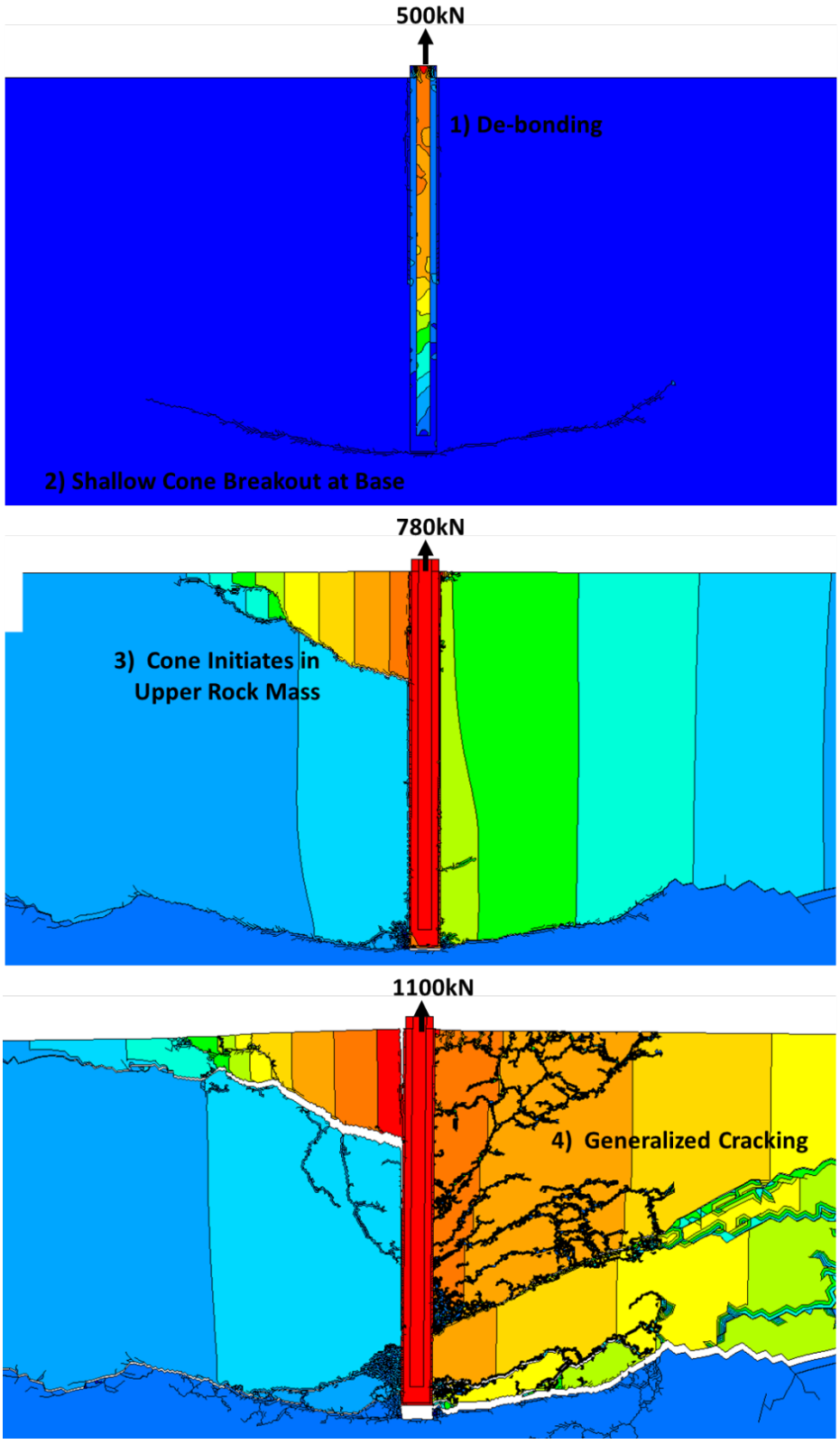

Figure 43– Principal Stress (upper), σ_1, at 500kN load step, and Vertical Displacement at 780kN (middle) and 1100kN (Lower) Load Steps of Model 2, comprising a Young's Modulus, E=1.5GPa rock mass

As shown in Table 2 and Table 3, Model 3 was run with the same elastic moduli, Mohr-Coulomb cohesion and friction angle, and tensile strength as Model 1. However, in this model the fracture energy parameter was calculated to be 1.4 which is slightly higher than the arbitrary value of 1.0 selected in the previous model run. As noted in Table 3, this change in fracture energy changes the development of failure in the rock mass. Similar to Model 1, cracking initiates with Mode 3 failure of the bond, however, this failure is followed by shallow cone failure at the base of the anchor (Mode 4.1) before a cone develops in the upper rock mass at 570kN. Ultimate failure of the anchor is observed at a load of about 980kN which is about 200kN less than that of Model 1. This illustrates the importance of calibration of all of the fracture energy parameters in the model. Similarly, Figure 45 provides a comparison of cracking observed in two different model iterations (Model 5b and Model 6) with the same fracture energy parameters but vastly different Young's Moduli of 1.5GPa and 50GPa respectively. Tensile strength and Fracture Energy were calculated to be 3.8 and 3.0 for the 50GPa rock mass and these values were arbitrarily used for the 1.5GPa rock mass. Failure was not observed in either of these models, however, crack development is shown for the 1425kN load step in Figure 44. The lower modulus in the left hand figure transfers the rock load deeper into the rock mass during elastic unloading. This allows for stress to develop at the distal end of the anchor (Mode 4.0 failure initiation). Alternatively, the right hand screenshot show crack development for the 50GPa modulus where cracking is observed along the bond (Mode 3) and in the upper rock mass (Mode 4.2). Furthermore, the stress concentrations in this model suggest a different location for Mode 1 Steel failure in the threadbar.

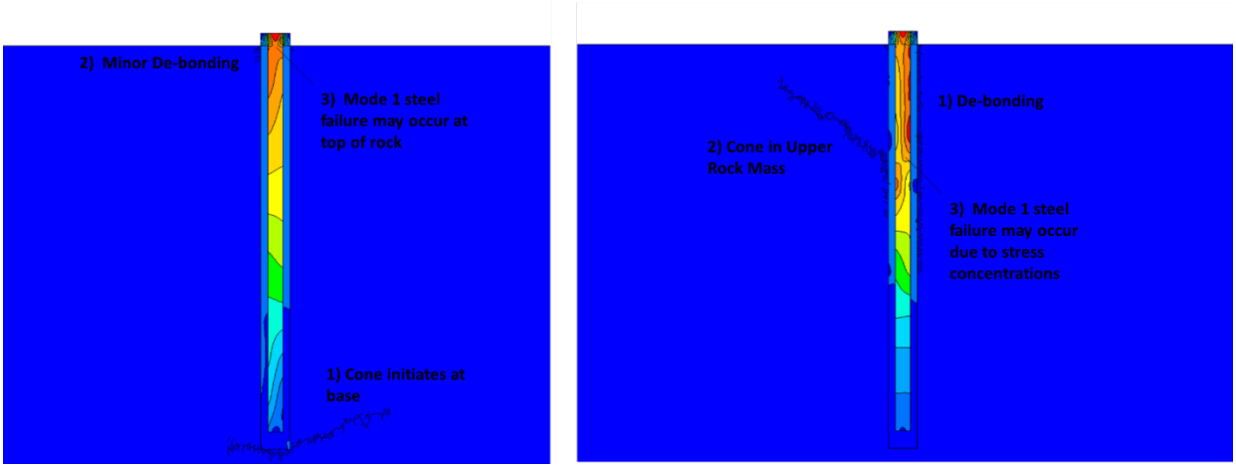

Figure 44– A comparison between 1425kN load steps for Model 5b and Model 6. Both models comprise the same fracture energy and tensile strength however, the left have screenshot was given a Young's Modulus, E = 1.5GPa and the right hand screenshot was given an E = 50GPa representing intact rock. The failure mode noted for each simulation varies depending on the stiffness of the rock.

The left hand screenshot shows stress concentrations at the proximal end of the anchor at the top of rock, while the right hand screenshot indicates that failure may occur at the base of the cone in the upper rock mass. Future models which consider plasticity of the steel anchor could be used to assess hybrid Model 1 and rock mass failure mechanisms near the yield strength of the bar of 1425kN for 517/690MPa steel.

The models noted above described the importance of all of the Rotating Crack (Rankine) failure parameters in model simulations. In reality, arbitrary values for this parameters will not be set in design. Figure 45 and Figure 46 provide a more realistic comparison of two different models run with the same Mohr-Coulomb parameters but representative Rotating Crack (Rankine) failure parameters that reflect the anticipated nature of the rock. The first model (Model 7) was run with E=30GPa, σ_t=3.0MPa and a calculated fracture energy of 6.3. This is compared to the second model (Model 11) which was run with E=3GPa, σ_t=0.3MPa and a calculated fracture energy of 0.6. Cracking is observed to be concentrated along the bond of the anchor in Model 7 and with a dominant Mode 3 failure mechanism developing until 1320kN where Mode 4.0 failure develops at the end of the anchor. This is very different to Model 11 where generalized cracking is observed in the rock mass at a load of 590kN and ultimate failure of the rock mass occurs at 715kN. It is anticipated that the steel will failure before the rock in Model 7, however, even if Grade 75 (517/690MPa) steel is used in Model 11 the yield strength of the steel should not be exceeded and the bar will fail as a combination of tensile breakout or generalized cracking within the area of the envisaged pullout cone (Mode 4.3 failure) and by means of bond slippage (Mode 3).

All of the models in this section were run using a continuum with no joints to reflect the nature of cracking in the rock mass based on adjustment of the Rotating Crack failure parameters (noteably E, σ_t, G_F). In reality, these models should be run with representative intact rock parameters and joints in the mesh domain, similar to Chapter 5. However, the sensitivity analysis completed has shown that various failure mechanism can be achieved by adjusting these parameters. This provides confidence that a variety of field observations of damage patterns can be modelled in ELFEN in the future, however, significantly more in-situ testing is required.

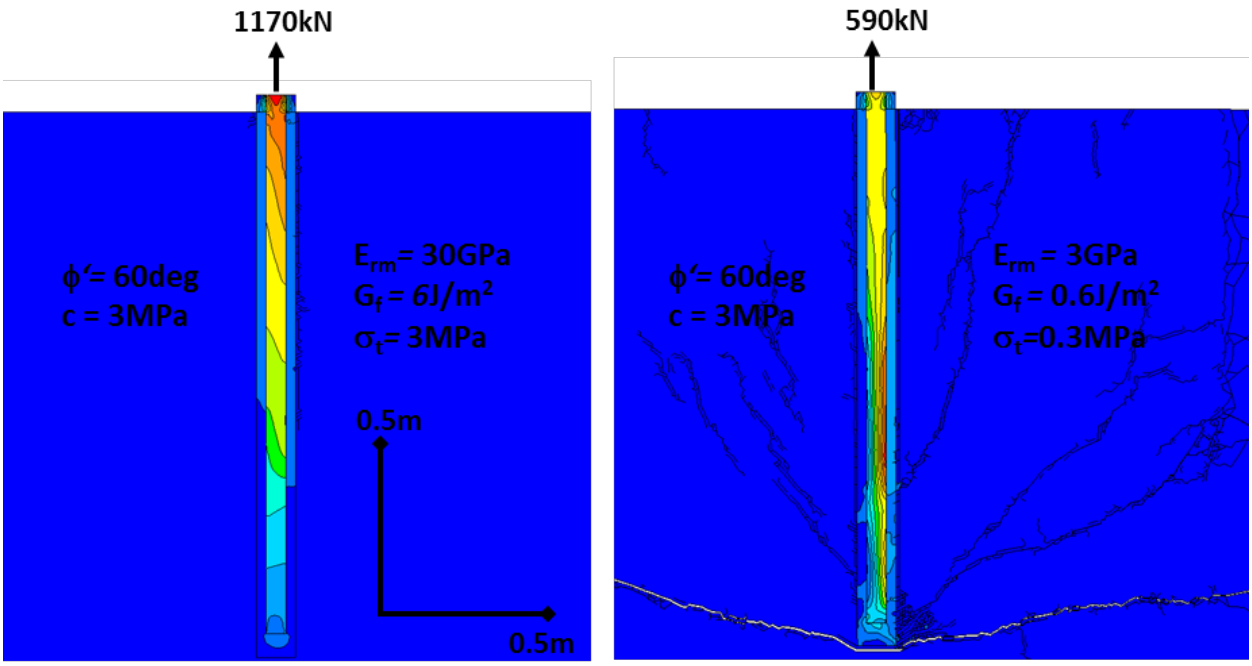

Figure 45– Observed Variation in Rock Mass Damage with varying Rotating Crack / Rankine Failure Parameters and Constant Mohr-Coulomb Friction Angle and Cohesion; Model 7 (left) and Model 11 (right) comprise different failure mechanisms based on these parameters;

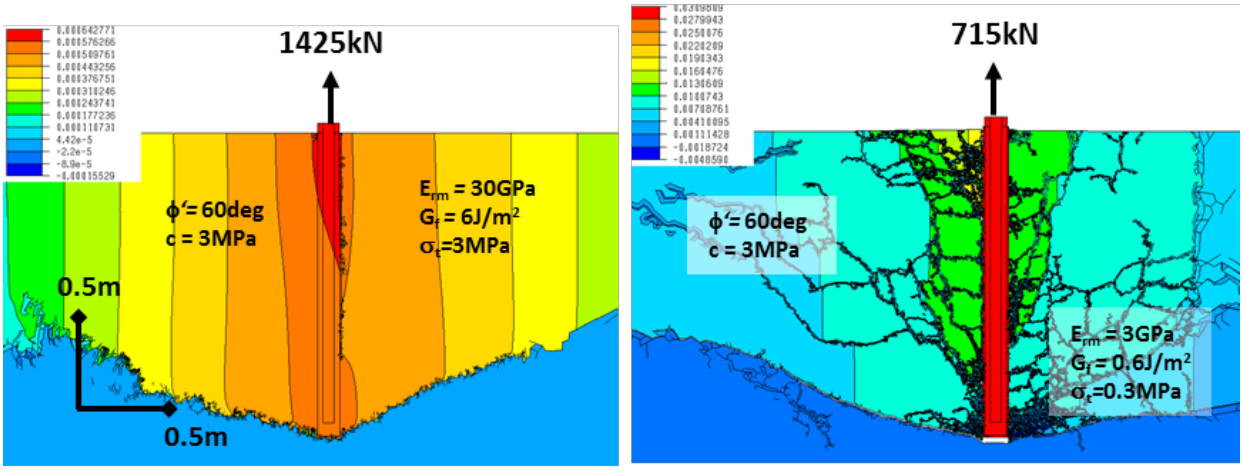

Figure 46– Observed Rock Mass Damage and Dilation at Final Load Steps (1425kN and 715kN) for two models with varying Rotating Crack / Rankine Failure Parameters and Constant Mohr-Coulomb Friction Angle and Cohesion;

***Note**: See Figure 45 for pre-failure crack propagation*

6.7 Discussion and Summary

The models presented in this section illustrated the initiation and progressive development of fractures in a continuum model for various ranges of loading. All of the models in this section were run using a continuum with no joints to reflect the nature of cracking in the rock mass based on adjustment of the Rotating Crack failure parameters (noteably E, σ_t, G_F). The sensitivity analysis completed has shown that various failure mechanism can be achieved by adjusting these parameters, and that failure of the rock mass is progressive, even within massive rock with no joints.

Carter (1995) completing testing in weak, structureless sandstone using a full scale apparatus on a 1.5m embedment anchor. Pre-failure deformation was noted in the sandstone with a radius of dilation of about 1.5m radius for the 1.5m anchor depth. Although global failure was not observed in this test, irrecoverable dilation or plastic deformation was observed around an anchor load of 200kN. The design capacity of the 25mm bars used by Carter is approximately 210kN and the bar snapped before the rock mass could develop to failure. Had a 44mm, high grade steel bar been used for the test, it is possible that the rock mass could have been taken further into the in-elastic range to ultimate failure. In reality, tensile fracturing processes between natural fractures in the rock, progressive rock mass failure, and deformation-induced softening behavior are important considerations in assessment of 'rock cone' pullout. While the results in this section prove to be interesting, to push the limits of engineering design the failure mechanism associated with failure and tensile crack initiation at low confinement need to be better understood both in massive and jointed rock masses.

This Chapter has illustrated that that one small change in a numerical model, such as the elastic modulus, E, can have implications on the tensile fracturing behaviour surrounding an anchor. This illustrates the importance of calibration. For the low stiffness model (1.5GPa) the serviceability of the anchor may not be the same as the stiffer model (15GPa or 50GPa) at similar loads, since cracking of the upper rock mass may occur which is very different to local de-bonding at the rock-grout interface. Furthermore, this Chapter also introduced the Rotating Crack / Rankine Failure Parameters which can be used to model tensile cracking in the same model domain as shear behaviour modelled with traditional Mohr-Coulomb friction angle and cohesion. The parameters used in the model were based on empirical correlations based on observed tensile cracks induced in a compressive stress field. It is possible that in a tensile loading scenario, in situations of low confinement, the tensile cracking behaviour may require new empirical relationships to be

developed for fracture energy and tensile strength cut off. Future work should include full scale testing to assess the specific influence of tensile strength and the Hoek-Brown mi parameter on the potential failure modes of anchors. It is envisaged that in very weak and in brittle rock, tensile and shear breakout may occur well within expected volume of rock predicted using the pullout cone approach.

Furthermore, it is also envisaged that where discrete blocks are mobilized with dilation of the upper rock mass, hybrid rock mass-bond failure (combined Mode 1, Mode 3 and Mode 4 failures identified by Brown (2015) and Brown et al (2015)) and combined inelastic deformation along both the rock-grout interface and within the rock mass may be a more feasible mechanism than simple cone pullout. The work by Bruce (1976) on shallow anchors in "strong, slabby" sandstone showed failure from the bottom of the fixed anchor, whereas, the work by Weerasighe and Littlejohn (1997) noted an active cone in the upper part of a "fissile" mudstone rock mass. This suggests that the failure mechanism, distribution of shear and tensile fracturing and load transfer are highly dependent not only on fracture statistics, but also, on intact rock properties. This concept was illustrated in this section.

While the work in this section was completed in a continuum mesh, it should be recognized that in jointed rock masses the orientation of naturally occurring fractures should be inserted into the model. The use of joints in numerical models can induce stress rotations and modulus "softening" in the model, which may reduce boundary affects and influences the failure mechanism observed. This is shown in Figure 47 where deformation and damage is observed to be progressive and controlled by pre-existing fractures. The persistent joint in the upper rock mass to the right of the anchor firstly facilitates elastic deformation perpendicular to this feature in the upper rock mass (1). As the load increases, cracking of the small rock bridge at the top of this joint occurs and the anchor load is transferred deeper in the rock mass (2) and facilitates cracking at the base of the anchor (3). As the load is increased further, stress rotations in the rock mass lead to de-bonding or cracking at the rock-grout interface (4).

This mechanism is very different than that which would have been expected in a continuum model, and had the proximity of joints been different that those shown in Figure 47 a different failure mechanism may have been observed. This illustrates the conclusions from Chapter 5 that multiple realizations of jointing are required when modelling brittle fracture in jointed rock masses.

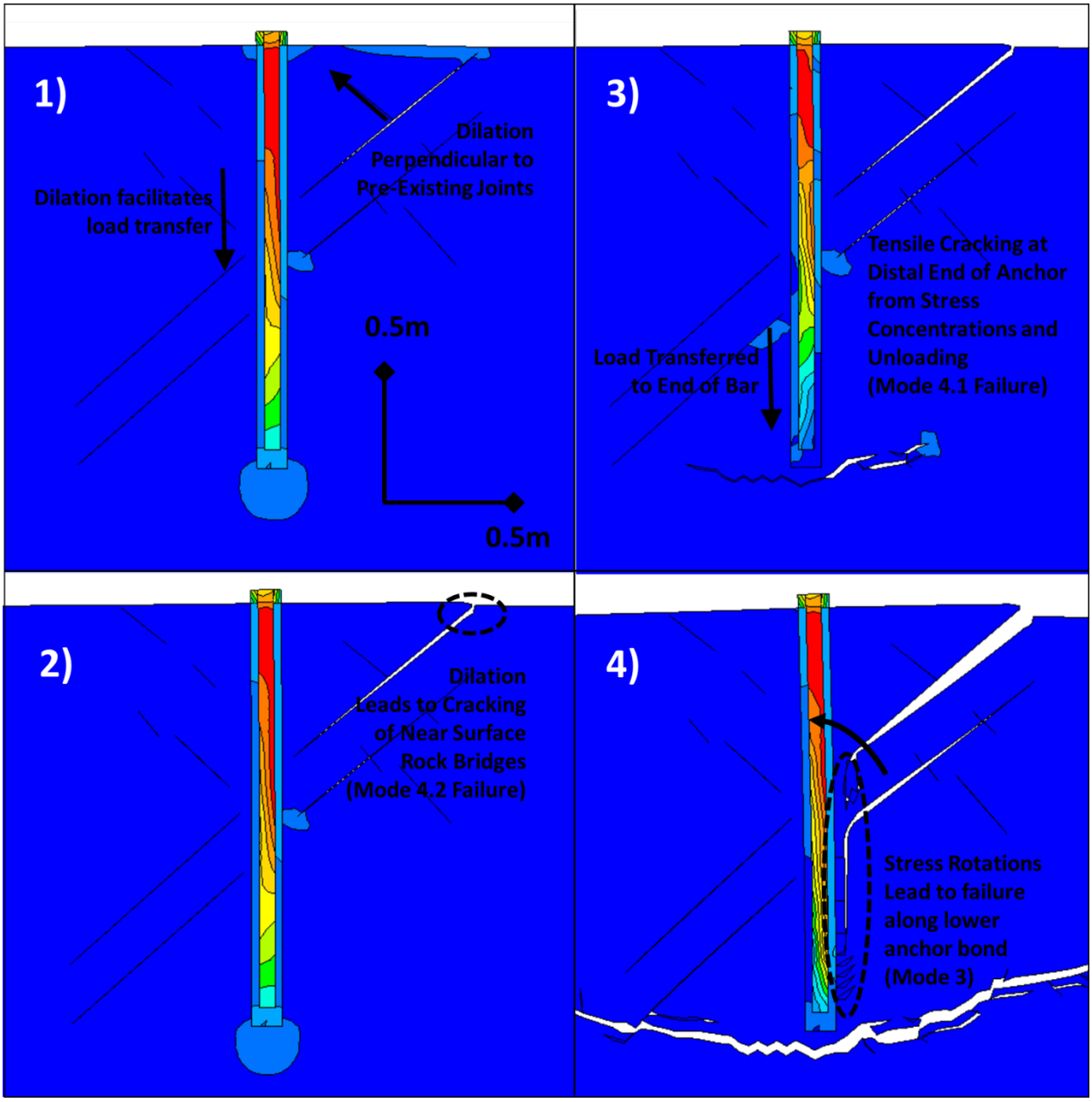

Figure 47– Influence of Pre-Existing Joints on the Failure Mechanism observed in ELFEN

7 Three-Dimensional Analysis

This Chapter (Chapter 7) presents the analysis of the cone pullout mechanism in three dimensions. The previous chapters identified the feasibility of two dimensional numerical simulations using an assumed softening criteria in a jointed rock mass (Chapter 5) and an alternative fracture energy based hybrid FEM-DEM method (Chapter 6) used to analyze of damage in intact rock. While the results from these sections proved to be interesting, each come with the caveat that in-situ testing is required for incorporation of these numerical methods in design. The same caveat applies to this section, however, for completeness the feasibility of numerical modelling of the cone pullout mechanism is also investigated in 3D.

7.1 Fracman Analysis of Removable Blocks

Chapter 5 illustrated that the capacity of the anchor may be dependent on the interconnectedness of the rock mass. This is no different in three dimensional space, where three or four intersecting joints sets may form a fully removable block within a proposed area of anchorage. If the joints are fully interconnected with no rock bridges, and the joint orientation is such that the fractures do not provide frictional resistance against block removal, the dead weight of the wedge may be the only viable resistance to pullout and external loading on an anchor. The failure mechanism in this case is different than most of the simulations in the previous sections, and the capacity provided by a dead weight block is not very different than that assumed in the "dead weight cone" assumption in the standard of practice.

Analysis of the resistance provided by or the stability of a removable block does not require sophisticated geo-mechanical numerical analysis, and the resisting forces can be analyzed using graphical, CAD-based, limit equilibrium methods. However, in order to determine the likelihood of forming a removable block across a sample foundations, an analysis rock mass interconnectedness was completed in Fracman 7 by Golder Associates. Using Fracman, a screening level check and be completed to assess the likelihood of removable blocks in the upper rock mass prior to completing more sophisticated three dimensional anchor simulations which consider the contribution of joints and intact rock to the pullout simulation.

The depth of the apex of a removable wedge and the "dead weight" of this wedge are two important considerations in the design of anchors. To illustrate this point, a four joint set network was generated in Fracman which is illustrated in Figure 48 below. The upper left screenshot of Figure 49 indicates how blocks are formed between joints in this model and the upper right screenshots

shows the same blocks without a graphical representation of the three dimensional fracture in the model. An important consideration shown on this figure is the depth of the apex of the block forming joints below the ground surface. It is important that the designed free stressing length for anchors extends beyond unfavourable persistent structural features that are present in the rock mass to generate confinement and avoid deformation in the upper rock mass during loading. In three dimensional space, the apex of the wedge formed by a discrete block in a DFN model may help define the length of the free stressing length in design. Measurement of this parameter is shown in the lower screenshot in Figure 49, along with a visual representation of the bonded and free stressing length of an anchor.

The likelihood of formation of a discrete removable block within an area of anchorage was assessed in more detail by extending the four joint set fracture network across a 50m x 200m area of anchorage in Fracman, as shown in Figure 48.

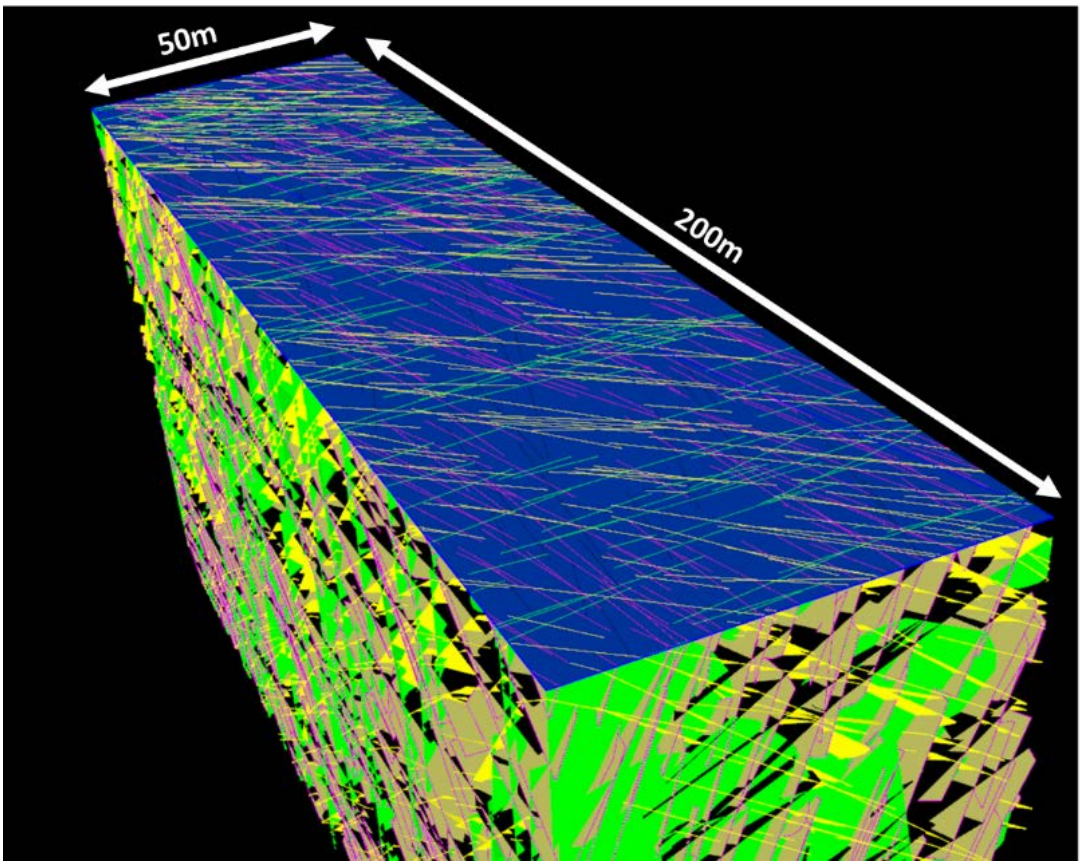

Figure 48 – Fracman Screenshots illustrating fracture traces on the 50m x 200m sample foundation area

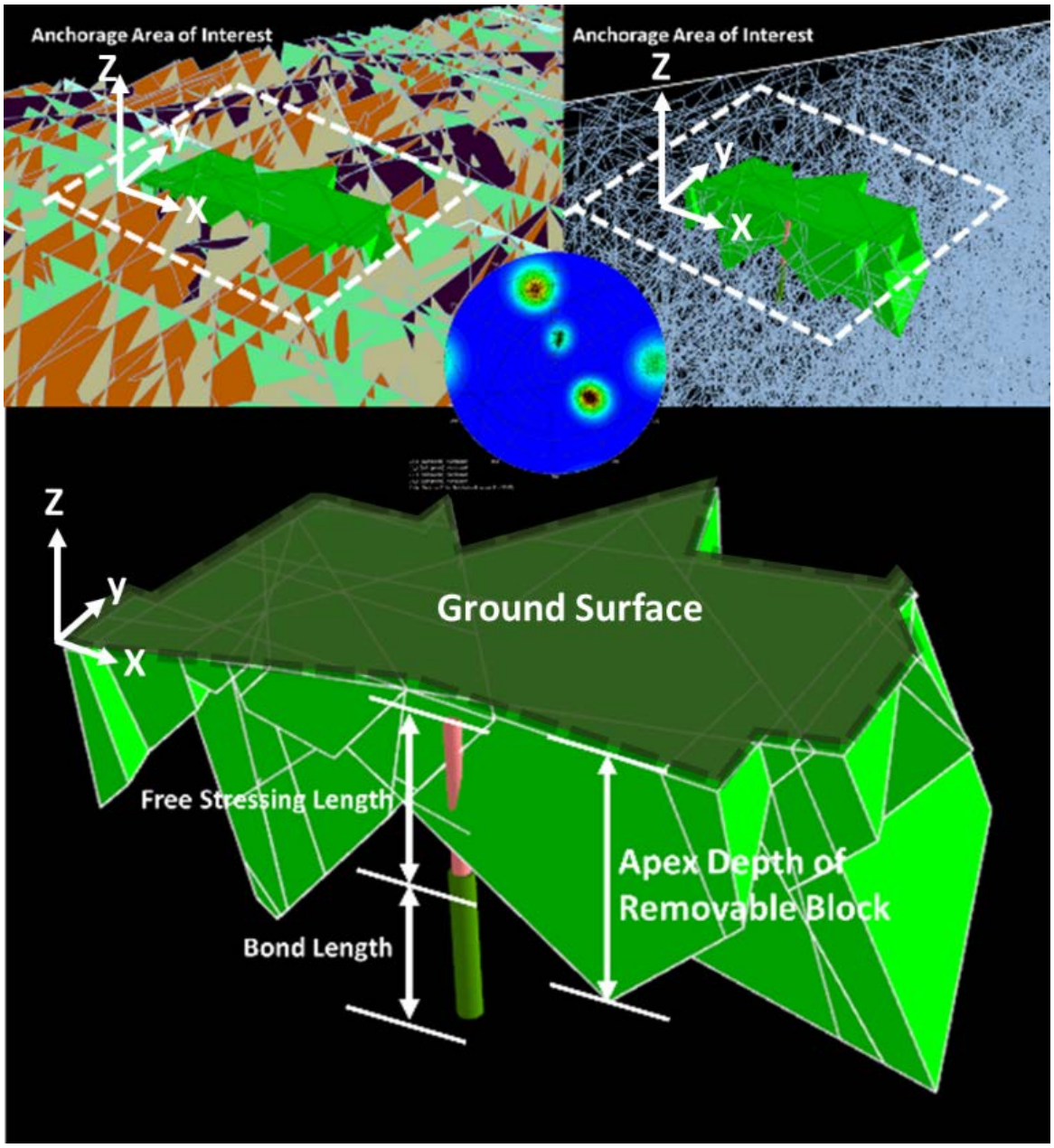

Figure 49 – A Fracman screenshot showing formation of removable blocks within a foundation area.

For the Fracman assessment, two different DFN's were generated with similar statistics for fracture orientation (shown in Figure 49), termination and intensity (P32), but different fracture radius distributions. It was assumed that the fracture patterns both followed an exponential distribution, however, the mean fracture radius for DFN1 and DFN2 were given as 10m and 20m respectively, with a maximum fracture length cut off of 20m and 40m. Fracture intensity was observed to be an important parameter in the two dimensional anchor simulations presented in Chapter 5 since this

parameter provides an indication of the interconnectedness of the rock mass. P21 or P32 is a measure of the fracture intensity over an area or volume and as this intensity increases the size and distribution of intact rock bridges generally decreases accordingly. However, when assessing the formation of discrete blocks and the depth of the apex of these block within an area of anchorage, it is contended that the fracture length or radius distributions in the model also may have a significant influence on the formation of these blocks. For this reason the P32 is left constant and ranged from 0.86 to 2.36 (due to spatial variability across the DFN domain) with an average of about 1.4 for both DFN's, despite different radius distributions. Five fracture network realizations were run to generate the distribution of blocks across the area of anchorage. As a secondary check, the P21 was also calculated across the area of anchorage for the five DFN realizations produced for both DFN1 and DFN2 and the average P21 was calculated to be 1.1. The fracture trace distributions for one realization from each DFN is provided in Figure 50. The left hand chart (labelled A.1) indicates the fracture trace distribution for DFN1 and the right hand chart (labelled B.1) indicates the distribution for one realization of DFN2.

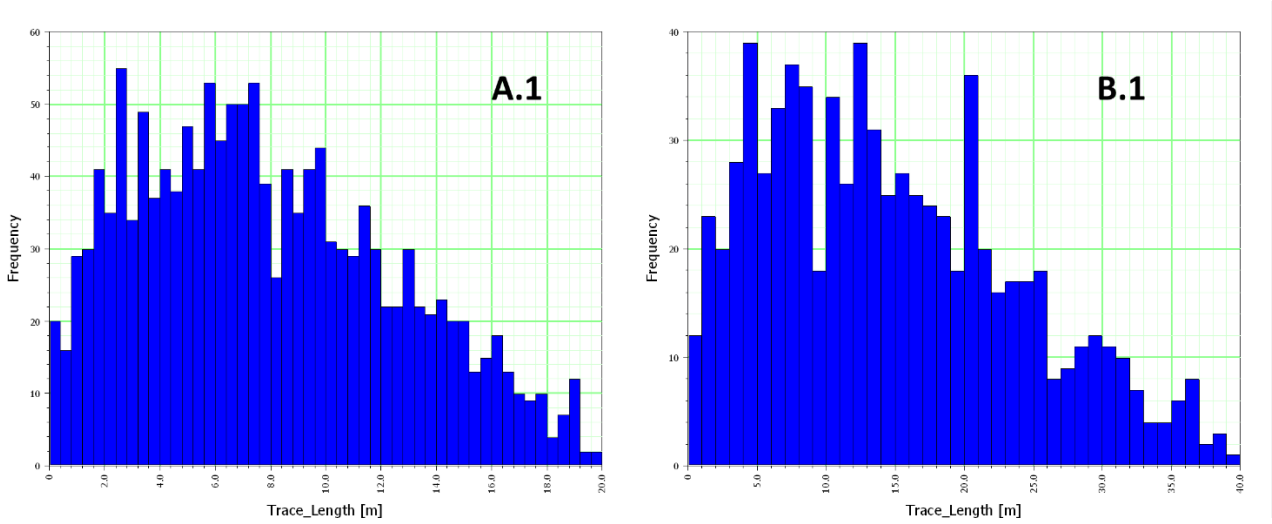

Figure 50 – A comparison between P21 fracture trace distributions for one realization of DFN1 (left-A.1) compared to that of DFN2 (right – B.1)

After five realizations were completed for each DFN fracture trace statistics and the distribution of removable blocks was assessed. Figure 51 provides a comparison of the weight of removable wedges for a given apex depth to curves produced based on recommendations by Littlejohn and Bruce. The authors recommend note that the typical designer considers the resistance provided by a cone initiation point at a depth of about 0.5-1.0 down the bonded length (BL) of an anchor. Cone breakout angles between 60-90 degrees are generally assumed at the base of the cone. These

assumptions are described in more detail in Chapter 3. Figure 51 provides a number of curves using these design assumptions. The uppermost curve being a 60 degree cone breakout angle imitating at 0.5xBL and the lowermost curve being a 90 degree cone breakout angle initiating at 1.0xBL. The point data plotted on this curve is the weight of the discrete wedges formed with the ground surface in the DFN realization on the x-axis, plotted against the apex depth for each removable wedge formed within the area of anchorage. The red points indicate individual wedges formed in the area of anchorage from the five realizations of DFN1 and the gray points indicate the wedges formed from the five realizations of DFN2. The "Weight of the Removable Wedge" should not be confused with the capacity of a given anchor since the anchor capacity may depend on friction developed by the normal force associated with sliding along joints, if this is a consideration for the structural geology at the site (i.e. dilation of sub vertical joints). It is apparent from this curve that the "dead weight" cone assumption does not consider the joint frictional or intact rock strength across a foundation. However, this type of curve can be used to assess the free stressing length requirements to achieve a desired bond length beyond removable blocks within a foundation.

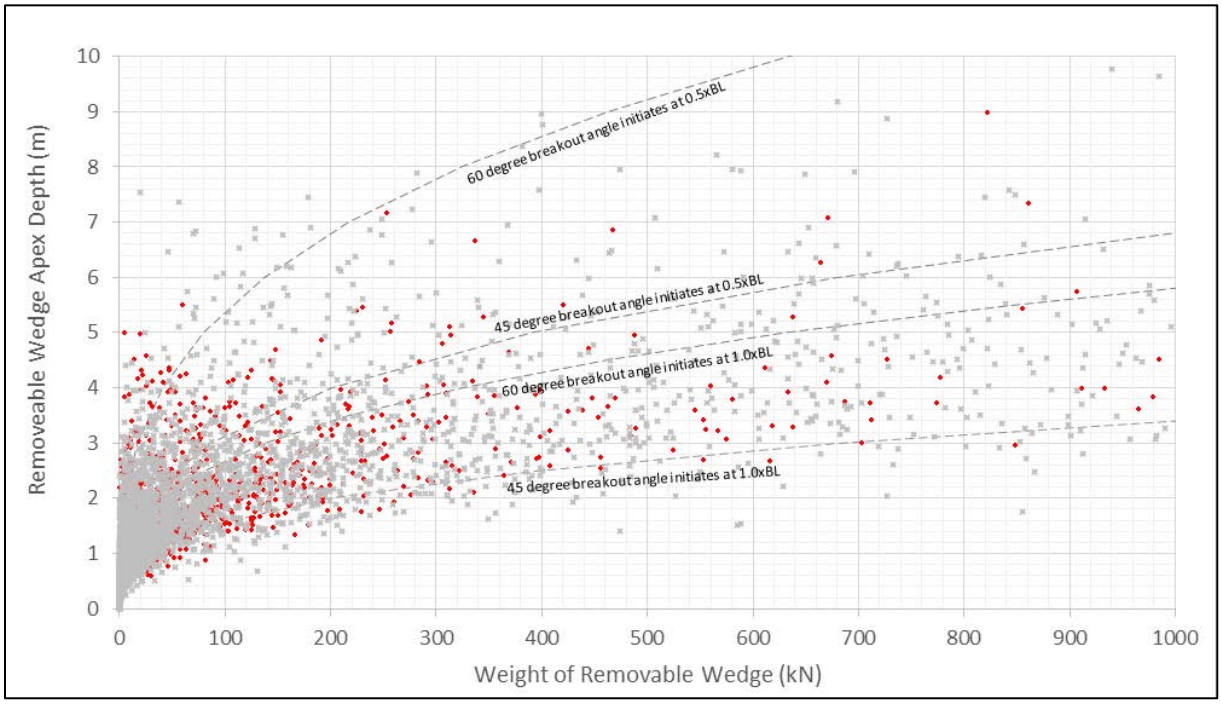

Figure 51 – A comparison of the weight of removable wedges for a given apex depth to curves produced based on recommendations by Littlejohn and Bruce.

The dead weight cone approach or assessment of removable blocks is one method which may be used to assess the required anchor lengths across a foundation and this method may be the most appropriate, and suitably conservative, depending on the risk tolerance and nature of the project.

If tensile strength is to be provided on the pullout area of the cone, the likelihood of encountering a removable block should be understood across the foundation area. As a starting point in the assessment of the contribution of intact rock in the design of anchors, the probability of encountering a removable block in the area of foundation anchorage can be considered. Figure 52 provides comparison between the distribution of removable blocks for one realization of DFN1 (A.2, A.3) and one realization from DFN2 (B.2, B.3). As noted above the P21 or fracture intensity on the trace plane shown in blue is 1.1 for both DFN's, however, the joint lengths used to develop this fracture intensity are longer in DFN2. This means that the intensity in DFN1 is developed by shorter joints, with more intact rock bridges, however, more small joints are required to develop the fracture intensity observed at the surface. In DFN2, less joints are present but these jints are longer and potentially more connected. As a result, the probability of encountering a wedge in the 50mx200m area of anchorage is between 33-43% for the five realization completed for the DFN2 statistics compared to 7-10% for the five realizations with DFN1.

The distribution of removable blocks and the probability of encountering a discrete block may be assessed using DFN based methods, however, it is up to the designer as to the level of risk that should be taken in the design. This may be based on how flexible the location of the foundation is or alternatively the size of the footprint. If changes can be easily made during design, the contribution of intact rock over a portion of the foundation may be considered, as described in the two dimensional simulations provided in Chapter 5.

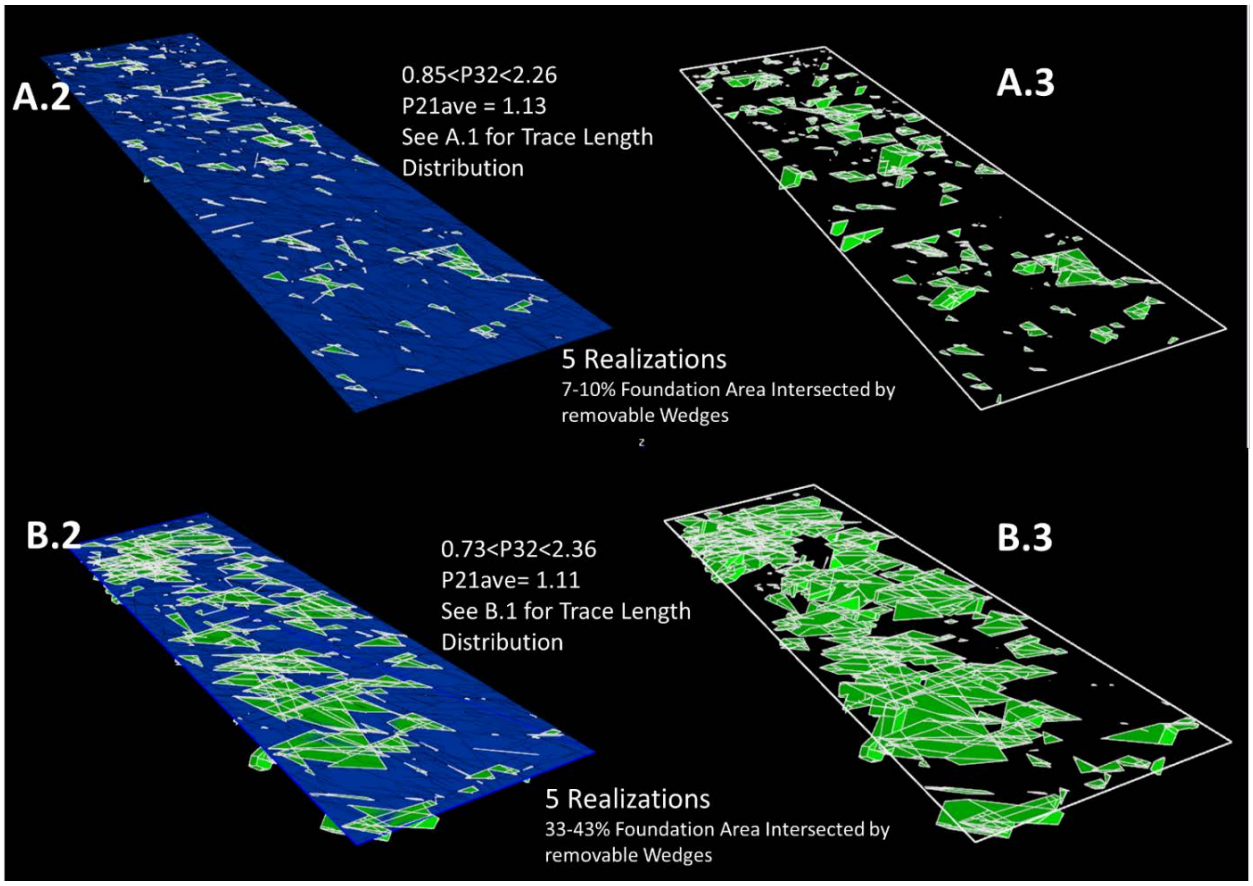

Figure 52 – A comparison between the distribution of removable blocks for one realization of DFN1 (A.2, A.3) and one realization from DFN2 (B.2, B.3)

7.2 Discussing the Challenges with 3D Simulation of Anchor Pullout

For completeness, geo-mechanical analysis of the cone pullout problem is also completed for this chapter in 3D. It is well understood that the cone pullout problem is 3 dimensional in nature, however, in Chapter 5 it is contended that cross sections cut perpendicular to stability controlling joint sets can be used to analyse the pullout failure mechanism in an efficient (quicker) manner. Furthermore, it is considered essential that the tensile fracture processes between joints can be simulated in the numerical model. This requires a very fine mesh between fractures (in some cases 1 cm element length) and most 3D models cannot accommodate this scale of meshing over a large area. However, numerical models do not have to be an exact representation of geology, since the purpose of a model is to simulate the behaviour of the rock mass.

The use of the 3dimensional discontinuum methods is common in the design and safety assessment of large arch dam foundations on rock. The first dam foundation failure through rock occurred in

1959, and since this failure three dimensional block models that consider sliding on rock discontinuities in 3D have been standard practice in dam design. Lemos, 2012 provides a review of dam foundation failure analysis in the context of discontinuum models. Figure 53 provides an example from the paper by Lemos where simplifying assumptions are made to represent the rock mass as a series of discrete blocks. Lemos notes that typically in a dam foundation there are a number of persistent faults or features with known intersection locations. These dicrete features can be input into the discontinuum model. Lemos notes that "*the purpose of the analysis directs the selection of the number and location of joints, as the intention is not to recreate in detail the joint structure, but to identify the possible failure modes and their likelihood*". This scale which is typically considered for a dam global stability model is provided in the 3DEC screenshots from Lemos (2012) in Figure 53. Global stability of a large structure is generally a concern is a discrete block is formed within the foundation area. Simplification of the site geology into a number of persistent, water bearing geological feature is a very appropriate method for conducting a coupled hydro-mechanical static or seismic stability analysis of a foundation. However, when it comes to brittle fracture of a short 2m embedment dowel or a 30-50m length anchor it is contended that a smaller scale block size is required to properly assess the resistance to failure.

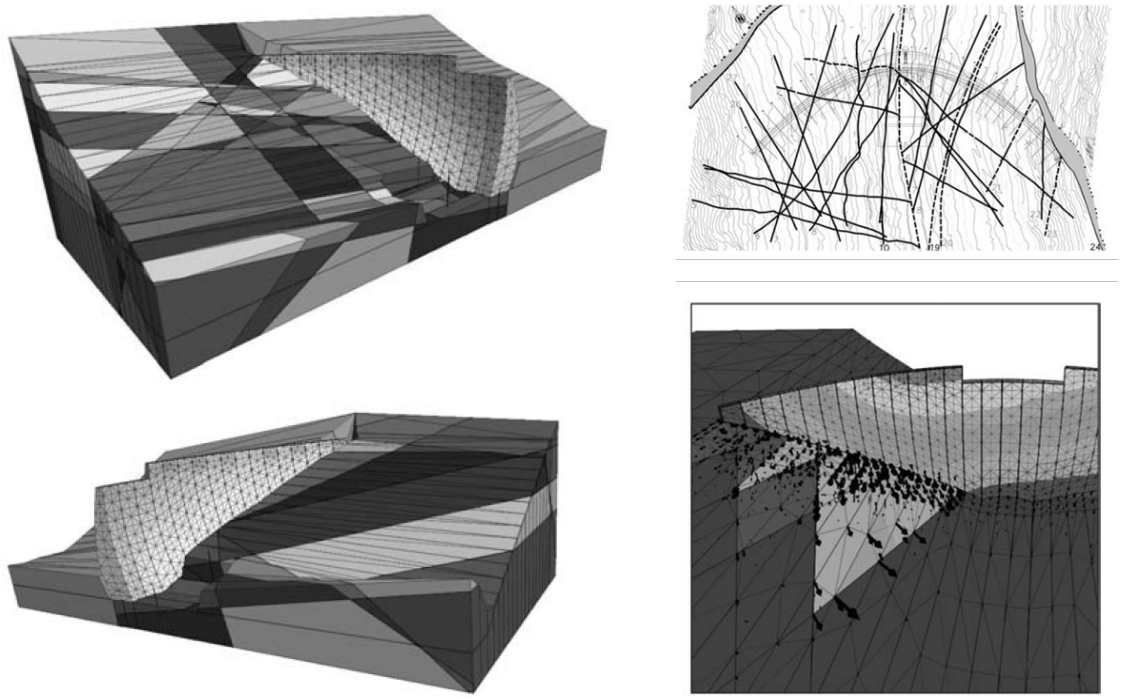

Figure 53– A 3DEC Screenshots showing numerical analysis of a dam foundation; Upper right screenshot indicates traceplanes of various faults at the site used to develop the models (Modified after Lemos 2012)

Further to large scale analysis of dam foundation, Chong et. al. (2011) analysed the effect of joints on p-y behaviour of laterally loaded piles into mudstone using 3DEC. In this model two full-scale pile load test results were used to validate a numerical model where elastic deformation was observed in a jointed rock mass. The validated model was used to extend the study to include the effects of various persistent joint sets on both the p-y and pile head load-deflection behaviour. Since the response of the rock mass is elastic in these models, the simulation of brittle fracture processes was not required. Chong completed analysis on a elastic model with a single persistent fracture, a two fracture conjugate intersection and a four joint wedge forming intersection. As expected, it was concluded that a single joint demonstrated a "higher capacity" due to mobilization of intact rock strength and the inability of the pile to move compared to the wedge movement experienced in the conjugate or four joint models.

The difference between the work in this thesis and the work by Chong is the direction of loading and the mechanism of which deformation occurs in the rock mass. Loading by Chong was lateral and the direction of the applied load was approximately 45 degrees to the moderately dipping joint orientations. To mobilize the wedge, the pile loads pushed against the natural direction of sliding and the wedge needed to be pushed upward. The normal force on the joint also provides additional friction against sliding. The deformation observed in the model was observed both from the elastic response of the rock mass to lateral loading and sliding along joints. However, if direct tensile loads were applied in the model the four joint model, which formed a discrete block in the area of anchorage, the capacity of the anchor would be limited to the dead weight of the block (analyzed in the previous section) with some losses due to elastic deformation. This model also does not allow for tensile breakout within the area of anchorage noted in Chapter 6. To allow for this mechanism, a different approach was taken in this thesis to 3DEC modelling.

An attempt was made to model breakout and deformation of intact rock by inputting additional fractures within the overall area of a large wedge, as shown in Figure 54. These smaller blocks allow for tensile cracks to develop within adjacent to the block to allow for in-elastic deformation to occur. This was completed for the assessment of a 1.5m embedment dowel and to allow for the scale of dilation shown in Figure 55 to be achieved.

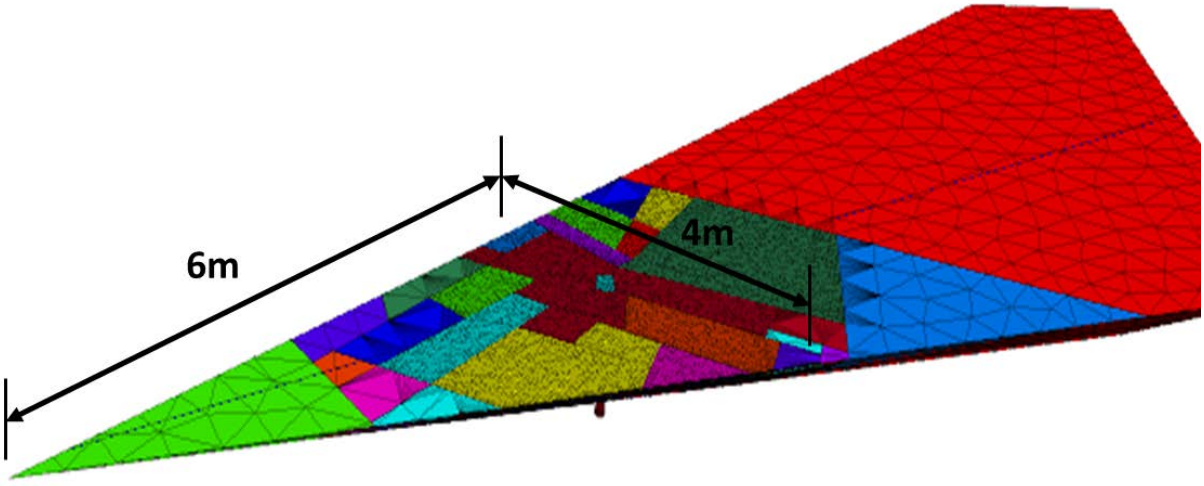

Figure 54– A 3DEC Screenshots indicating the minimum scale required to calibrate the rock anchor pullout model.

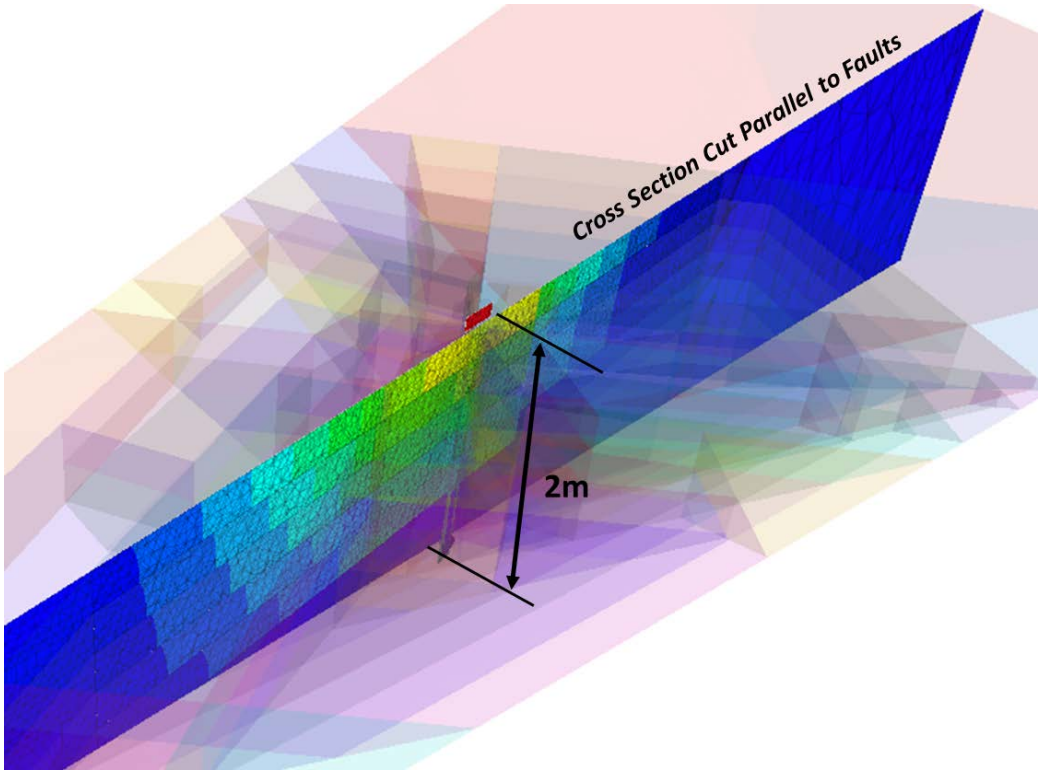

Figure 55– A 3DEC screenshot indicating interblock dilation induced by anchoring within a larger scale wedge formed by prominent faults. The scale of modelling required to simulate interblock dilation and tensile fracturing is much smaller than that of typical discontinuum foundation models.

Ideally, the three dimensional model would be developed using the synthetic rock mass approach noted in the previous section. In a perfect model, a discrete fracture network would be developed, similar to that presented in Section 7.2, and a 3D voronoi network would be developed between each discrete fracture location in the model. At the start of this research, this was the approach taken to analysis of 3D cone pullout, however, the run times required to generate tensile fracturing between joints were very long and it was not realistic to run multiple DFN realizations with voronoi / interblock cracking simulations at a centimeter scale between joints. Furthermore, voronoi tend to "lock up" with dilation and for this reason a tetrahedral blocks were considered between discrete fractures in the model. Developing these blocks and cleaning the mesh is a very time consuming process, and while likely more geologically representative, model simulations at this scale are not feasible with multiple DFN realizations in Engineering design.

With long run times and difficulties in cleaning the geometries a new approach was required. The literature presented in Chapter 2 and the simulations noted below suggest that cone breakout behaviour can be controlled by the site structural geology. It is not certain whether it is solely the contribution of naturally occurring fractures or alternatively whether it is bedding / foliation parallel microdefects that control tensile failure in rock. To simplify the computational requirements of the model, it was assumed that interblock tensile cracking will occur along preferential orientations. Cleaner model geometries can be prepared using standard 3DEC commands, such as the standard JSET command, which allows for fracture patterns to be generated within a model. This is a much simplier process than generating and cleaning a DFN with non-persistent discontinuities represented as disks. Input parameters for use of this command include fracture orientation, spacing, and persistence and distributions of each. The persistence allows for fractures to terminate on other joint orientations, this is inputted by specifying a percentage of terminations in the model. Inputting interblock fractures in the model allows for various pre-determined fracture breakout patterns to be assessed within the overall wedge. Persistent natural or pre-existing fractures can be modelled by the use of frictional parameters for joints. Interblock fractures or micro defects that are modelled as joints in the model can be modelled with calibrated intact rock strength properties. Interblock microstructure is shown in the Figure 56 and 60 for moderately dipping structural and sub vertical-horizontal conjugate jointing respectively.

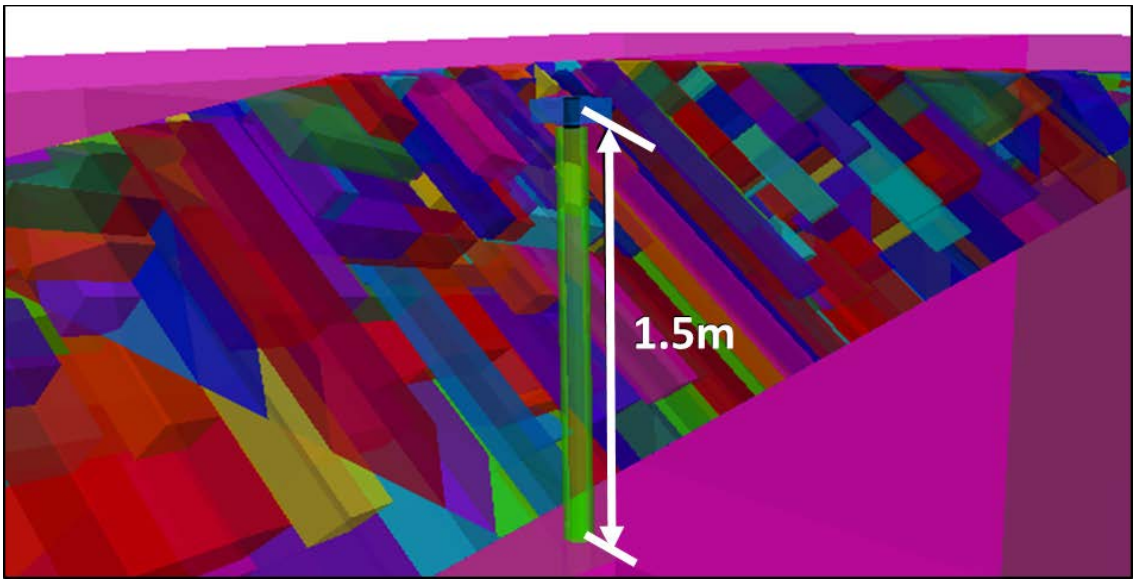

Figure 56– A 3DEC Screenshot showing interblock fracture patterns with moderately dipping orientations

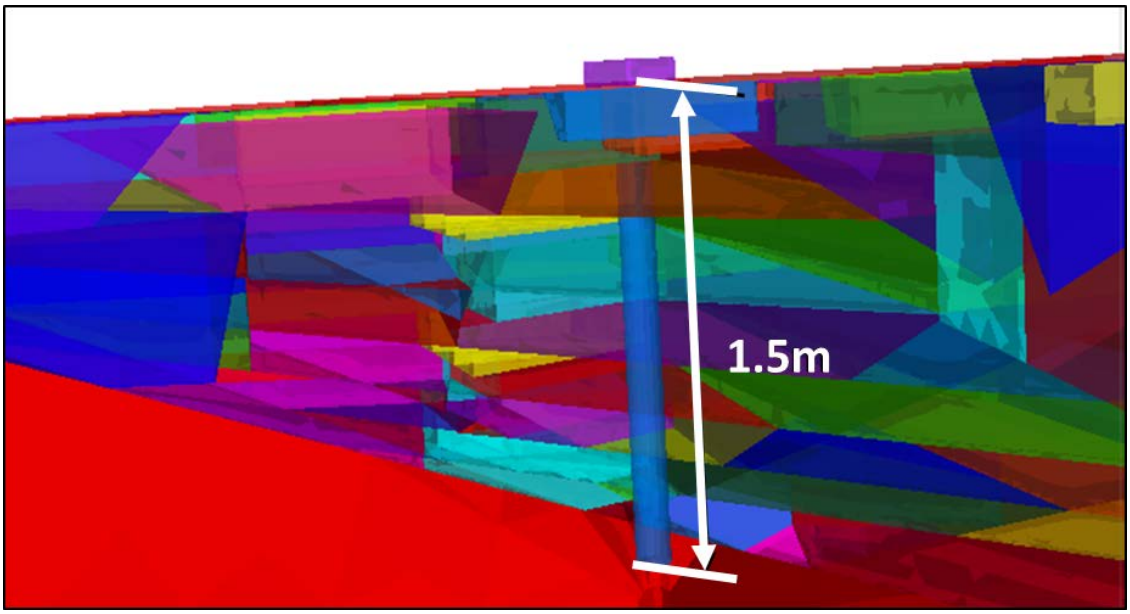

Figure 57– A 3DEC Screenshot showing interblock fracture patterns with subvertical-subhorizontal orientations

The strength properties for the interblock micro defects can be calibrated using full scale pullout cone data, similar to that described for the continuum mesh in Section 5. In three dimensions, dilation in the rock mass can be calibrated to historic test data. Figure 58 provides a 3DEC screenshot with block forming joints shown in plan view with a fracture dilation overview from Bruce (1979). Similar to the methodology noted in the the previous section, discrete fracture dilation data should be used at the basis for calibrating both two dimensional and three

dimensional pullout models. In three dimensional space, the blocks are represented a sub vertical – sub horizontal conjugate joint set similar to that shown in Figure 57. The traces of the sub vertical "jointing" are represented by the traces and different block colors shown on this figure. These blocks do not represent pre-existing "joints" in the model since intact rock parameters are applied to the surfaces of the blocks. By using intact rock parameters, these blocks represent imperfections in the synthetic rock mass and provide the possibility or model freedom for intact rock breakout within a larger wedge. It is the opinion of this thesis author that introducing pre-existing fracture patterns in the rock mass is a step backwords compared to the DFN based approach represented in 2D, however, this was deemed the only reasonable approach to analysis of the cone mechanism in 3D. As noted in the previous section, dilation can be calibrated to the loading overlain on Figure 58.

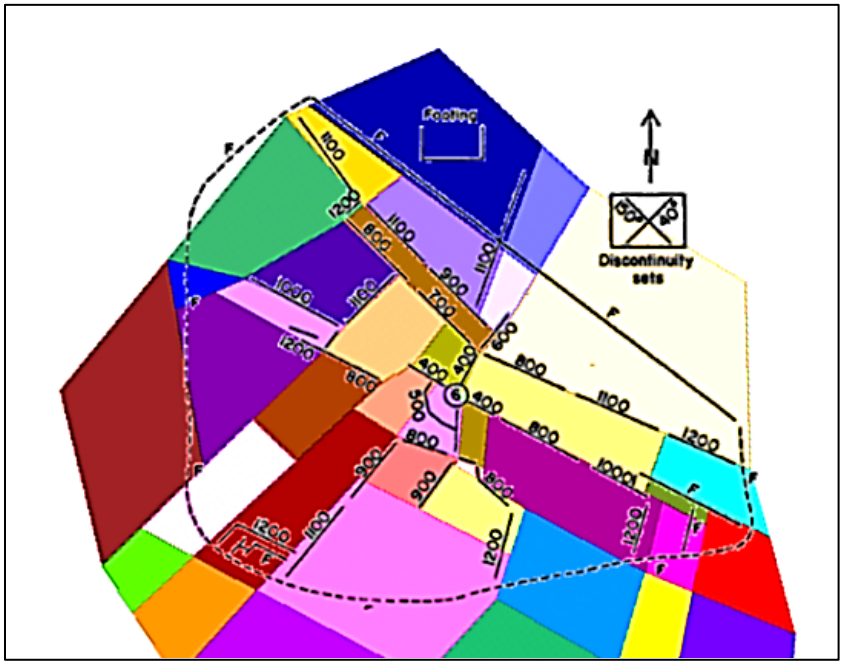

Figure 58 – An overlay from Bruce (1979) on a plan view screenshot taken from a 3DEC model. The different colors in the model indicate blocks which have the freedom to dilate with applied loading. The numbers annotated on the overlay indicate the load (in kN) in which various factures were observed to dilated during a full scale field test

An important component of this calibration is the stiffness at the rock – grout interface and the load transfer from this interface to the rock mass. Historically, numerical modelling with cable anchors has used the Kbond and Sbond parameters to calibrate this stiffness which are the stiffness and bond strength of grout respectively. Similarly, the deformation properties of the steel are governed by an elastic modulus with a plastic yield cutoff.

For modelling the cone pullout mechanism, it is also contended that the volume of the grouted hole and the load transfer mechanism that occurs within this volume are important in modelling the cone mechanism. For this reason, the cable bolt node based element in 3DEC are combined with a grouted volume in the calibration models. To apply the load to the anchor and then the grout a loading block is used in the simulations, similar to the two dimensional simulations described in Chapter 5 and as shown in Figure 59. The elastic properties of the grout volume, the grout stiffness and strength modelled with the cable element, and the properties of the steel modelled using the cable element are all calibrated together. A target of approximately 5mm of dilation is assumed for the top of the grout column for a load of 1200kN. This estimate reflects the deformational properties of a #14 threadbar. In the model, the ultimate strength of the steel is given as 1800kN and the parameters are adjusted until a uniform deformational load transfer is achieved as shown in Figure 59.

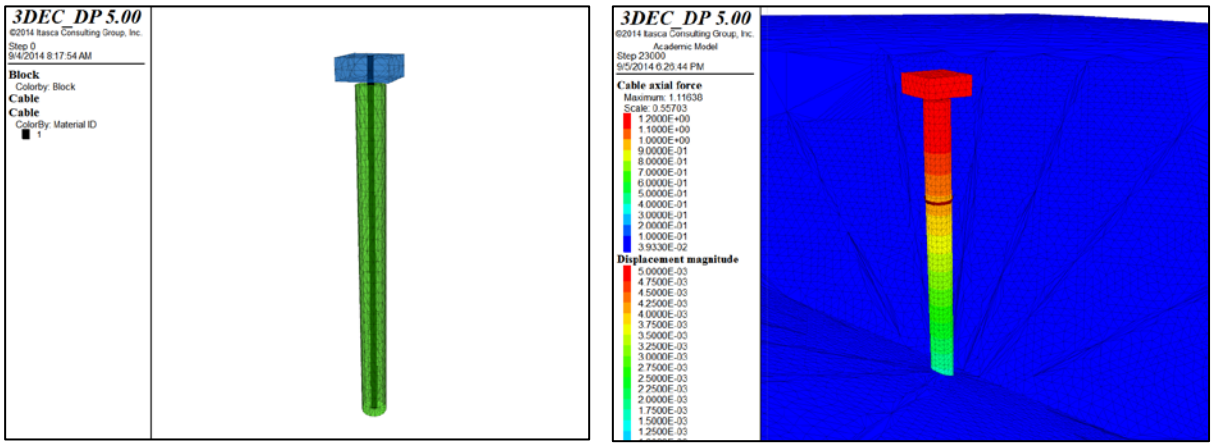

Figure 59– 3DEC screenshots showing the loading block, cable bolt element and grouted volume used to analyze the cone pullout mechanism;

After the steel – grout region is calibrated, the rock mass region can be generated in the model in the model. The geometric constraints of the model are described above and the failure criteria must be determined by the model. Historical test data suggests that 5mm of displacement for the limit of failure in the model. Since simplifying assumptions have been made on the shape of the interblock fractures in the model, attention must be paid to this deformation to determine when failure has been achieved. An issue with modelling the grouted volume as a discrete block is the poisons effect of grout shrinkage with loading. In reality roughness of the drill hole may prevent limit the influence of this mechanism and to add some interlocking between the grout and the rock mass in the model some individual blocks were joined to the bolt in the simulation. Again, this is

not an ideal assumption, however, it may represent reality if a high strength anchor grout, such as Microsil Anchor Grout which is capable of achieving 50MPa compressive strengths after 7 days, is selected. For loading of the anchor, a displacement boundary is set on the loading block at 1E-02 mm/sec to allow the load to be transferred to the rock mass. After 20,000 cycles the load is increased to 1E-01mm/sec for the remainder of the pullout test. Figure 60 shows the non-uniform displacement of the anchor at load step 20,000 where a load of 250kN is applied to the anchor bolt. At this load, a maximum of about 1mm displacement is observed in the rock mass surrounding the anchor. This formation is elastic at this stage of the model, although the shape of deformations is controlled by the interblock structure assumed to model microdefects in the 3DEC model. Furthermore, the wedge forming fracture traces in the model shadow the deformation as shown in the cross section cut perpendicular to this dominant structure. The cross section cut parallel to these joint sets indicates more deformation in the upper rock mass which accurately depicts the unloading that is ongoing as the stress is increased in the model. Figure 61 shows the deformational behavior of the rock mass at a load of 1600kN. At this load, it is anticipated that the steel threadbar may be deforming plastically in reality. At this loading stage the load is transferred near the base of the wedge, however, debonding is observed in the model with slippage at the rock-grout interface when the joined blocks are released and local "cracking" or interblock deformation is observed to exceed 5mm displacement.

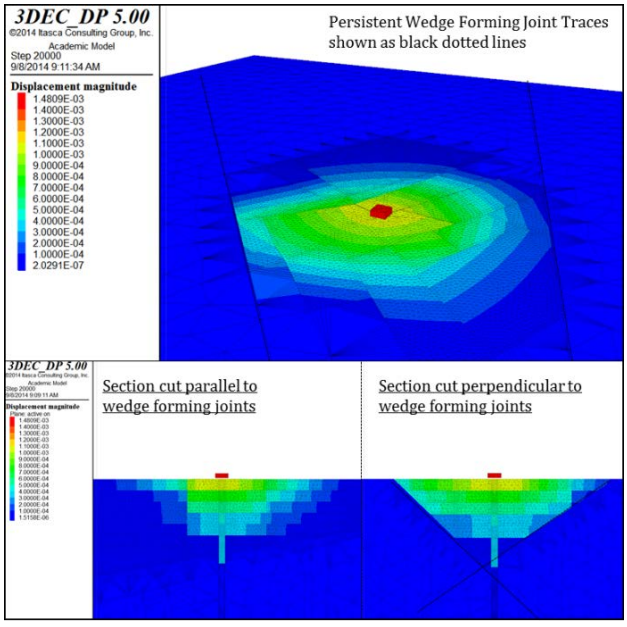

Figure 60- 3DEC Screenshots showing maximum deformation and dilation in the rock mass of approximately 1mm in the upper rock mass at maximum loading of 250kN loading in anchor.

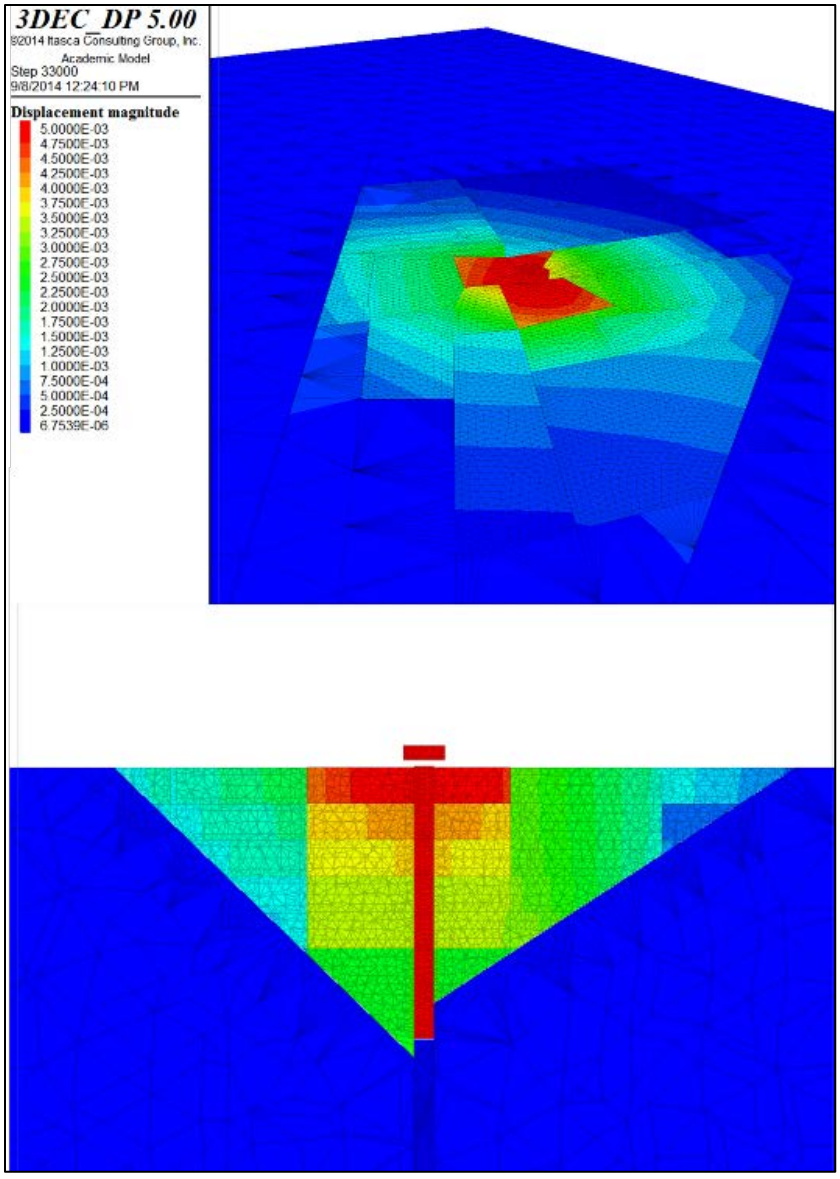

Figure 61 – 3DEC Screenshots showing dilation at 1600MN load with over 5mm interblock deformation occurring within the maximum probable wedge

The current state of practice of the design of rock anchors does not account for the deformational behavior of the rock mass in design, however, it is assumed that the current design practice is conservative enough that deformation may not be observed if the methods recommended by Littlejohn and Bruce are employed. For example, for this 1.5m length anchor the Littlejohn and Bruce pullout cone approach would calculate an ultimate failure load of 85 kN if a breakout angle of 90 degrees is considered to initiate from the base of the anchor. At 85kN the maximum deformation behavior in the 3DEC model is less than 1mm. By applying a tensile or shear strength

of 100kPa to the outside of this pullout cone an ultimate resistance of 785 kN can be calculated for the anchor. By assuming a factor of safety of 3 for this scenario (as recommended by Wyllie, 2004) an allowable anchor capacity of 260kN is calculated. For this load, the 3DEC model calculates a maximum deformation of about 1mm in the rock mass immediately adjacent to the anchor. At the 517MPa yield capacity of 'Grade 75' steel threadbar the strain in the bar for the 200GPa Young's modulus is calculated to be 2.585E-03. If the strain is applied over a 1500m bar length, 4mm of elastic deformation is expected in the bar before experiences plastic deformation. The rock mass deformation is less than 25% observed in a #8 threadbar at this load (at 517MPa yield) and this is likely considered reasonable for most designs. However, if the designer chooses to push the standard of practice of anchor design by considering a factor of safety less than 3, choosing tensile strength estimates that are very high or alternatively considering that a large wedge size provides resistance to failure (as shown in Figure 62) the deformational behaviour or tensile breakout within the maximum wedge should be considered in the design of anchors. This is particularly the case where multiple anchors are installed in close proximity and these anchors induce overlapping stresses or stress concentrations in the rock mass.

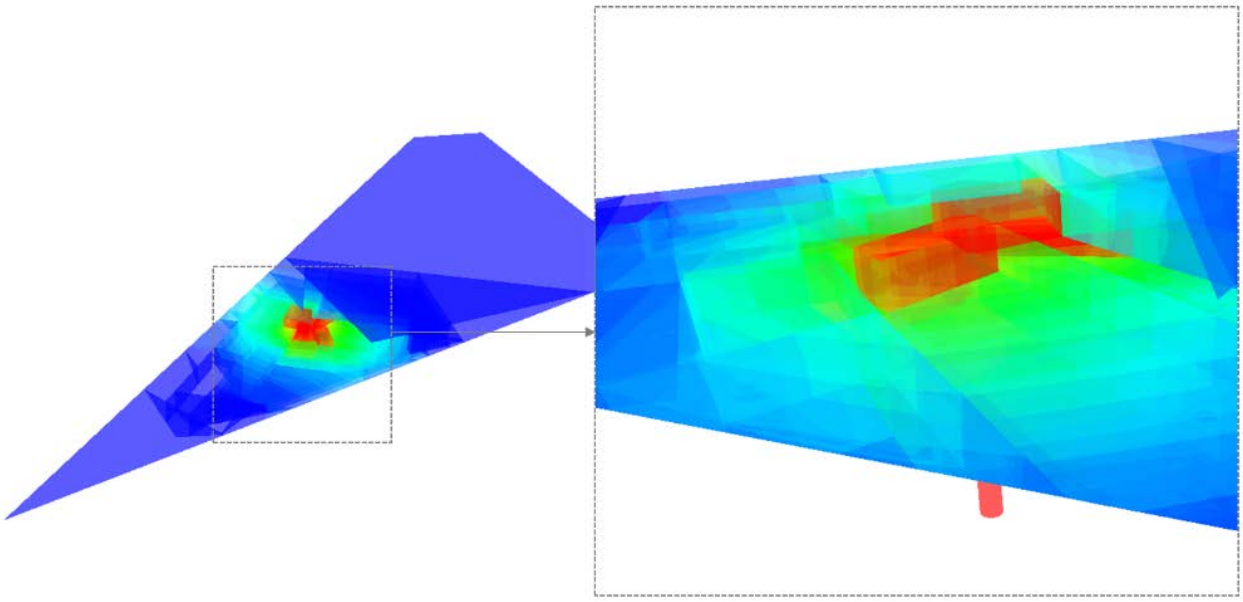

Figure 62 - 3DEC Screenshots showing dilation at 1600MN load with over 5mm interblock deformation occurring within the maximum probable wedge

7.3 Comments on Up-scaling Numerical Models in 3 Dimensions

This Chapter (Chapter 7) has illustrated some of the limitations of modelling rock anchor pullout in three dimensions. The 3DEC models provided in this Chapter are capable of producing similar dilation of in the rock mass observed in field pullout tests, however, the mechanism used to generate this dilation is an oversimplification of reality. The advantage of the three dimensional Distinct Element Code (3DEC) is that it allows for larger strain deformations and kinematics to be accommodated, which may be useful at the large scale of a faulted dam foundation. However at the brittle fracture scale, while structural geological constraints were used to reflect the likely cracking behavior of the rock mass, the results presented are no more sophisticated when it comes to crack initiation and damage than the ubiquitous joint model applied to a continuum code, such as that used in FLAC3D. Furthermore, the mesh spacing required to assess the cone pullout mechanism is 3D is very wide, as shown in the continuum ELFEN 3D model, in Figure 63 below.

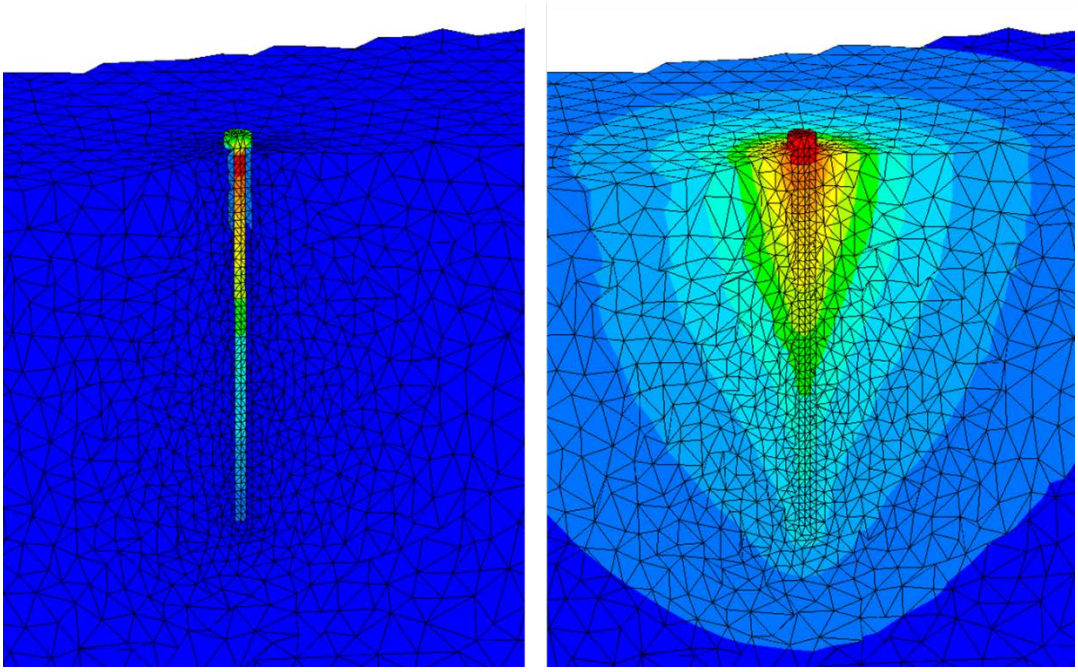

Figure 63 – ELFEN screenshot showing 3D anchor model; Principal Stress distribution on left and Total Displacement plot on right.

It should be recognized that the purpose of simulation of 1.5-2m "pullout" tests in the past three chapters is for calibration of the numerical model parameters. Full scale testing data was available for pullout failures at this scale and this information provided a convenient starting point for this assessment. However, in engineering design the failure of a 2m embedment dowel is not a

profound problem. It is proposed that if field testing is completed on shorter dowels, and simulation is completed at this scale, the calibrated intact rock and fracture parameters can be used for larger scale anchor pullout problems to study the group effect or to design the pullout capacity of longer anchors with a free stressing length. For proper calibration, the same representative scale of stability controlling joints and a representative mesh size needs to be maintained for the calibration at the small scale if the same material parameters are to be used to model a larger scale mechanism. The issue with three dimensional modelling is the limitation on the number of elements that can be generated in the model. Figure 63 shows a mesh spacing that is feasible in a 3D ELFEN simulation. It should be noted that cracking was not observed in this model. It is possible that the lack of failure may have been due to the wide (0.1m) mesh spacing used in the simulations. Figure 55 compares two additional 2D ELFEN simulations completed with the same material properties but different mesh sizing. The screenshot on the left shows brittle fracture development for a model run with a 1cm mesh size, while the right hand screenshot shows the same model run with a 10cm mesh size. The smaller mesh size allows for fractures to propagate with more freedom, and multiple mechanisms for fracturing can develop, such as upper cone failure, generalized cracking, and fracturing developing at the distal end of the anchor as shown in the figure. In contrast, the wider mesh spacing is dominated primarily by bond failure with a simplified cone breaking out between the wider nodes. It is contended that the model with the finer mesh spacing more appropriately simulates brittle fracture in the rock mass, especially in the case where joints are inputted in the mesh domain. Furthermore, by employed 3D tetrahedral elements instead of triangular elements used in 2D, additional complexity and roughness is added to the model.

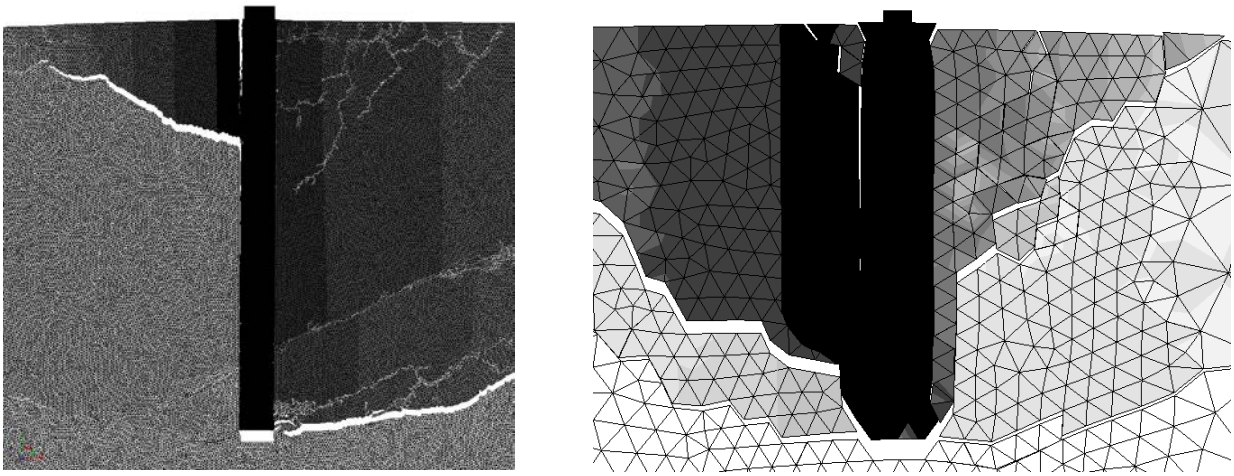

Figure 64 – A comparison between two ELFEN models run with the same material properties but different mesh sizes; 0.01m mesh size on left, 0.1m mesh size on right

Due to the large mesh sizing that would be required in 3D for large scale pullout problems, it is the opinion of the author of this thesis that future studies should spend time understanding the rock mass pullout mechanism in the field rather than developing new 3D numerical approaches for the cone mechanism.

In a recent review paper on fracture initiation and propagation in intact rock, Hoek and Martin (2014) note that the improvements in computing power the discrete element codes, specifically bonded particle or grain based codes, have been useful in studying the tensile cracking behaviour at the laboratory scale. However, the authors note that "*while this approach holds much promise, the current grain-based models are still limited to two dimensions, and much research needs to be carried out before this approach becomes state of practice*". As an alternative to the grain based models, 3D voronoi and 3D tetrahedral trigon methods have also been used to model tensile failure at the laboratory scale in 3DEC (Gao and Stead, 2014). However, until research shows that tensile failure behaviour can be simulated at the laboratory scale in 3D, and numerical codes are sophisticated enough to input multiple DFN realizations without significant manual processing, modelling of the cone pullout mechanism should be completed in two dimensions.

It is contended that as an alternative to the complex 3D models described above, the design of anchors in 3D should be completed using a combined approach using Fracman and 2D numerical simulations. A proposed design methodology is presented in Figure 65. It is contended that if two dimensional cross sections are cut parallel and perpendicular to persistent discontinuities, the brittle failure behaviour of the rock mass can be more appropriately characterized. Furthermore, where problems are truly 3dimensional in nature. It is contended that a limit equilibrium approach can be used, and the likelihood of encountering removable blocks can be assessed in 3D using fracman. Additional details and commentary on incorporation of numerical modelling in the design process is presented in the next chapter.

1) Map discrete fracture locations across the propose foundation; measure dilation and D21 cracking patterns during pullout test on a 1.5m-2m fully bonded anchor with the same bar sizing and hole diameter proposed for long length anchor installations. AE can be used to monitor the onset and propagation of D21 damage in 3D.

2) Develop DFN with the deterministic discrete fracture locations observed at the surface in the field and generate stochastic fractures based on field mapping input (P21, fracture orientation, fracture length and fracture terminations, etc.).

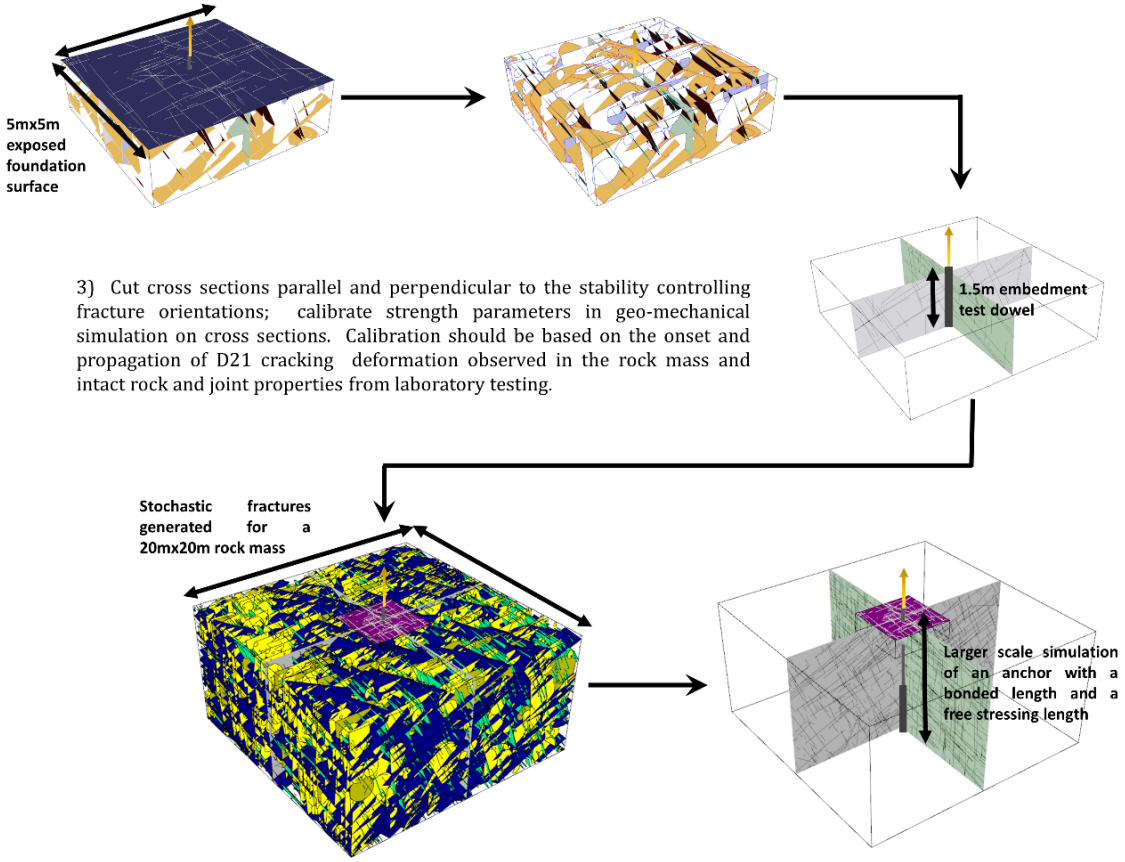

3) Cut cross sections parallel and perpendicular to the stability controlling fracture orientations; calibrate strength parameters in geo-mechanical simulation on cross sections. Calibration should be based on the onset and propagation of D21 cracking deformation observed in the rock mass and intact rock and joint properties from laboratory testing.

4) After calibration is complete, the same DFN inputs can be used to generate stochastic fractures in a randomly generated DFN realization. Multiple DFN realizations can be completed to assess the stability of longer anchors at a large scale. This is only possible if the longer anchor is installed in the same structural domain as that of the smaller scale calibration.

5) Cross sections can then be cut parallel and perpendicular to the same stability controlling joint sets as the smaller scale calibration simulation. The same scale of fracturing can be simulated using the calibrated parameters and mesh size of the smaller scale model. The distribution of tensile and shear fracturing can then be assessed in the simulations and the distribution damage and deformation can be assessed under higher loading conditions at the larger scale.

Figure 65– A Proposed Design Methodology for Analysing the Three Dimensional Cone Pullout Problem using Discrete Fracture Networks combined with Simulations on 2D Cross Sections.

8 FOUNDATION ENGINEERING ANALYSIS AND APPLICATIONS

8.1 Incorporation of the Combined DFN-Numerical Approach into Anchor Design

8.1.1. Comparing the Numerical Approach to the "Dead Weight Assumption"

Evaluation of the Type D rock mass failure mechanism is typically completed using the "rule of thumb" that the dead weight of an inverted cone of rock provides resistance to failure. Different cone breakout angles and initiation points are based loosely on the "competency" of the rock, judged by the designer, without clear guidance from a recognized design code. For this reason the design of rock anchors is usually only undertaken by experienced geotechnical engineers. Since there is significant uncertainty and lack of knowledge associated with the cone pullout mechanism a Factor of Safety of 3 is recommended for this design approach, which is considered suitably conservative (Bruce, 1976; Bruce, 2013).

For simple anchor designs, the generally conservative standard of practice may calculate anchor lengths that are reasonable for many applications. It should be recognized that more data collection (including full scale anchor testing to failure) is required to improve the design practice and various design inputs are noted in Figure 66. It may be argued that the costs of collecting this data may not outweigh the benefits for simple problems, but for large dam structures where anchor lengths now exceed 140m a less conservative design approach may be warranted.

It is recognized that the dead weight cone assumption may be valid for rock masses where joint lengths are continuous or fully persistent, and joint sets have the potential to form a removeable wedge within the area of anchorage. In Chapter 7 Fracman was used to calculate the weight of removable wedges for in multiple DFN realizations and this dataset is compared to various design curves generated using the dead weight cone assumption. It is contended that Fracman or other DFN models can be used as a screening level analysis tool to assess the probability of encountering a wedge within the proposed area of anchorage, prior to undertaking geo mechanical modelling simulations. It is also recommended that the structural geology of the site is used to identify the shape and block size that makes up the envisaged pullout surfacing. Using structural geology and block size analysis, the breakout angle and cone initiation point can be revised and the designer can move toward a 3D limit equilibrium calculation of "cone" resistance that is more consistent with kinematic analysis used in rock mechanics.

For many projects and rock masses, this approach to design may also be more appropriate than the combined DFN-numerical approach presented herein, however for other projects neglecting rock mass strength and the frictional properties of joints may be unacceptable.

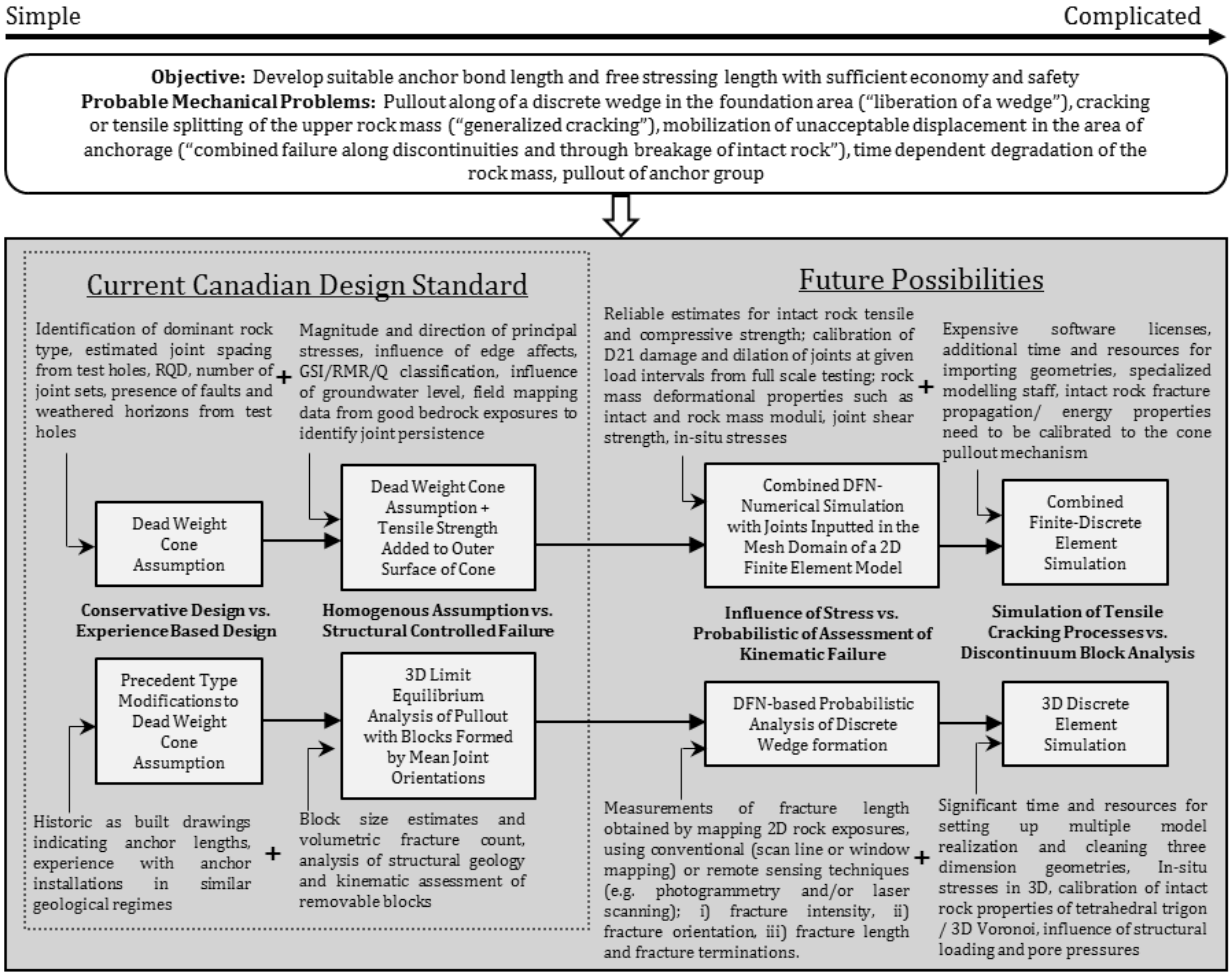

Figure 66– A Design Flow Chart indicating design inputs for various anchor design approaches

Where jointing in the rock mass is observed to be non-persistent, and the Owner or Owner's Engineer have determined that the design lengths calculated using the dead weight cone assumption are unacceptably long, moving to a numerical approach to anchor design may be warranted.

Significant reduction in anchor lengths may be realized by developing site specific strength parameters for rock strength and analyze the failure mechanism associated with anchorage. The rock bridges between these non-persistent joints are anticipated to have an influence on anchor

capacity, as intact rock cohesion or tensile strength provides a significant measure of strength. The dilation of joint roughness and the frictional properties of joints may also contribute to the rock mass failure mechanism.

For a 1.5m embedment rock anchor, the "dead weight" cone assumption calculates a failure load of between 30-100kN, depending on the assumed breakout angle and cone initiation point. Assuming a ninety degree breakout angle (initiating at the base of the anchor) calculates an un-factored dead weight cone capacity of about 80kN. This value is plotted on the chart provided in Figure 67. It is apparent from this figure that the "dead weight" assumption significantly underestimates the ultimate failure load for anchors. Testing by Bruce 1976 suggest that for the sedimentary rock at the Withnell Central Quarry test site ultimate failure loads between 1000-2000kN may be applicable for 1.5m embedment anchors in this rock type.

Anchor test 6 reported an ultimate failure load of 1200kN, which indicates a Factor of Safety of about 15 when compared to the dead weight cone assumption. This test result is annotated in red on Figure 67, and this test result was used to calibrate the Finite Element models presented in Chapter 5. The variation in loads from all anchor simulations from the Finite Element Models is also presented on this Figure.

It should be recognized that the range of finite element model failure loads from 400kN to 1600kN are lower on this chart than the results presented by Bruce 1976. This is due to the fact that calibration was initially completed using the relatively conservative Anchor test 6 result in the initial finite element model calibration, and the P21 fracture intensity was either increased or decreased in these models to illustrate the influence of fracturing on the calculated anchor capacity in the model. The variation in P21 from about 3-30 generally provided lower anchor capacities than Anchor 6, due to the influence of higher fracture intensities than the Bruce (1976) rock mass, however, it should be recognized that even conservative estimates for fracturing provide a higher calculated resistance compared to the dead weight cone assumption.

It is contended that by properly characterizing jointing and calibrating numerical simulations, design calculations can be completed which more accurately reflect the strength values measured in the field. However, it should also be recognized that while Anchor Test 6 calculated an ultimate pullout load of 1200kN, cracking was observed at about 400kN at the surface prior to ultimate failure. This cracking was noted by Bruce, 1976 to be within the area of the anticipated "pullout cone" surface and this inter-block breakout failure mechanism should be considered by designers when designing anchors.

For comparison purposes, the onset of crack initiation is also plotted in Figure 66 from the sensitivity analysis complete in the ELFEN FEM-DEM model simulations presented in Chapter 6. By varying the Rankine Rotating Crack parameters in ELFEN, the onset of cracking was observed in the models between 200kN-1200kN for intact rock tensile strength and modulus values ranging from 0.15-3MPA and 1.5MPa-50MPa respectively.

A flow chart is provided in Figure 68 which may be used to assess whether the current design state of practice may be an appropriate design assumption for a given project.

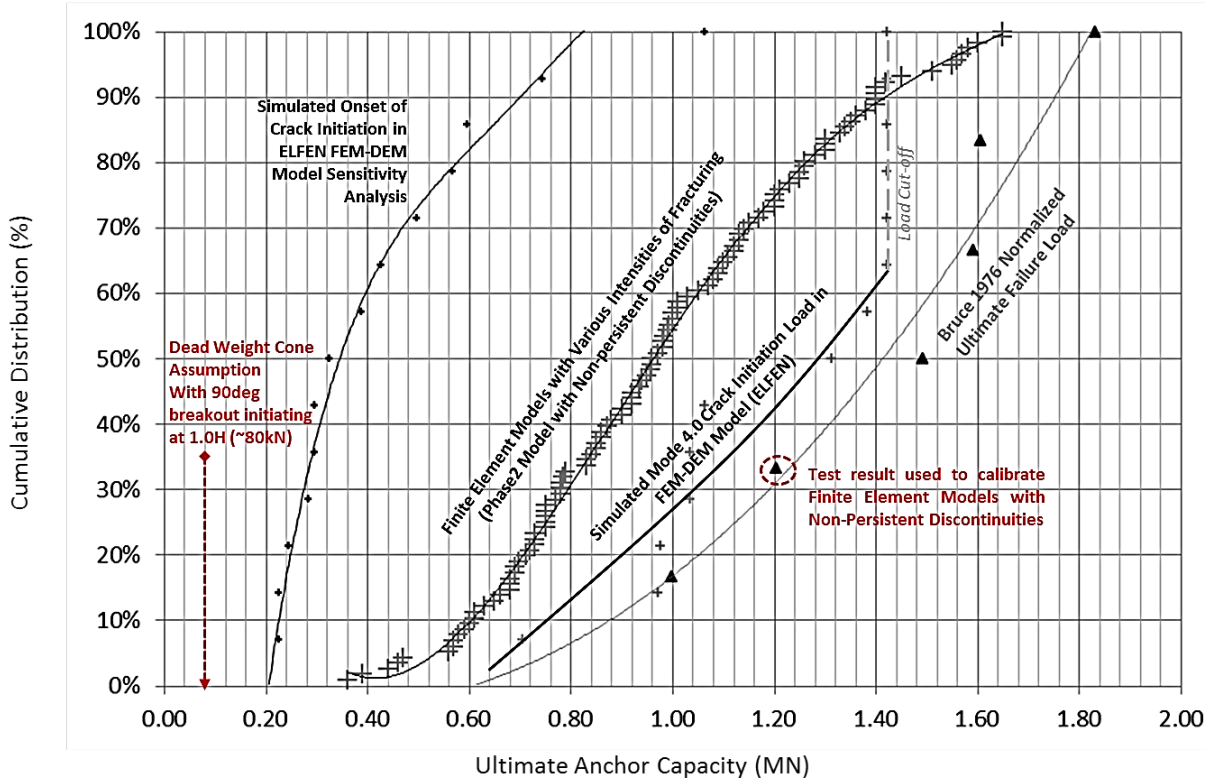

Figure 67 - A cumulative distribution chart showing anchor capacity variation for the rock mass generated from numerical simulations and compared to testing data by Bruce (1976) and the "dead weight" assumption.

Note: It should be recognized that the difference in anchor capacities is due to variation in joint intensity in the Finite Element model and fracture propagation properties in the FEM-DEM model. The purpose of the assessment was not to calibrate the testing curve, but rather, calibrate to one anchor test result and vary the joint properties and Rankine rotating crack parameters to illustrate that these values are important parameters in numerical models. The Mohr-Coulomb plasticity properties were left constant for all model iterations. Even with conservative estimates for jointing, the frictional properties of joints provide higher capacities than the dead weight cone assumption which indicates that this assumption is conservative. Additional discussion on the onset of crack initiation is provide in the next section.

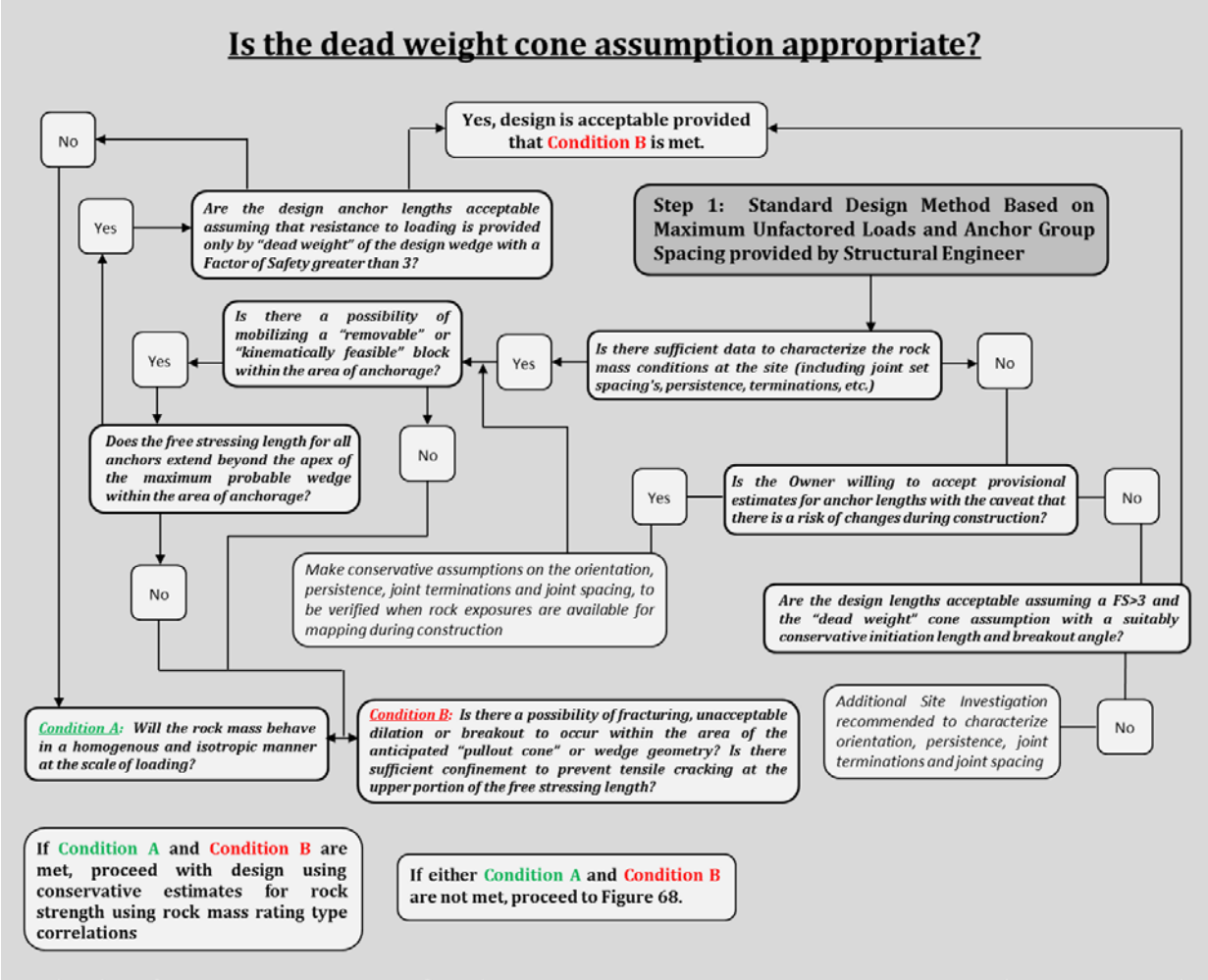

Figure 68 - A Flow Chart which can be used to assess whether the dead weight assumption is appropriate

8.1.2. Comparing the Numerical Approach to "Equivalent Cone Strength"

It is contended that the numerical approach can be used to better understand the failure mechanism associated with anchorage. This approach can also be used confirm design strength values assumed using the "Equivalent Cone Strength" assumption, where a strength value is assigned to the outer surface of an assumed breakout angle and cone initiation point.

The results from the ELFEN model simulations are compared to the "Equivalent Cone Strength" approach using the geometries provided in Figure 69.

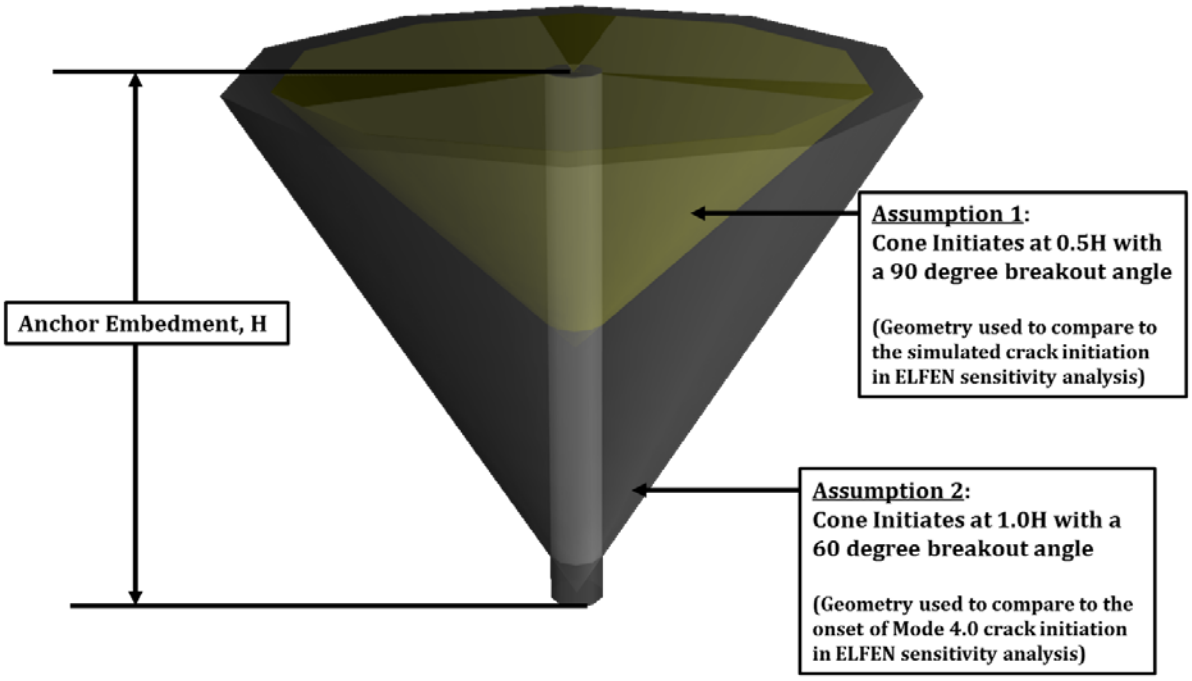

Figure 69 - A cone pullout illustration showing to two geometric assumptions used to compare to the onset of brittle fracturing in the ELFEN model results shown in the chart on the next figure.

For this analysis, a cone initiating at the midpoint of the anchor (0.5H) was assumed to have a 90 degree breakout angle and equivalent strength was applied to the outer surface of this cone area. This geometry can be considered "Assumption 1" for the purposes of discussion. This upper strength is added to the dead weight of the cone volume in this calculation. A similar calculation can be completed for a cone initiating at the base of the anchor (1.0H) and this cone was assumed to have a breakout angle of 60 degrees. This geometry can be considered "Assumption 2" for the purposes of discussion. The Ultimate Anchor Capacity for each geometric assumption is plotted in

Figure 70 for a range of tensile strength values of 80-300kPa and these calculated values can be compared to crack initiation in the ELFEN models, both for the onset of crack initiation and initiation of the Mode 4.0 failure mechanism noted in Chapter 6 to be breakout of a cone surface at the base of the anchor.

It is anticipated that the upper rock mass will dilate first and for this reason the upper cone or Assumption 1, could be considered as an assumed representation of the onset of cracking in the rock mass surrounding the anchor. The larger cone initiating at the base of the anchor or Assumption 2 could be considered to represent the onset of development of a global failure surface. For example, for a 200kPa "equivalent cone strength", Assumption 1 calculates a capacity of about 500kN and Assumption 2 calculates a capacity of 1000kN. It should be recognized that while the 200kPa average cone strength is applied uniformly across the outer surface of the cone in these calculations, in reality the load is not uniformly distributed along the anchor at depth. This non-uniform stress distribution may affect the location of crack initiation at depth, as shown in Chapter 6.

It is contended that the practitioner with experience with anchor design may be able to use very conservative assumptions for cone strength using assumptions similar to those presented in Figure 69. However, it should be recognized that this "equivalent strength" may not be directly a function of rock mass rating type relationships developed using Q, RMR or the Hoek Brown failure criteria. The load distribution within the rock mass is a complex distribution of both shear and tensile loads. Assuming that the resistance to pullout is provided by solely tensile strength, the equivalent cone strength range of 80kPa-300kPa could be calculated using the Hoek-Brown failure criteria for and an R3 strength Sandstone (UCS = 45MPa; mi=13) for the respective GSI range of 50-70.

It should be recognized that while assumptions seem to provide a representation of the load at which cracks initiate in the rock mass, it is contended that if pre-existing fractures produce an an-isotropic rock mass response the load at which cracks are observed to initiate in the rock mass may be very different than predicted using the Hoek-Brown failure criteria applied to the outer surface of an assumed cone.

While engineering judgement can be used to evaluate the suitability of the "Equivalent Cone Strength" approach on a case by case basis, the following conditions should be met if this approach is taken:

- Condition 1: The rock mass strength and deformation properties are considered homogeneous and isotropic;
- Condition 2: Generalized cracking or extensive deformation is not anticipated within the area of the envisaged pullout cone (i.e. interblock rock strength is strong);
- Condition 3: The likelihood of encountering a removable block within the area of anchorage is considered low;

If any of these conditions are not met, it is recommended that the "dead weight cone" assumption is considered in design with a Factor of Safety of 3, or alternatively, a numerical modelling approach should be undertaken, with full scale testing to validate the onset of cracking and joint frictional properties.

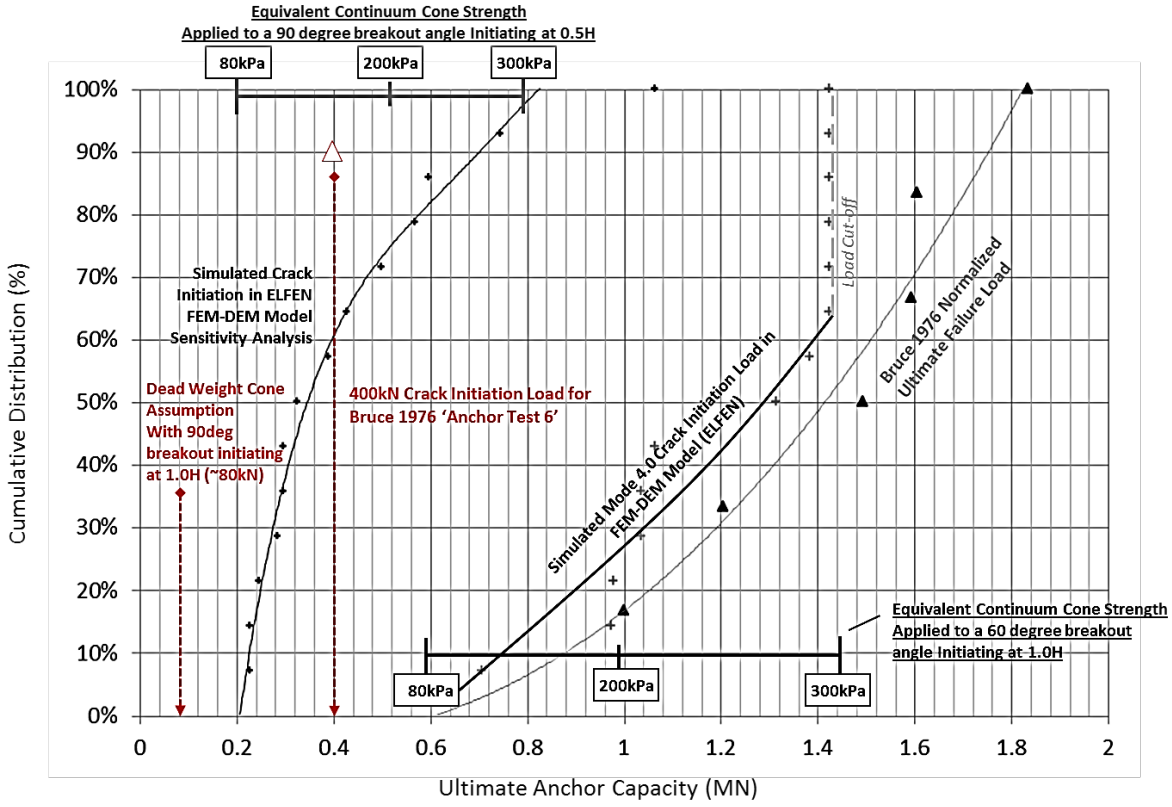

Figure 70– A cumulative distribution chart showing anchor capacity variation for ELFEN simulations compared to the capacities calculated using various equivalent continuum cone strength estimates. ***M-C plasticity parameters were left constant in models and the variation in capacity is observed due to variation in Rankine parameters***

8.1.3. Choosing an Appropriate Numerical Model for the Project.

It is contended that the numerical method presented more appropriately captures the load transfer mechanism (both shear and tensile loading) from the structure to the rock mass, and combining numerical modes with discrete fracture networks allows for the variability in the rock mass to be quantified.

In the current standard of practice, where the "dead weight" cone assumption is deemed over-conservative designers use rock mass rating type relationships to analyse anchor capacity. In some cases, "equivalent cone strength" is applied to the outer surface of this cone.

Representing rock mass capacity by an equivalent cone strength assumes that the rock mass deformational behaviour and strength are homogeneous and isotropic. At the scale of many anchor problems, rock mass failure may be influenced by individual fractures and for this reason this assumption may not be valid. The load transfer mechanism from the anchor to the rock mass is also influenced by the stiffness of the rock mass which may lead to further anisotropy. It is also possible for breakout or extensive fracturing to occur within the assumed cone shape. Rock mass anisotropy and the consideration of interblock breakout / generalized cracking are noted as Condition A and Condition B on Figure 68, and if these conditions are encountered, going to a numerical modelling approach is recommended. Numerical modelling may also allow for the influence of groundwater pressures, confinement provided by the overlying structure and in-situ stresses to be considered in anchor design.

If more full scale pullout testing is completed, a better understanding of the rock mass pullout mechanism can be developed and rock mass behaviour can be more appropriately characterized in models. Figure 71 provides a flow chart and recommendations for various modelling approaches dependent on the availability of field data, the nature of the anticipated failure mechanisms and design requirements for the project.

It should be recognized that the numerical model iterations presented in this thesis were run with the same Mohr Coulomb plasticity parameters, and the observed variation in pullout capacities were a result of variation in (P21) joint intensity or proximity of individual joints in the Finite Element model and fracture propagation properties in the combined FEM-DEM model. This illustrates the importance of these properties in calculations of anchor capacity.

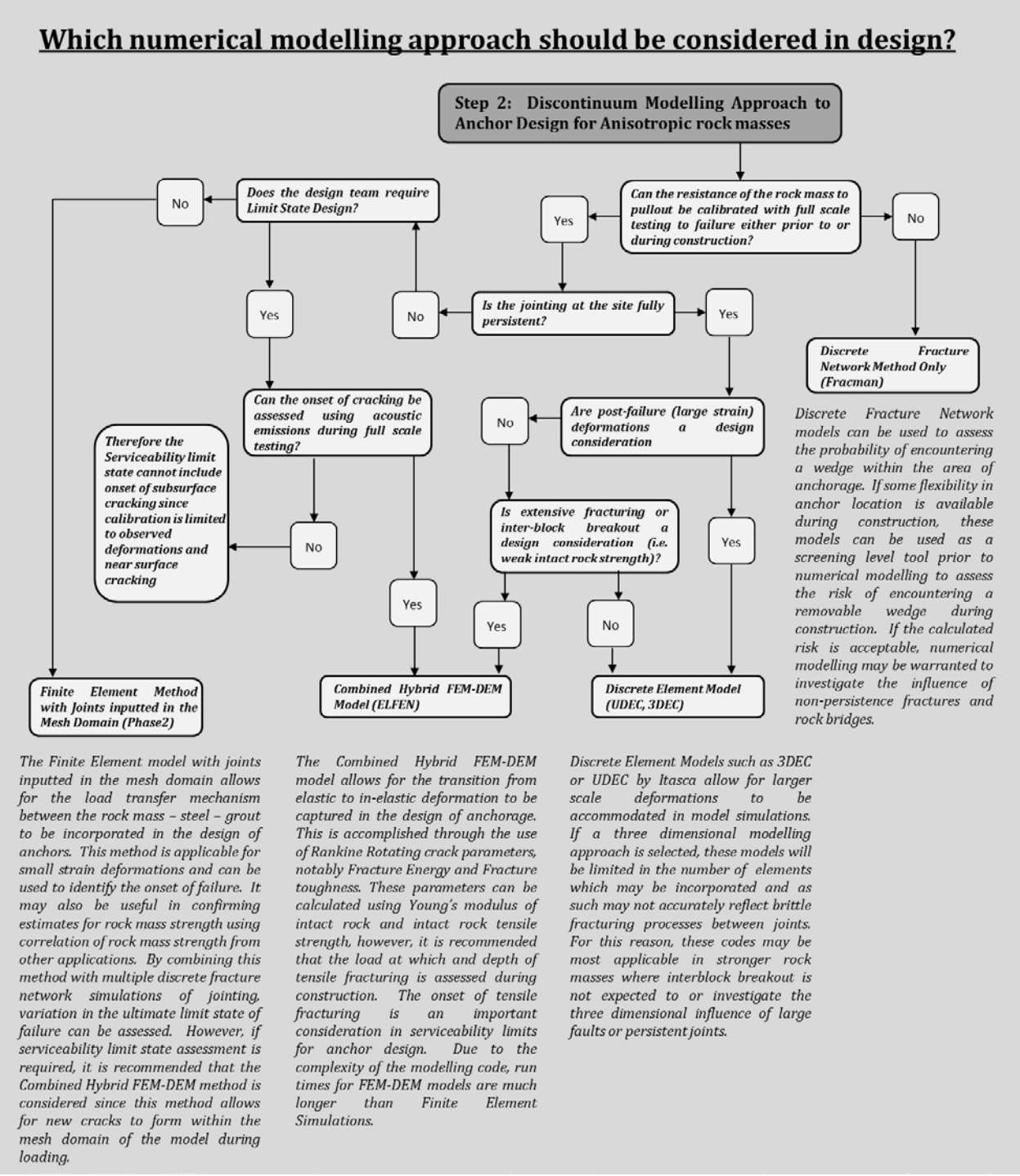

Figure 71- Numerical Models Considerations Flow Chart for Design of Anchors

8.2 Assessing the Load Transfer Mechanism for Post-Tensioned Anchors

8.2.1. Calibration using a 10m Embedment Fully Grouted Dowel

The previous section outlined advantages to a numerical modelling approach to design and this section provides a validation of the numerical approach for longer anchors.

The numerical simulations in Figure 72 illustrate a comparison between two 10m length anchors fully grouted cable anchors tested to 18MN. While these loads are very high, it is possible to test anchors to this load using a very large testing jack. These simulations comprise the same input parameters and softening relationship calibration presented in Chapter 5. These two simulations suggest that the anchor load is not transferred to the distal end of the bond length in either of these simulations, however, up to 5mm deformation of the rock mass was observed at surface. The right hand screenshot indicates the distribution of failed elements in the model for different joint orientations. In the upper 3m of the rock mass tensile and shear fractures propagate outward into the rock mass from the bond length, while below this depth, tensile fracturing is concentrated next to the bond. While ultimate failure was not observed the deformation and damage observed on the surface could be recorded for calibration of numerical models, in addition, acoustic emissions sensors installed at the surface during testing could be used to assess the onset of tensile fractures at depth with increased loading.

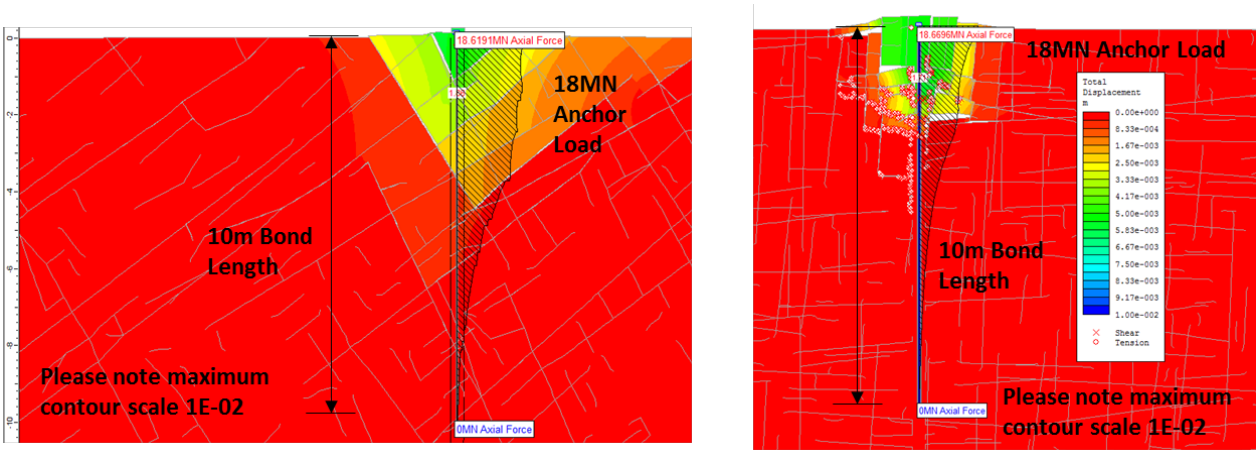

Figure 72– Comparison of calibration of a 10m length fully grouted bolt with moderately dipping conjugate jointing shown on the left and subvertical-subhorizontal jointing on the right. A 1H:1V stress ratio is applied in these models which is different from other model iterations presented in this section.

The observation in these numerical simulations presents an interesting question for the rock mechanics community. Is "cone pullout" mechanism feasible at the scale of the 30-50m free

stressing lengths required for large dams, and if not, why is this approach the documented standard of practice. It is hypothesized that the load is dissipated into the rock mass prior to reaching the end of the bond length for these long anchors. It is also contended that rock mass confinement at depth may result in localized deformation closer to the ground surface. It is recommended that testing is completed to failure of the rock mass at a scale larger than 2m embedment to investigate this point.

8.2.2. The Important Consideration of In-Situ Stresses in Calibration

An important consideration in rock mechanics that has been overlooked so far in this study is the orientation of the major principal stress. It is noted by Hoek and Brown (1980) that at depths likely to be encountered in civil engineering projects, in 92% of the case studies the horizontal stress exceeds the vertical stress component, it is contended that this has an influence of the behaviour of the rock mass in anchor simulations.

To test this theory, a second numerical simulation was completed on the 10m dowels loaded in the previous section. For this model a 2.5H:1V stress ratio was applied in the model. The results shown in Figure 73 indicate that at a load of 18MN the surface displacement is less than 1mm, which might be considered acceptable for some foundation designs. The distribution of tensile fracturing is concentrated closer to the rock-grout interface and as a result, even at a load of 18MN the displacement is much less than that the same model, provided in Figure 72, with a 1H:1V stress ratio. This may be due to the fact that the subvertical pre-existing fractures in the model have higher normal force acting on the frictional surfaces and which may results in clamping of fracture in the model. As a result, it is anticipated that failure at the rock-grout interface may be more feasible than rock mass pullout in this model.

However, the orientation and persistence of jointing in the model has a significant influence on model behaviour and if sub-horizontal discontinuities are inputted as the persistent joint set in the model the influence of horizontal stresses is much less significant and up to 2cm of displacement is observed at the surface under the same loading conditions but in models with different jointing patterns / joint statistics. This displacement is shown in Figure 74.

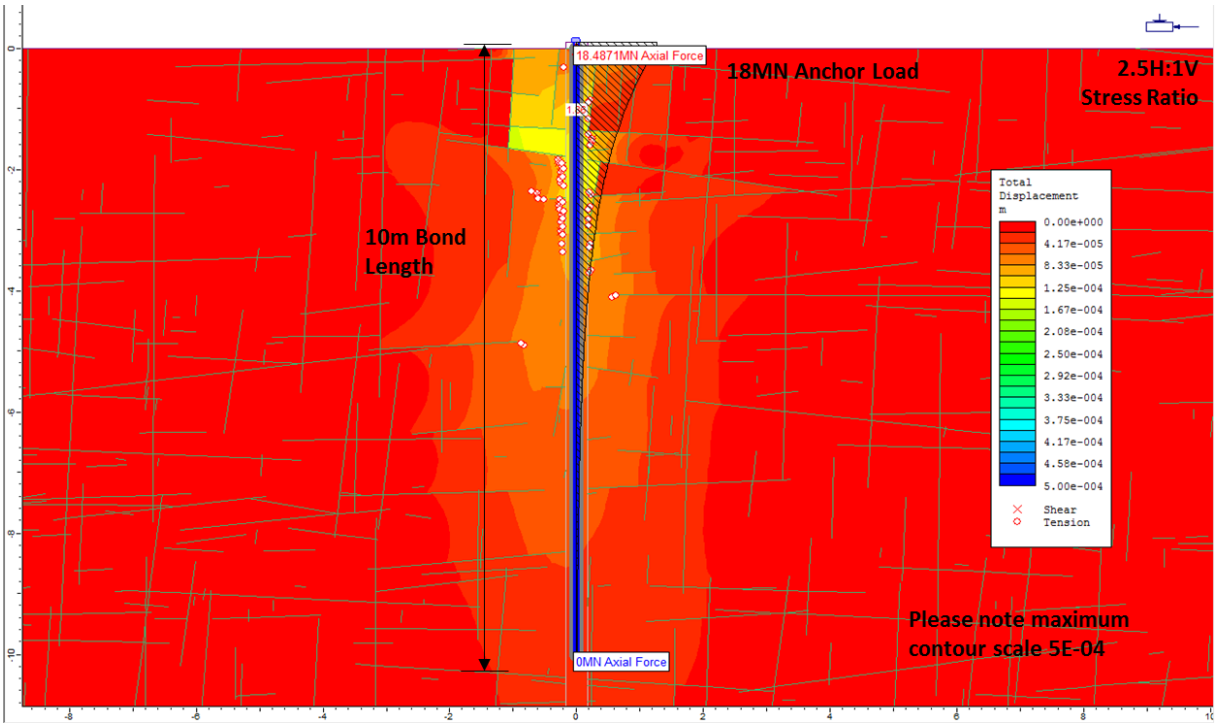

Figure 73– An example of calibration of a 10m length fully grouted bolt with non-persistent, subvertical-subhorizontal conjugate jointing and a 2.5H:1V stress ratio applied in the model. Applying the major principal stress in the horizontal direction limits dilation at the surface to less than 1mm at the surface at 18MN.

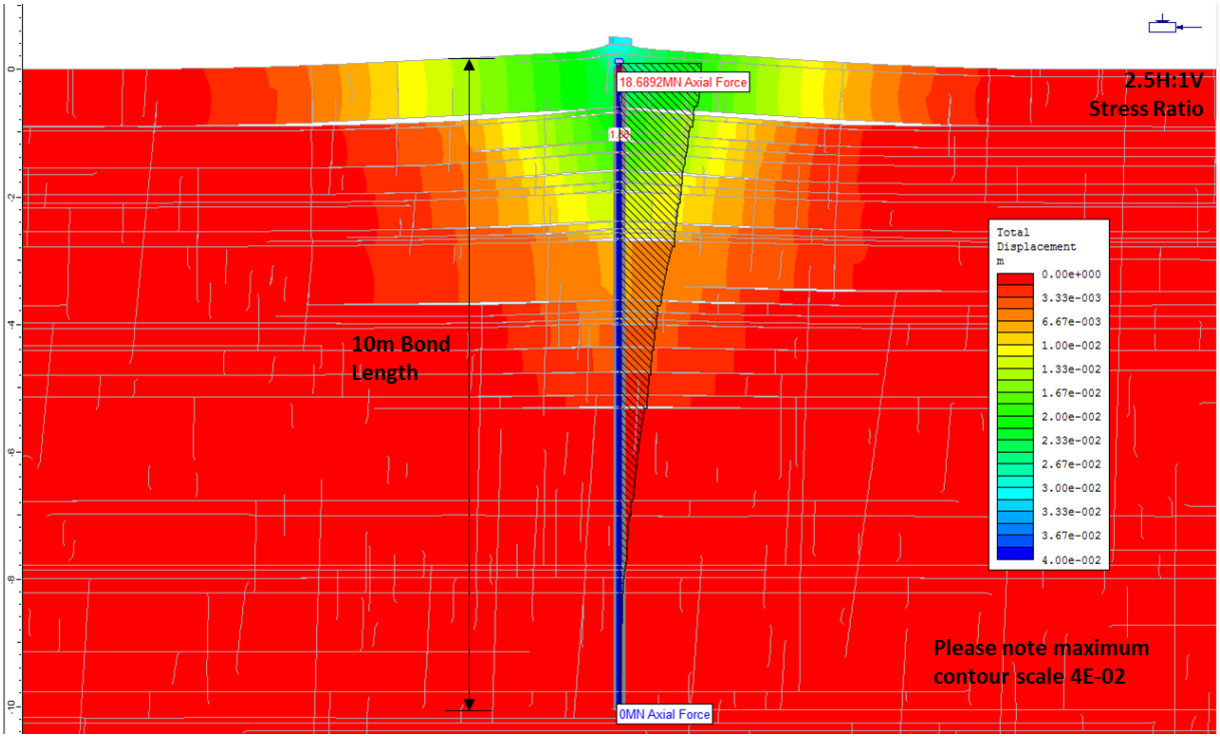

Figure 74– An example of calibration of a 10m length fully grouted bolt with persistent, sub-horizontal jointing and non-persistent sub-vertical jointing and a 2.5H:1V stress ratio applied in the model. Applying the major principal stress in the horizontal direction has less of an impact on dilation since clamped sub-vertical joints do not control the stability in this models

8.2.3. Designing the Free Stressing Length and Verification of Anchor Load Distribution

The previous two sections indicated that calibration of rock mass parameters should be completed on a dowel longer than 1.5m embedment since numerical simulations indicate that the failure mechanism observed may be different for this length of dowel compared to a 10m embedment dowel. This calibration should consider the discrete location of joints and in situ stresses if possible in the model. Once the model is calibrated, the synthetic rock mass parameters can be used at a larger scale to analyze more sophisticated anchor problems. Figure 75 provides a comparison between the 10m anchor length presented in Figure 72 to the same anchor with a four meter free stressing length. It is apparent for the 13MN anchor load step that deformation occurs in a very different manner based on the confinement provided by this free stressing length. At a load of 13MN about 5mm deformation is observed at the surface where the deformation observed in the model with the free length is less than 1mm. As the load is increased to 18MN, a failure cone develops in the upper 5m of the rock mass in the fully grouted model while the anchor with the free length has only minor tensile fracturing occurring next to the anchor bond. At a load of 25MN the anchor with the free stressing length fails as a result of mobilization of a "cone" of deformation initiating at the top of the free stressing length. At this load, considerable deformation is also observed in the fully grouted model and both anchors have effectively failed.

While 25MN seems like a very high test load, this is becoming the standard cable anchor capacity for the seismic upgrade of dams described in Chapter 2. Figure 76 shows the results of an anchor test completed on a 25MN capacity, 17m length test anchor at the Canning Dam site (Sinclair and Rodd, 2011). The anchor length comprises a 10m bond length and a 7m free stressing length. It is contended that even if anchors are not taken to failure, post-design validation can be completed by analyzing the deformational behaviour of the anchor, as shown in Figure 77. This figure presents numerical simulation of the rock mass behavior for the Canning anchor length. Minor tensile cracking is noted near the proximal end of the bond length in this model, however, dilation in this model is less than 1mm due to the confinement provided by the free stressing length. The load distribution in the anchor is similar to that observed in the Canning Dam test anchor with the point of zero load in the bond length at about 11m below the ground surface as shown in the right hand screenshot.

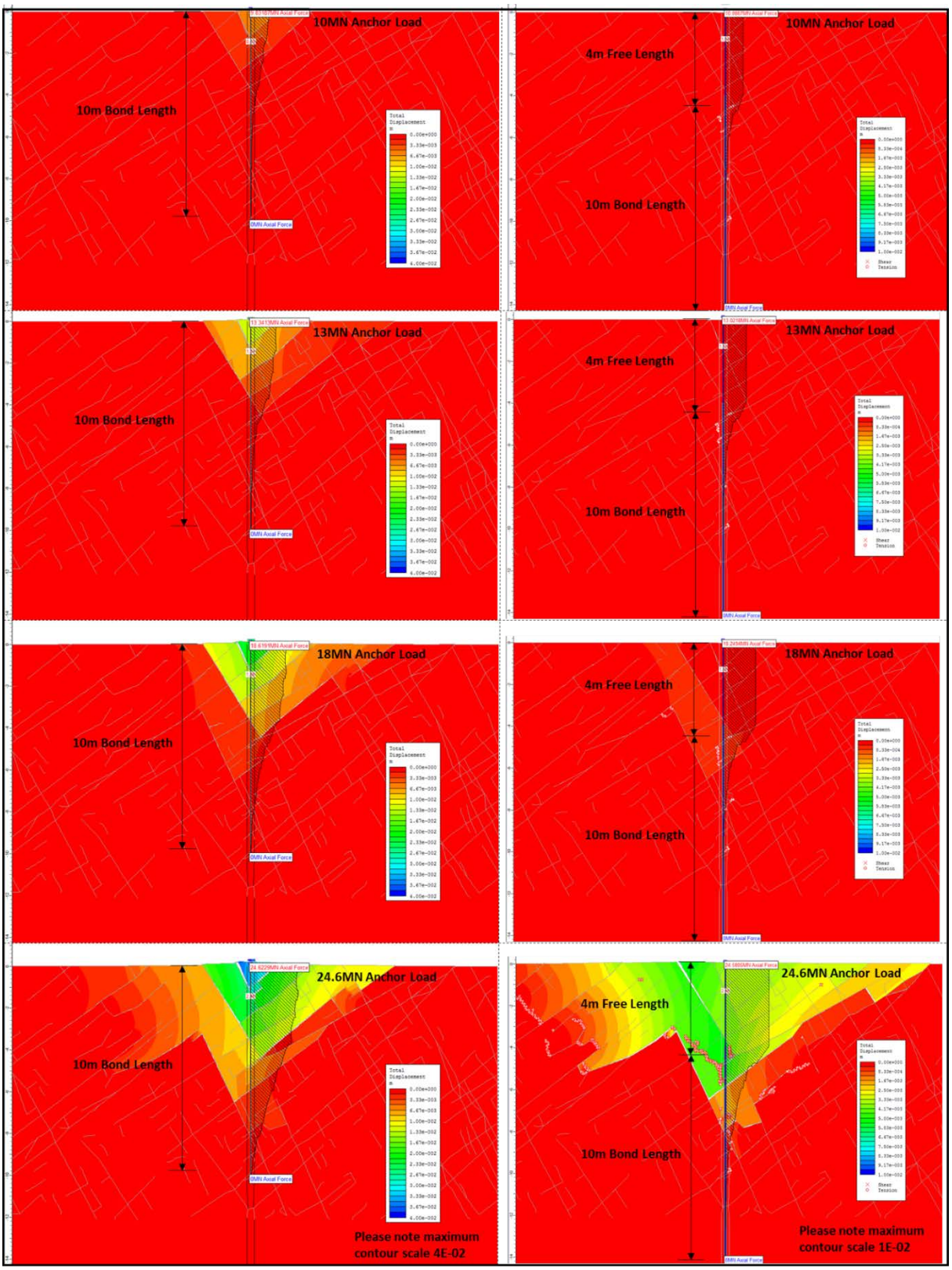

Figure 75– A comparison between the dilation observed for a 10m length fully grouted cable anchor compared to a 14m long anchor comprising a 10m bond length and a 4m free length. Please note the difference in scale between these two models.

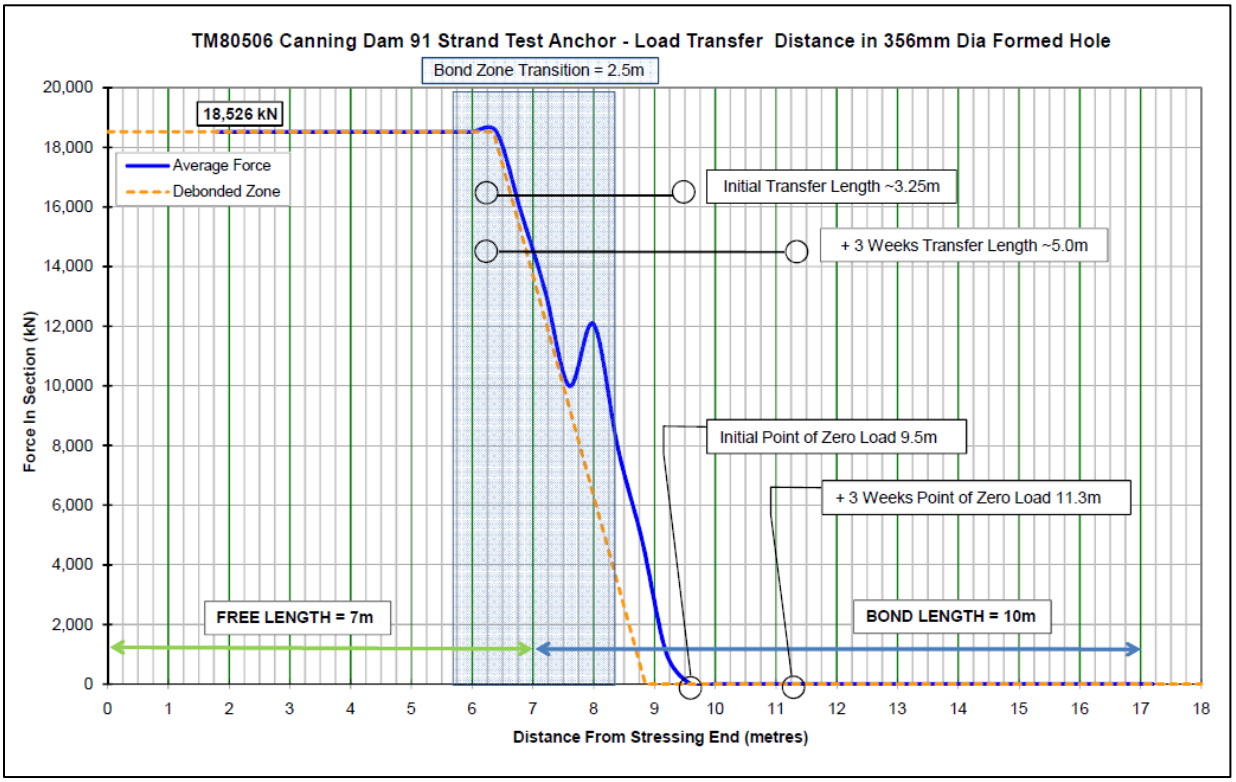

Figure 76– An example anchor test on a 17m length test anchor at the Canning Dam site. The anchor length comprises a 10m bond length and a 7m free stressing length (modified after Sinclair and Rodd, 2011)

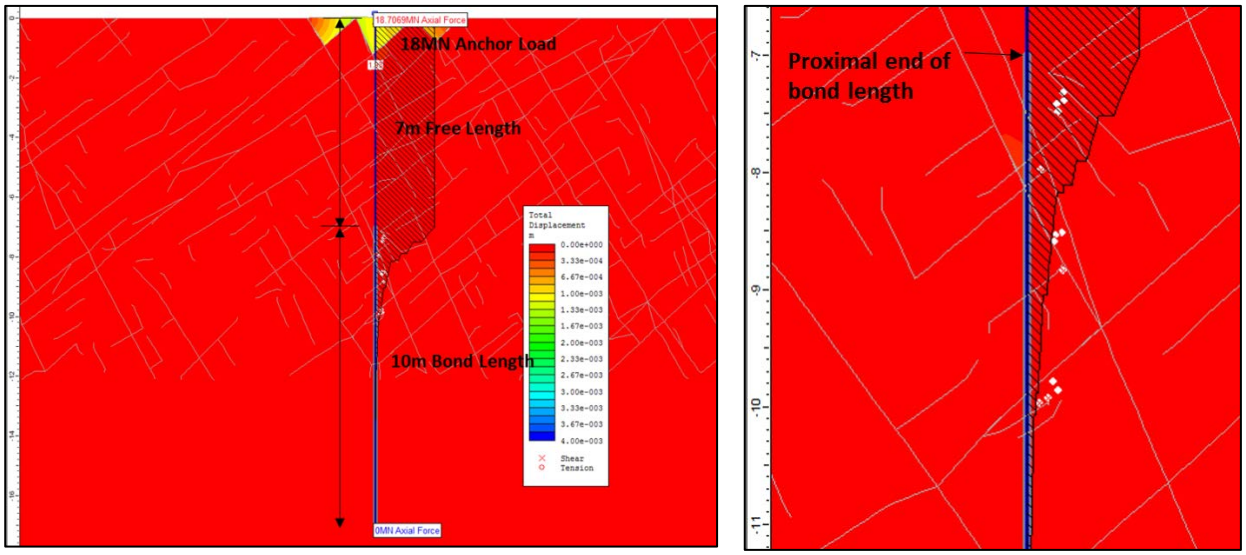

Figure 77– A numerical simulation of the rock mass behavior for a 17m length anchor with the anchor length comprising a 10m bond length and a 7m free stressing length. Minor tensile cracking is noted near the proximal end of the bond length in this model, however, dilation in this model is less than 1mm due to the confinement provided by the free stressing length. The load distribution in the anchor is similar to that observed in the Canning Dam test anchor with the point of zero load in the bond length at about 11m below the ground surface as shown in the right hand screenshot.

8.2.4. Group Effect and Confining Influence of Overlying Structure

Further to the design of single anchors, the numerical method can be used to model the complex interactions and load transfer from the structure to anchors / piles and the rock mass. Confinement provided by the overlying structure may have an influence on the failure mechanism observed in the models. Figure 78 provides two example foundation problems where overturning of concrete foundations were assessed.

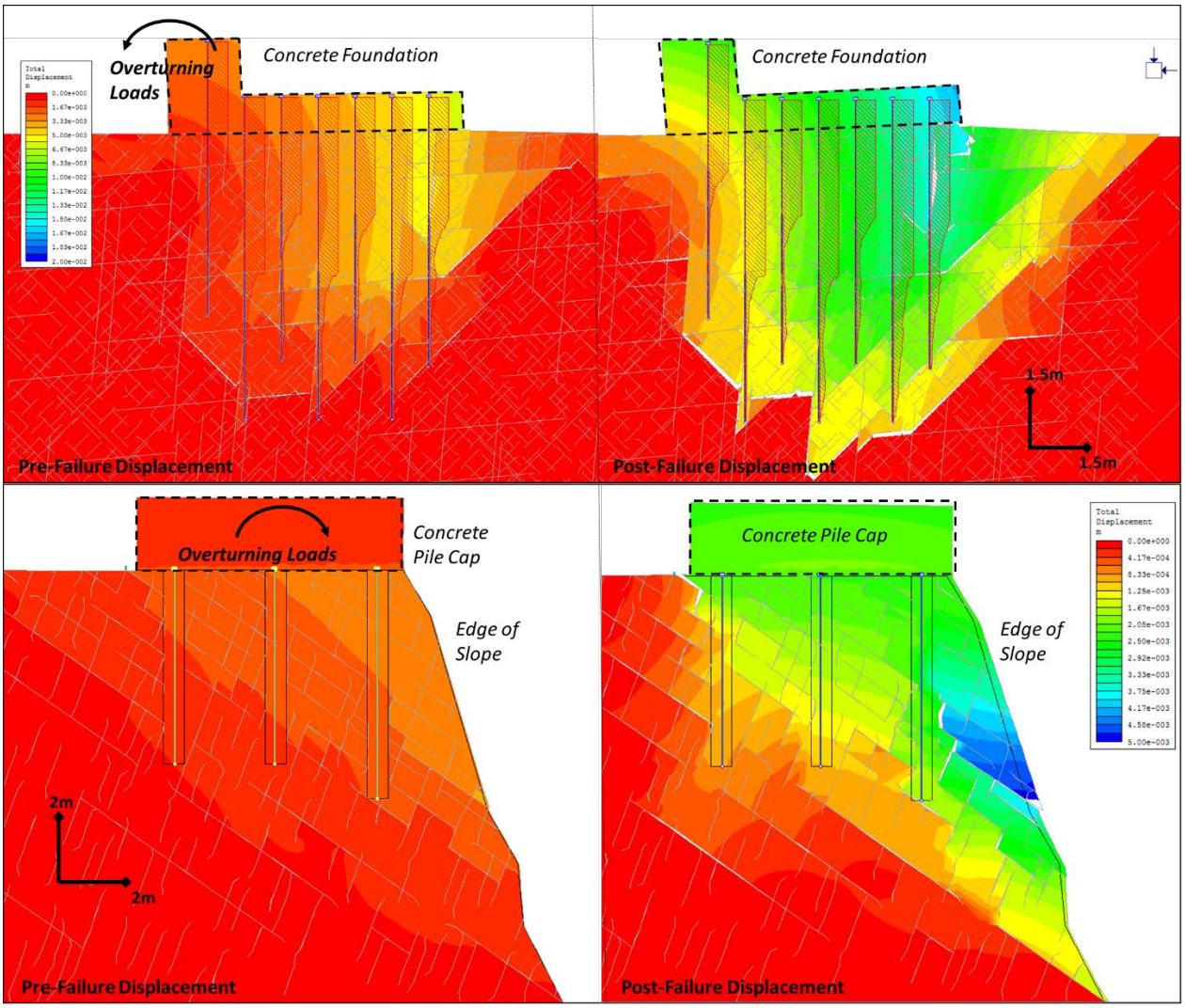

Figure 78– Examples of how structural interaction can be considered in anchor design; The upper two figures show displacement contours for overturning about the toe of a foundation, while the lower two figures indicate the "edge effect" or the influence of reduced confinement at the edge of a slope.

In the upper two figures, it is apparent that the overturning loads have an influence on the shape of deformation observed in the model due to compression in the rock mass at the toe of the

foundation and point of rotation. Similarly the overturning loads in the bottom two screenshots of Figure 78 provide an example of how lack of confinement on a slope may also have an influence on the stability of an anchor. In these models a complex distribution of compressive, shear and tensile forces are present in the rock mass. The numerical approach is much better at assessing these complex load distributions compared to limit equilibrium methods. At a minimum, the numerical method can be used to better understand the failure mechanism associated with foundation overturning loads, including anticipated stress distributions in the rock mass.

While it may be appropriate to assess the failure mechanism using one model iteration, in order to properly assess the stability of the foundations multiple DFN realizations are required to assess the failure load distributions associated with fracturing in the model. This concept is introduced in Chapter 5 and is also discussed in more detail below.

8.3 Incorporation of Reliability in the Assessment of a Foundation

8.3.1. Principles of Limit State Design

The principles of limit state design (LSD) stem from structural engineering with the limit state being the condition "*beyond which the structure no longer fulfils the relevant design criteria*" (Harrison, 2014). Two limit states are applicable for design; firstly the serviceability limit state (SLS), which is defined as "*conditions beyond which the specified service requirements are no longer met"* and the ultimate limit state (ULS) which is associated with collapse or other similar forms of structural failure (Harrison, 2014). Limit state design has been accepted in structural engineering design for some time and in the past 10 years design guidelines for incorporation of LSD in geotechnical engineering have been developed for seismic assessment of "lifeline" and "emergency route" bridges in British Columbia (BCMOTI, 2005). BC Hydro also has adopted similar performance criteria for large dams in BC.

Limit state design requires designers to account for variability in attributes such as applied loads, material properties and structural geometry and this variability is accounted for using probabilistic methods. The concept of reliability comes out of this probabilistic method which is defined in terms of a probability of structural failure.

In Europe, limit state design is being proposed for geotechnical design in recent revisions to Eurocode 7 (EC7), which is the reference design code for the European Union. Some difficulties have been faced with this new mandate since it is very difficult to incorporate the epistemic nature of rock mechanics parameters, traditional deterministic analysis, the observational approach, and engineering judgement in the new context of the EC7. Not only will EC7 require designers to distinguish between SLS and ULS for rock mechanics problems, it also requires designers to verify that no limit state is exceeded under design conditions (Harrison, 2014). Given the current lack of understanding of the cone pullout mechanism in the standard of practice, and the lack of consideration of deformation in the deterministic "pullout cone" method, the serviceability limit state will be very difficult to assess in anchor design.

Langford and Diederichs (2013) describe a proposed reliability based design approach for rock mechanics projects. The authors focussed on various parameters (such as UCS, and the Hoek-Brown parameters GSI and mi) associated with developing an equivalent continuum for the assessment and numerical simulation of the plastic zone radius and displacement in a tunnel. The authors addressed the uncertainty associated with a design in a quantitative sense and suggested a method for determining the probability of unsatisfactory performance. The authors' also noted that in addition to data collection and rock mass characterization, determination of potential failure mechanisms and statements of failure conditions (or criteria) are important components of the definition phase of the RBD method.

It is understood that factors such as tensile and shear strength are important considerations in anchor design and the variability or sensitivity in these parameters should be considered in design. However, for this section, tensile strength and strength softening parameters are not varied and the variation in anchor capacities are observed only due to the proximity of persistent joints to the anchor in different fracture set realizations. Chapter 5 has illustrated that the discrete location and interconnectedness of joints may have a significant influence on the capacity of a rock anchor. It is also contended that the failure mechanism of an anchor also changes with spacing and variation in the length of discontinuities.

8.3.2. Ultimate Limit State Analysis using DFN Based Methods

If limit state design methods are adopted it is considered essential that the data used for probabilistic assessment is properly characterized. This includes the strength, tensile fracturing, and deformational properties of the rock mass, as well as proper statistical characterization of the distribution of naturally occurring fractures in the rock mass. Chapter 3 has described the necessary geotechnical data collection requirements for DFN models and more detail and additional guidelines are provided by Elmo et. al. 2015 who note that variability or randomness of natural geological processes can be quantified by objective sampling through scanline and window mapping of rock exposures of various orientations. Variability cannot be characterized by stochastic models using probability theory if subjective sampling or unrepresentative spot mapping is carried out. This is a key consideration to adopting the limit state design method proposed in the new Eurocode 7 revision.

Despite attempts to make geotechnical design consistent with structural analysis using Limit States Design (LSD), Eurocode 7 does not provide standards for how calculations should be completed to assess the various anchor failure modes using the LSD. Bond and Harris (2008) note that "*no guidance is given in Eurocode 7 on how to design anchorages by calculation…. Presumably, calculations would need to consider all possible failure modes and compare these with the design anchor load derived from the ultimate and serviceability limit state verifications of the structure. In the absence of suitable guidance, we recommend that designs are based on testing instead.*" (Bond and Harris, 2008). Assuming that proper data collection is undertaken and a representative and calibrated DFN model has been developed, it is contended that a combined DFN-numerical models can be used to develop reliability curves for the use in limit states design. In this section, the ultimate limit state is selected for analysis since the serviceability limits are dependent on the performance requirements for a specific structure. The calibrated strength and softening parameters used in Chapter 5 were also used for this assessment.

The previous chapters have illustrated that the discrete location and interconnectedness of joints may have a significant influence on the capacity of a rock anchor. It is also contended that the failure mechanism of an anchor also changes with spacing and variation in the length of discontinuities. For the limit states assessment, a variation in fracture statistics (including both fracture intensity and trace lengths) were run and are summarized in Table 4.

Table 4. Foundation Variability using DFN Sections

Symbol and Number of Model Iterations		No. Sets *	P32	P21 Range**	Fracture Trace Length Distr. (in meters)**	
					Mean	Max
✕	10	4	7.5	10-13	0.4	2.3
■	10	2	4.5	6-7	0.4	2.3
□	10	2	4.5	6-7	0.4	2.3
▲	6	4	7.5	9-13	0.8	3.2
◆	3	4	7.5	11-13	1.3	4.2
●	2	4	15	22-27	1.3	4.6
●	2	4	3.75	6-8	0.4	1.8

**Only two sets with 45 degree conjugate jointing for '■', two sets with subvertical-subhorizontal conjugate jointing considered for '□'.*

***From 2D Cross Sections Cut from 3D DFN for Numerical Models*

Different DFN iterations were run to simulate the spatial variability of various structural domains in the rock mass which may be present across a large foundation area. The number of realizations run for each DFN were based on the conceptual spatial distribution of the domain across the foundation area. Ten realizations were run for the '□' domain which indicates that this domain is present for about 20% of the foundation area, where only two realization were run for the '●' domain which indicates that this domain is present for less than 5% of the foundation area. The different symbols indicate the different structural domains with the properties notes in Table 4. For statistically representative anchor values, more realizations should have been run for this conceptual exercise, however, this approach represents the likely distribution of test results if the entire foundation surface was tested randomly at set intervals. A total of 43 anchor simulations were completed across the seven geological domains.

Interpretation of anchor capacity across the foundation area can be completed using a number of different approaches. For example, the data could be lumped into one limit states design curve as shown in Figure 79. As shown in this figure the outlier capacities in Domain '●' represent the lowest values on the Relative Frequency vs. Ultimate Capacity curve. The "Inferior" Characteristic Value ($X_{k,inf}$) is calculated to be 0.4MN, which is represents by the lower 5% of the data as marked by the transparent grey shading on the graph. The mean value is represented by the peak on the capacity distribution curve.

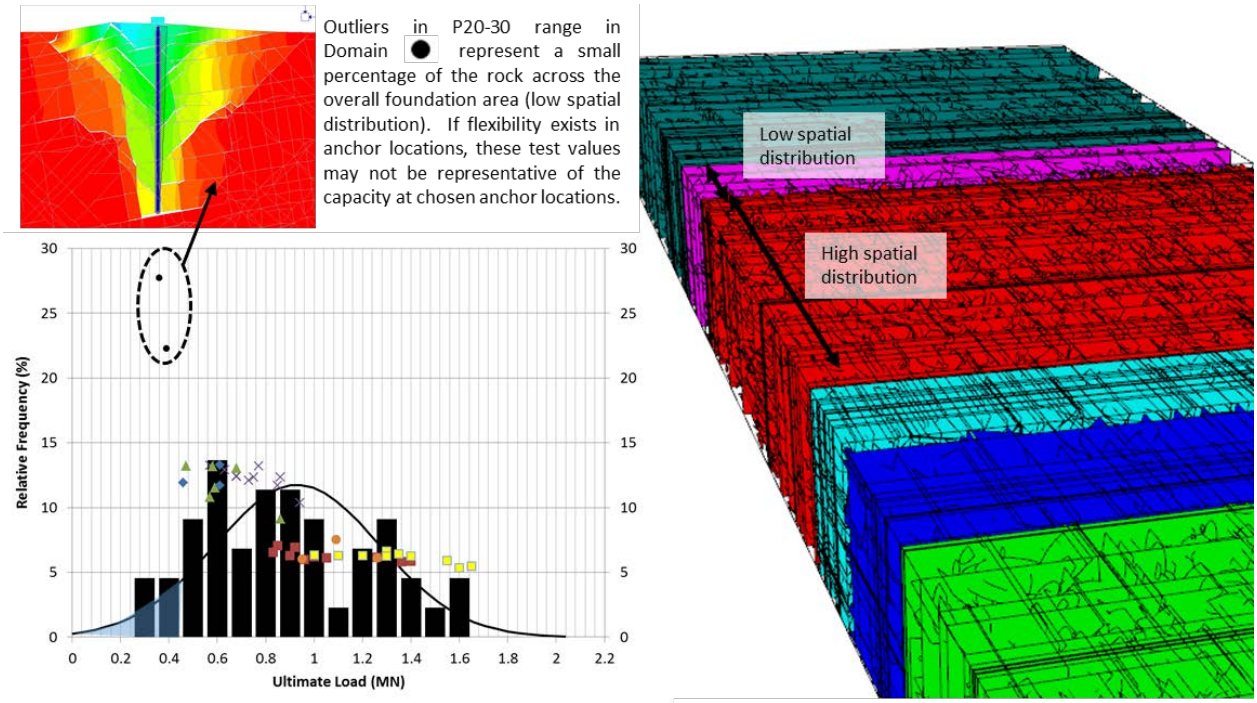

Figure 79 –Relative Frequency vs Ultimate Anchor Capacity Plot for All 43 Realizations; Mean Capacity Value of 0.93MN is shown by peak of Load Distribution Curve and the 'Inferior' Characteristic Value is 0.4MN for the data.

A conservative designer may selected the $X_{k,inf}$ value as a representative design value. Other designers may compare this ultimate capacity curve to an ultimate load distribution curve and assess a probability of failure. The problem with this approach is that data with different geological compositions (possibly due to rock type or geological origin) is being lumped into the same dataset. This creates an artificially low $X_{k,inf}$ value due to the low lying outliers present in Domain '●', which has a low spatial distribution. For this fractured or blocky rock the capacity of an anchor will likely be governed by the frictional properties of joints, and anchor capacities may be less than 0.4 MPa. Conversely, in rock masses with more widely spaced discontinuities strength will be developed by intact rock bridges governed by the length or persistence of fractures. This is observed in two joint set networks where P21 intensity values were as little as 6 (see symbols '■' and '□'). The anchor capacity that could be considered in a design is likely greater than 0.8 MN.

If good geological understanding is developed for the site then different strength estimate ranges could be applied at different areas of the foundation, as shown by the different structural domains in Figure 80. Where there is some flexibility in the location of anchors across a foundation, the higher quality rock mass such as Domains '■' ,'□' or '×' may be selectively chosen across the foundation. In this conceptual foundation model this higher quality rock mass represents 70% of

the foundation area in the model. Therefore, where some risk can be accepted going into construction, it may make sense to design for these upper range values instead of combining all of the rock across the foundation into one dataset. Alternatively, different anchor groups could be designed with different embedment length depending on the domain that each anchor lies across the foundation. If this is the case, the mean or inferior characteristic values provided in Figure 80 could be used to design different anchor length across the foundation. If poorer quality rock such as that noted in Domain '●' manifests with a greater spatial extent than expected a contingency plan could be in place to increase the anchor lengths throughout selected locations of the foundation. As with the current practice of anchor design, a plan for testing should also be devised to reveal if the actual anchor behaviour falls within acceptable limits, and monitoring should be completed at early stages of anchor installations so design adjustments can be made, if required, during construction.

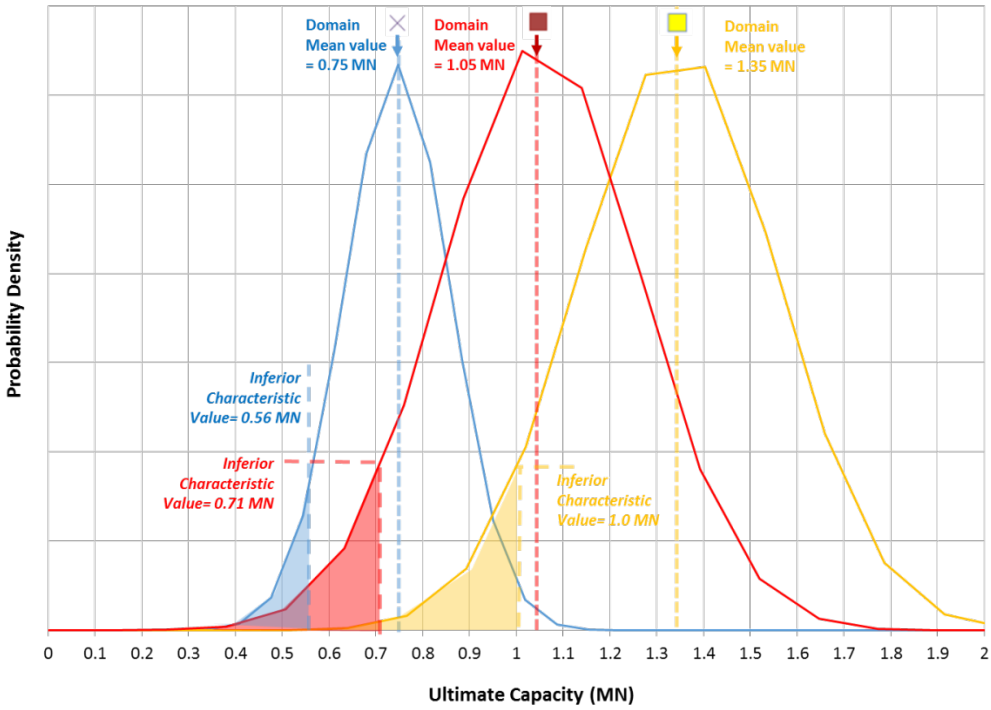

Figure 80 –Structural Domains Specific Relative Frequency vs Ultimate Anchor Capacity Plots

If a reliability based design approach is adopted it is important that the geological data is included with the histograms and resistance curves so various geological assumptions can be verified by an Engineering Geologist during construction.

8.3.3. Discussion on Anchor Serviceability Limit State and Damage

It should be recognized that up to this point in this thesis the design anchor capacity has been related to the ultimate failure or ultimate limit state of the rock mass. However, the previous chapters outlined that damage to the rock mass prior to failure is progressive and tensile fracturing may initiate at loads as little as 30-40% of the ultimate anchor load. Examples of pre-failure deformation are provided in Figure 81, where a figure from Wyllie describing failure mechanisms is overlain on an ELFEN model screenshots. If a Factor of Safety of 3 is employed in working stress design, the in-elastic deformation in the rock mass should be limited, but if lower resistance factors are used in limit states design, the performance of the anchor may be affected by tensile cracking processes. Crack initiation prior to failure may lead to serviceability issues for the structure, particularly if in-elastic deformation occurs in the rock mass.

Uncertainty remains inherent in our lack of understanding of tensile crack initiation at low confinement and strength softening and dilation of the rock mass surrounding a loaded rock anchor. It is contended that these crack initiation, crack propagation and strain softening properties can be determined from full scale pullout testing, however the long term performance of damaged rock due to weathering and fatigue from cyclical loading is also uncertain. For this reason, it is not recommended that in-elastic damage of the rock mass is permitted in the assessment of allowable deformations in the assessment of the serviceability limit state until a better understanding of the tensile fracturing processes in the rock mass are understood. In addition, the influence of blast damage and construction disturbance of the rock are important considerations that are not discussed in this thesis but may have an influence on the stability and serviceability of a foundation anchor. More research is required in this area of study.

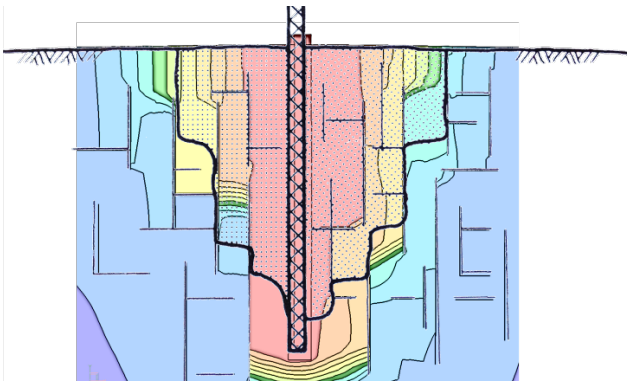

Figure 81 –ELFEN Plots overlain on failure mechanism descriptions from Wyllie (modified after Wyllie, 1999)

9 CONCLUSIONS AND RECOMMENDATIONS

9.1 Research Conclusions

The standard approach for design against the Mode 4 rock mass failure mechanism is to assume that the dead weight of an inverted cone of rock provides resistance to failure. Different cone breakout angles and initiation points are based loosely on the "competency" of the rock, judged by the designer without clear guidance by code, and for this reason the design of rock anchors is usually only undertaken by experienced geotechnical engineers. Since there is significant uncertainty and lack of knowledge associated with the cone pullout mechanism a Factor of Safety of 3 is recommended for this design approach, which is considered suitably conservative (Bruce, 1976; Bruce, 2013).

For simple anchor designs, the generally conservative standard of practice may calculate anchor lengths that are reasonable for many applications and it should be recognized that by going to a more sophisticated analysis approach requires more data for calibration. Proper data collection is more expensive and for simple anchor problems it may not make sense to move toward a numerical approach to anchor design.

It should also be noted that the dead weight cone assumption may be valid for rock masses where joint lengths are continuous or fully persistent. This assumption was verified in Chapter 7 using Fracman to calculate the of removable wedges across a foundation surface and comparing the distribution in weights to design curves developed using the dead weight assumption. It is contended that Fracman or other DFN models can be used as a screening level analysis tool to assess the probability of encountering a wedge within the proposed area of anchorage, prior to undertaking geo mechanical modelling simulations.

Where the probability of encountering a wedge is low, and jointing in the rock mass is observed to be non-persistent, a significant reduction in anchor lengths may be realized by developing site specific strength parameters for rock strength and analyze the failure mechanism associated with anchorage. The rock bridges between these non-persistent joints were shown in this thesis to have an influence on anchor capacity, as intact rock cohesion or tensile strength provides a significant measure of strength. The dilation of joint roughness and the frictional properties of joints also contribute to the rock mass failure mechanism.

Since the preliminary work of Bruce (1976) it has been well understood that jointing has an influence on the behaviour of the rock mass. More recently, Bruce noted that the deformation behaviour of the rock mass is also an important consideration that is often overlooked. In the proceedings of "*Ground Anchorages and Anchored Structures*" edited by Littlejohn (1997), Bruce provides commentary in a discussion session on the load transfer mechanism of anchors:

"*So, in all the anchor tests that I have done I have only ever mentioned the E value twice, and yet we are all saying that it is extremely important. So, I raise the question, perhaps if we truly believe confinement is important, then what are we going to do about it?*"

In response to Bruce, the numerical simulations summarized in this research have confirmed a number of controls and suspected considerations in the design of anchors. More specifically, this research discussed the influence of jointing by presenting the results of anchor capacity simulations where joint persistence and orientation were scaled and adjusted. Although not presented in this research, additional fracture network statistics such as the number of joint sets, joint spacing (particularly important in bedded in sedimentary rock) and fracture termination should also be considered. By using numerical simulations that allow the load transfer mechanism from the anchor to the rock mass to vary with stiffness and the discrete locations of joints in the rock mass, the failure mechanism of the rock mass under the applied loading can be better understood.

A better understanding of the Mode 4 rock mass failure mechanism and load transfer mechanism may allow for a significant reduction in anchor lengths for large dam structures. In addition, the numerical method developed in this thesis can also be used as a tool to confirm equivalent cone strength values applied to assumed cone breakout geometries. It is recognized that results from field testing of anchors also results in variability. It is contended that this uncertainty or variability is associated with pre-existing fractures in the rock mass which can be quantified using probabilistic DFN-based approach.

A summary of the current state of practice and the numerical analysis is presented in this thesis. In Chapters 1-2 of this thesis the cone pullout problem was introduced and the current standard of practice of anchor design was reviewed. Chapter 3 provided a review of mapping requirements for use of the DFN method. Chapters 4-8 were the research chapters in this thesis which can be summarized as follows;

In Chapter 4, the suitability of the Phase2 finite element code by RocScience, with joints inserted in the mesh domain, was validated and the calibration process required to model the rock cone

pullout failure mechanism and dilation prior to failure was described. It should be recognized that the numerical model iterations presented using this method were run with the same Mohr Coulomb plasticity parameters, and the observed variation in pullout capacities were a result of variation in (P21) joint intensity or proximity of individual joints in the Finite Element model. This illustrates the importance of explicit representation of joints in the numerical simulation of anchor capacity.

Chapter 5 investigated the influence of DFN statistics on modelled anchor capacity. Specifically, the influence of fracture intensity (P21), the interconnectedness of jointing and joint persistence, and joint orientation are observed. Cracking of "rock bridges" was also observed in a numerical model (D21). This damage represents breakage of intact rock and where little damage is observed in a model, dilation occurs as a consequence of slippage along joints due to the interconnected nature of the rock mass. The influence of confinement, in particular the influence of closely spaced testing jack outriggers, was also investigated and models showed that the testing apparatus used may have an influence on the failure mechanism observed in field tests.

Chapter 6 investigated damage of intact rock by adjusting fracture energy parameters in the hybrid FEM-DEM model ELFEN 4.4.0 by Rockfield. The Rotating Crack (Rankine) failure parameters, notably E, σ_t, G_F, were adjusted and the load transfer mechanism and damage associated with loading were assess for a variety of input parameters. The mohr-coulomb plasticity parameters were left constant in the models which illustrates that fracture energy is an important component of the model. In this section, the progressive nature of the cone pullout mechanism and damage is also validated using the code and the influence of intact rock modelling parameters is also investigated.

Chapter 7 outlines the difficulties with three dimensional analysis of the cone pullout problem which are investigated using Fracman and 3DEC. The limit equilibrium block method in Fracman proved to be useful in analysing the likelihood or probability of encountering a fully removable block within the area of anchorage of a foundation. By analyzing the apex angle of removable blocks, the capacity across the foundation could be assessed assuming that these blocks are rigid. This data was compared to the Littlejohn and Bruce dead weight cone assumption and it was shown that for rock masses with persistent joints the dead weight cone assumption may be suitably conservative. However, where intact rock exists more sophisticated models are required or tensile strength may need to be applied to the outer surface of the limit equilibrium blocks. In this section tensile breakout was investigated using 3DEC and limitations are discussed. Due to the longer run-times and the difficulties with manual meshing and block formation of non-persistent blocks in 3D

models it is recommended that alternative 2D methods are used to represent 2D problems. This section provides an alternative where cross sections are cut parallel and perpendicular to the stability controlling joint sets. An advantage to doing this is that models can be calibrated at a 2m test anchor scale and the same mesh size can be used when upscaling to larger anchor problems.

Finally, Chapter 8 presents a methodology and flow charts for incorporation intended to provide some guidance on the incorporation of models in design. 2D modelling iterations presented in this thesis proved be fast enough that this methodology can incorporate multiple Discrete Fracture Network (DFN) realizations for efficient integration with reliability based design methods.

Specifically, this work showed that the dead weight cone assumption is very conservative and the numerical method provides an alternative analysis method that can reproduce results similar to those observed in field testing. In the current design practice, experienced practitioners apply some equivalent strength to the outer surface of the pullout cone to make up for the difference in strength between the "dead weight" cone method and observations from field tests. However, the methods used to analyze this strength assume that rock mass deformations and strength are homogenous and isotropic. It is contended that the numerical simulations presented in this thesis are suitable for confirming that equivalent strength estimates reflect the possibility of crack initiation within the envisaged cone surface. Furthermore, rock mass properties can be calibrated on shorter anchors where failure can be observed, and these intact rock and joint frictional properties can be used to analyze more sophisticated applications such as the group effect of anchors.

Further engineering applications for the combined DFN-numerical approach are also outlined in Chapter 8. It is contended that the numerical method presented is capable of capturing the load transfer mechanism (both shear and tensile loading) and confinement provided by the overlying structure to the rock mass in anchor calculations. Consideration of a more global influence of overturning loads and confinement at depth may allow for designers to better understand the design considerations for anchors.

Numerical modelling at a larger scale could prove to be highly beneficial in assisting designers in understanding this complex load transfer mechanism, and a better understanding may help lead to less conservative anchor and pile designs in the future.

9.2 Recommendations for Further Studies

Uncertainty remains inherent in our lack of understanding of tensile crack initiation at low confinement and strength softening and dilation of the rock mass surrounding a loaded rock anchor. In 1979, Littlejohn and Bruce noted that there is a "*dearth of data on anchor failures in the rock mass"*, and in 1993 Carter presented the same message.

A literature review and experience by this thesis author in Canadian engineering practice suggests that practitioners often forgo full scale testing to calibrate rock mass properties and use conservative estimates for rock mass strength developed for other applications. While "anchor testing" is almost always completed during to validate the pullout strength of the grout and steel using ASTM method designation 4435-84, it should be recognized that this testing methods does not test the Mode 4 rock mass failure mechanism. This is due to the fact that the recommended test setup using this method provides a reaction force within the zone of rock mass dilation. Where the opportunity exists, it is recommended that practitioners take the opportunity to test the rock mass surrounding an anchor so the failure mechanism associated with anchors can be better understood. It is recommended that testing is completed with outriggers placed well outside of the influence of the anchor load transfer to allow for rock mass dilation to occur.

In addition, for anchors greater than 2m embedment the failure mechanism may be different than that observed in shallower anchor installations due to increased confinement at depth. This is illustrated in numerical simulations presented in this thesis and this should be investigated in the field. It is understood that the practicality of running such tests to failure may be difficult but the data provided by these tests would be very useful in advancing the standard of practice.

If feasible, it would be very useful to instrument such installations with load gauges so the load transfer mechanism can be analyzed during the test. Furthermore, the onset of damage could also be monitored using acoustic emissions which may allow for the three dimensional cracking behaviour to be mapped. It is also considered essential that the discrete locations of joints are mapped during such a test and the load at which various joints are observed to dilate are also important considerations. Using this information, numerical models can be calibrated and the tensile fracturing and dilation nature of the rock mass could be better understood.

At this time 3 dimensional numerical models are not considered practical for analyzing large scale anchor problems with multiple DFN realization and a fine mesh. This is in part due to the time it takes to develop a 3D model with non-persistent joints. In the future, it would be useful for industry to produce 3D models with user-friendly interfaces for incorporating DFN's into numerical simulations.

At the current time, significant manual processing is required to clean fracture networks and produce quality meshes and it would be very useful if this procedure could be more automated. Current research is ongoing for simulating brittle fracture in 3D at the laboratory scale using PFC3D, ELFEN3D, and 3DEC with Trigon Logic and once these fracture processes can be simulated in an efficient manner research combining in-situ anchor testing with a combined DFN-3D Numerical anchor simulation would be interesting to study.

References

1. Anon (1996) Rock foundations – technical engineering and design guidelines as adapted from the US Army Corps of Engineers. No. 16, ASCE Press. New York. pp 129

2. ASTM 4435-84 (2002) Standard test method for rock bolt anchor pull test. pp 662-666

3. R. Ballarini, S.P. Shah and L.M. Keer (1986) Failure characteristics of short anchor bolts embedded in a brittle material. Proceedings of the Royal Society of London, A404. pp 35-54

4. Bandis, S.C. (1993) Engineering properties and characterization of rock discontinuities, in Comprehensive Rock Engineering: Principles, Practice and Projects (ed. J.A. Hudson) Vol. 1. Pergamon Press, Oxford. pp 155-83

5. Barton, N.R. and Choubey, V. (1977) The shear strength of rock joints in theory and practice. Rock Mech. 10(1-2). pp 1-54

6. Barton, N.R. and Bandis, S. (1983) Effects of block size on the shear behaviour of jointed rock. Issues in Rock Mechanics - Proc. 23rd US Symp. on Rock Mechanics, Berkeley, CA, Soc. Mining Eng. of AIME. pp 739-60

7. Barton, N. and E. Quadros (2014) Anisotropy is everywhere, to see, to measure and to model. Rock Mechanics and Rock Engineering 48. pp 1323-1339

8. Bedi and Orr (2014) On the applicability of the Eurocode 7 partial factor method for rock mechanics. Rock Engineering and Rock Mechanics: Structures in and on Rock Masses. pp 1517-1523

9. Bedi, A., & Harrison, J. P. (2013). Characterisation and propagation of epistemic uncertainty in rock engineering: A slope stability example. Rock Mechanics for Resources, Engineering and Environment, 105-110.

10. British Columbia Ministry of Transportation (2005) Seismic Retrofit Design Criteria Supplement, June 2005

11. British Columbia Ministry of Transportation (2007) Bridge Standards and Procedures Manual, Volume 1 Supplement to the Canadian Highway Bridge Design Code S6-06, August 2007

12. Bond and Harris (2008) Decoding Eurocode 7, London: Taylor & Francis, 616pp

13. Brown D.G. (1970) Uplift capacity of grouted rock anchors, Ontario Hydro Research Quarterly, 22 (4). pp 18-24

14. Brown, E. T. (2015) Rock engineering design of post-tensioned anchors for dams – a review. Journal of Rock Mechanics and Geotechnical Engineering, 7(1). pp

15. Brown, E. T. Carvalho, J. Panton, B. (2015). Uncertainty in the design of post-tensioned rock anchors. Proceedings of the 13th ISRM Congress. Montreal, May 10-13th. Paper 711.

16. Bruce, D.A. (1976). The Design and Performance of Pre-Stressed Rock Anchors with Particular Reference to Load Transfer Mechanisms. Ph.D. Thesis, University of Aberdeen, Scotland, Oct. 1976. Reproduced by EPRI publication (Technical Report No. EL-3777). Load Transfer Mechanisms in Rock Sockets and Anchors. pp 31-42 142-143, 288-315, 440-454

17. Bruce and Wolfhope (2007) Rock anchors for North American dams: The National Research Program bibliography and data base. Ground anchorages and anchored structures in service, Proceedings of the International Conference, London, Thomas Telford, London (2007), pp. 121–131

18. Bruce and Wolfhope (2012) "Specialty construction techniques for dam and levee remediation. Chapter 6 - Prestressed rock anchors. PP 334-380. *Retrieved from http://ezproxy.library.ubc.ca/login?*"

19. Bruce, D.A. (2013) A Review of Specialty Geotechnical Construction Techniques for American Dams and Levees. International Commission on Large Dams, ICOLD 2013 International Symposium - Changing Times: Infrastructure Development to Infrastructure Management, Seattle, WA, August 12-16. pp 11

20. Bruce D.A., Fiedler W.R., Randoph M.D., Sloan J.D. (1991) Load Transfer Mechanisms in High Capacity Prestressed Rock Anchors for Dams. Association of State Dam Safety Officials, 8th Annual Conference, San Diego, CA. September 29 - October 2, 1991. pp 15

21. Carter T.G. (1995) Observations on cone pull-out behavior in very weak rock. In Anchors in Theory and Practice, Widmann (ed.), pp 17-23

22. Chong W.L., Haque A., Ranjith P.G., Shahinuzzaman A. (2011) Effect of joints on p–y behaviour of laterally loaded piles socketed into mudstone, International Journal of Rock Mechanics and Mining Sciences, Volume 48, Issue 3, April 2011. pp 372-379

23. Coates D.F., Yu Y.S. (1970) Three-dimensional stress distributions around a cylindrical hole and anchor. Proceedings of the 2nd Congress, International Society for Rock Mechanics, Belgrade. pp 175–182

24. Cundall P.A. (1971) A computer model for simulating progressive, large scale movements in blocky rock systems, Proc. Symp Int. Soc. Rock Mechanics, Vol. 1.

25. Dados (1984) Design of anchors in horizontally jointed rocks. Journal of Geotechnical Engineering, ASCE, 110 (11). pp 1637–1647

26. Diederichs M.S. (1999) Instability of hard rockmasses: the role of tensile damage and relaxation PhD Thesis University of Waterloo, Waterloo, Canada

27. Dershowitz, W.S. (1984) Rock Joint Systems. Ph.D. Dissertation, Massachusetts Institute of Technology, Cambridge, MA.

28. Rockfield Software Ltd., (2004) ELFEN 2D/3D numerical modelling package, Swansea, UK

29. Elmo (2006) Evaluation of a hybrid FEM/DEM approach for determination of rock mass strength using a combination of discontinuity mapping and fracture mechanics modelling, with particular emphasis on modelling of jointed pillars , PhD thesis, University of Exeter, Cornwall

30. Elmo and Stead (2010) An integrated numerical modelling – discrete fracture network approach applied to the characterisation of rock mass strength of naturally fractured pillars Rock Mechanics and Rock Engineering, 43. pp 3–19

31. Elmo D., Schlotfeldt P., Beddoes R., and Roberts D. (2011) Numerical simulations of scale effects under varying loading conditions for naturally fractured rock masses and implications for rock for rock mass strength characterization and the design of overhanging rock slopes. Proc. 45th US Rock Mechanics Symposium, San Francisco, CA, June 27–30, 2011.

32. Elmo D., Stead D., and Rogers S. (2015) Guidelines for the quantitative description of discontinuities for use in Discrete Fracture Network Engineering. Proceedings of the 13th ISRM Congress. Montreal, May 10-13th. Paper 587.

33. Fairhurst C. & Crouch S.L. (1977) Design Methods in Rock Mechanics, Proceedings of the 16th Symposium on Rock Mechanics, Minneapolis, 22-24 September 1975. New York: ASCE. pp 151-160

34. Fang Z., and Harrison J.P. (2002) Development of a local degradation approach to the modelling of brittle fracture in heterogeneous rocks International Journal of Rock Mechanics and Mining Sciences, 39 (4). pp 443–457

35. Farmer I.W. (1975) Stress distribution along a resin grouted anchor International Journal of Rock Mechanics and Mining Sciences and Geomechanics, 12 (11). pp 347–352

36. Feng, X. T., & Hudson, J. A. (2011). Rock engineering design. CRC Press/Balkema.

37. Gao, F. (2013) Simulation of failure mechanisms around underground coal mine openings using discrete element modelling. PhD. Simon Fraser University, Burnaby

38. Gao, F., Stead, D., & Coggan, J. (2014). Evaluation of coal longwall caving characteristics using an innovative UDEC Trigon approach. Computers and Geotechnics, 55, 448-460.

39. Golder Associates (2015) Fracman Version 7.4 Geomechanics Edition

40. Goodman R.E., Taylor R.L., Brekke T.L. (1968) A model for the mechanics of jointed rock. Journal of the Soil Mechanics and Foundation Division, ASCE, 94 (4). pp 637–660

41. Hadjigeorgiou, J. & Harrison, J. P. (2011). Uncertainty and sources of error in rock engineering. In Q. Qian & Y. X. Zhou (eds), Harmonising Rock Engineering & the Environment, Proceedings of the 12th Congress, International Society for Rock Mechanics, pp. 2063-2067

42. Hamdi, P., Stead, D., & Elmo, D. (2014). Damage characterization during laboratory strength testing: A 3D-finite-discrete element approach. Computers and Geotechnics, 60. pp. 33-46

43. Hammah R.E., Yacoub T.E., Corkum B., Wibowo F., Curran J.H. (2007) Analysis of blocky rock slopes with finite element shear strength reduction analysis. Proceedings of the 1st Canada–US Rock Mechanics Symposium. E. Eberhardt, D. Stead, T. Morrison (Eds.), Vancouver, Canada. pp 329–334

44. Hammah R.E., Yacoub T.E., Corkum B., Curran J.H. (2008) The practical modelling of discontinuous rock masses with finite element analysis. Proceedings of the 42nd US Rock Mechanics Symposium and 2nd US–Canada Rock Mechanics Symposium. San Francisco, USA

45. Harrison J.P. (2014) Eurocode 7 and rock engineering: current problems and future opportunities. Rock engineering and rock mechanics: structures in and on rock, Proceedings of Eurock 2014, ISRM European Regional Symposium, Vigo, CRC Press/Balkema, Leiden, pp 1531–1536

46. Havaej, M., Stead, D., Mayer, J., & Wolter, A. (2014, August). Modelling the relation between failure kinematics and slope damage in high rock slopes using a lattice scheme approach. In 48th US Rock Mechanics/Geomechanics Symposium. American Rock Mechanics Association.

47. Hobst and Zajic (1977) Anchoring in rock Elsevier, Amsterdam

48. Hoek E., Brown E.T. (1980) Empirical strength criterion for rock masses. Journal of the Geotechnical Engineering Division, ASCE, 106 (9) (1980), pp 1013–1035

49. Hoek E. (1983) Strength of jointed rock masses Geotechnique, 33 (1). pp 187–223

50. Hoek E., Kaiser P.K., Bawden W.F. (1995) Support of underground excavations in hard rock. Taylor & Francis/A.A. Balkema

51. Hoek, E. and Brown, E.T. (1997) Practical estimates of rock mass strength. Int. J. Rock Mech. Min. Sci., 34. pp 1165-1186

52. Hoek E., Carranza-Torres C.T., Corkum B. (2002) Hoek-Brown failure criterion – 2002 edition Proceedings of the 5th North American Rock Mechanics Symposium. Toronto, Canada. pp 267–273

53. Hoek, E. and Marinos, P. (2006). A Brief History of the Hoek-Brown Failure Criterion, unpublished document. *Retrieved from Hoek's Corner at http://www.rocscience.com*

54. Hoek, E., Carter, T.G., and Diederichs, M.S. (2013), Quantification of the Geological Strength Index Chart. 47th U.S. Rock Mechanics / Geomechanics Symposium, June 23 - 26, 2013 , San Francisco, California

55. Hoek E. and Martin C.D. (2014) Fracture initiation and propagation in intact rock — a review. J. Rock Mech. Geotech. Eng., 6 (4). pp. 287–300

56. Hudson, J. A., & Feng, X. T. (2015). Rock engineering risk (Vol. 1). CRC Press.

57. Hyett A.J., Bawden W.F., Macsporran G.R., Moosavi M. (1995) A constitutive law for bond failure of fully-grouted cable bolts using a modified Hoek cell. International Journal of Rock Mechanics and Mining Sciences, 32 (1). pp 11–36

58. Hyett A.J., Moosavi M. , Bawden W.F. (1996), Load distribution along fully grouted cable bolts, with an emphasis on cable bolt reinforcement, Int. Journal of Numerical and Analytical Methods In Geomechanics. 20. pp 517-544

59. Ismael, N. F., Radhakrishna, H. S. and Klym, T. W. (1980), "Uplift Capacity of Anchors in Transmission Tower Design", IEEE Transactions on Power Apparatus and System, Vol.PAS-98, No.5, pp.1653-1658

60. Ismael, N. F. (1982), "Design of Shallow Rock-Anchored Foundations", Canadian Geotechnical Journal, Vol.19, No.2, pp.469-471

61. ISRM(1982), Suggest methods for rock bolt testing, Pergamon Press. pp 163-168

62. Itasca (2015) 3DEC Version 5.0 dimensional distinct element code. Itasca Consulting Group Inc., Minneapolis, MN

63. Ivars, D. M., Pierce, M. E., Darcel, C., Reyes-Montes, J., Potyondy, D. O., Young, R. P., & Cundall, P. A. (2011). The synthetic rock mass approach for jointed rock mass modelling. International Journal of Rock Mechanics and Mining Sciences, 48(2), 219-244.

64. Jing, Lanru, and J. A. Hudson. "Numerical methods in rock mechanics." International Journal of Rock Mechanics and Mining Sciences 39.4 (2002): 409-427.

65. Kim, H-K. & Cho, N. J. (2012). A design method to incur ductile failure of rock anchors subjected to tensile loads. Electronic Journal of Geotechnical Engineering, 17(T), pp 2737-2746

66. Kim, D. H., & Lee, S. R. (2005). Uplift capacity of fixed shallow anchors subjected to vertical loading in rock. International Journal of Offshore and Polar Engineering, 15(04).

67. Klerck P.A. (2000) The finite element modelling of discrete fracture in quasi-brittle materials PhD Thesis University of Wales, Swansea, UK

68. Klerck P.A., Sellers E.J., Owen D.R.J. (2004) Discrete fracture in quasi-brittle materials under compressive and tensile stress states Computer Methods in Applied Mechanics and Engineering, 193 (27–29). pp 3035–3056

69. Krenchel, H., & Shah, S. P. (1985). Fracture analysis of the pullout test. Materials and Structures, 18(6), 439-446.

70. Lamas, L., Perucho, A., & Alejano, L. R. (2014). Some key issues regarding application of Eurocode 7 to rock engineering design. Rock engineering and rock mechanics: structures in and on rock, Proceedings of Eurock.

71. Langford, J.C., and Diederichs, M.S. (2013), Evaluating uncertainty in intact and rock mass parameters for the purposes of reliability assessment. 47th U.S. Rock Mechanics / Geomechanics Symposium, June 23 - 26, 2013 , San Francisco, California"

72. Langford JC (2013) Application of reliability methods to the design of underground structures. PhD Thesis, Queen's University, Kingston, Ontario, Canada

73. Langford, J. C., & Perras, M. A. (2014, August). Obtaining Reliable Estimates of Intact Tensile Strength. In 48th US Rock Mechanics/Geomechanics Symposium. American Rock Mechanics Association.

74. Lemos (2012) Discontinuum models for dam foundation failure analysis Q. Qian, Y.X. Zhao (Eds.), Harmonising rock engineering and the environment, Proceedings of the 12th Congress, International Society for Rock Mechanics, Beijing, CRC Press/Balkema, Leiden (2012). pp 91–98

75. Littlejohn, G. S., & Bruce, D. A. (1975). Rock anchors-state of the art. Part 1: design. Ground Engineering, 8(3).

76. Littlejohn, G. S. (1993). Overview of rock anchorage. In Comprehensive Rock Engineering, Pergamon Press, UK, Vol. 4, Ch. 15. pp 413–450

77. Littlejohn G.S. and Bruce D.A., (1977) Rock anchors – design and quality control. In Fairhurst, C. & Crouch, S. L. (Eds.), Design Methods in Rock Mechanics, Proceedings of the 16th Symposium on Rock Mechanics. pp 77-88

78. Littlejohn, G. S., Bruce, D. A., & Deppfier, W. (1977). Anchor Field Tests in Carbonferous Strata. Revue Franoaise Geotechnique, 82-86.

79. Morgan, S. P., Johnson, C. A., & Einstein, H. H. (2013). Cracking processes in Barre granite: fracture process zones and crack coalescence. International journal of fracture, 180(2). pp 177-204.

80. Panton, B., Elmo, D., Schotfeldt, P., & Carvalho, J. (2014). Design of rock foundation anchorage using Discrete Fracture Networks. In Proceedings of the International Discrete Fracture Network Engineering Conference, Vancouver.

81. Panton B., D. Elmo, J. Carvalho and E.T. Brown. (2015). Numerical simulation of rock cone pullout and the influence of discrete fracture network statistics on foundation anchor capacity. Proceedings of the 13th ISRM Congress. Montreal, May 10-13th. Paper 711.

82. Panton, B., Elmo, D., Stead, D., & Schlotfeldt, P. (2015). A discrete fracture network approach for the design of rock foundation anchorage. Mining Technology, 124(3), 150-162.

83. Park, J., Qiu, T., & Kim, Y. (2013). Field and laboratory investigation of pullout resistance of steel anchors in rock. Journal of Geotechnical and Geoenvironmental Engineering, 139(12), 2219-2224.

84. Pease K.A., Kulhawy F.H. (1984) Load transfer mechanisms in rock sockets and anchors. Report EL-3777 Electric Power Research Institute, Palo Alto.

85. Rocscience Inc. (2011) Phase2 Version 8.0—Finite Element Analysis for Excavations and Slopes, Toronto

86. Preston, R. (2014). Application of Photogrammetry to Estimates of Mine Pillar Damage and Strength. MSc.. Simon Fraser University, Burnaby.

87. Post Tensioning Institute (2004) Recommendations for Prestressed Rock and Soil Anchors, Fourth Edition. PTI, Phoenix AZ"

88. Saliman, R. and Schaefer, R. (1968), Anchored Footings for Transmission Towers, ASCE Annual Meeting and National Meeting on Structural Engineering, Pittsburge, PA, Sept. 3~Oct. 4, Preprint 753. pp.15-38

89. Schlotfeldt, P., Panton, B., Humphries, R., & Elmo, D. (2013, January). New Park Bridge, Kicking Horse Canyon; Pier 5—A Difficult Foundation on Rock. In 47th US Rock Mechanics/Geomechanics Symposium. American Rock Mechanics Association.

90. Sinclair, M R & Rodd, R J, (2011) The recent development and application of large ground anchors for dams. The Future of Dams, Proc ANCOLD 2011 Conf, Melbourne, 27-28 October, 8

91. Stead, D., & Eberhardt, E. (2013). Understanding the mechanism of large landslides. In Proceedings of the International Conference on Vajont-1963-2013-Thoughts and Analyses After 50 Years Since the Catastrophic Landslide (pp. 85-112).

92. Sutton J. J, Fenwick G. J, Stephenson N. G. Spring 2004. Seven Mile Dam: Dam Safety Improvements. Canadian Dam Association. pp 12-17

93. Thomas-Lepine (2012) Rock bolts – improved design and possibilities MSc Thesis Norwegian University of Science and Technology, Trondheim.

94. Tuckey, Z. (2012). An integrated field mapping-numerical modelling approach to characterising discontinuity persistence and intact rock bridges in large open pit slopes. MSc.. Simon Fraser University, Burnaby.

95. U. S. Army Corps of Engineers (1994), Engineering and Design Rock Foundations, EM 1110-1-2908, Nov. 30. pp.69-73

96. Weerasinghe R.B., Littlejohn G.S. (1997) Uplift capacity of shallow anchorages in weak mudstone G.S. Littlejohn (Ed.), Ground anchorages and anchored structures: Proceedings of the International Conference, London, Thomas Telford, London. pp 23–33

97. Weerasinghe R.B. and Adams D. (1997) A technical review of rock anchorage practice 1976–1996 G.S. Littlejohn (Ed.), Ground anchorages and anchored structures: Proceedings of the International Conference, London, Thomas Telford, London. pp 481–491

98. Wiles, T. D. (2006). Reliability of numerical modelling predictions. International Journal of Rock Mechanics and Mining Sciences, 43(3), 454-472.

99. Wolfrum S.G., Serrano A., Olalla C. (2007) Model failure tests on rock anchors. Proceedings of the 11th ISRM Congress Volume III. Lisbon PORTUGAL, in 2007 July 09-13. pp 339-342

100. Wong LNY, Einstein HH (2008) Coalescence behavior in Carrara marble and molded gypsum containing artificial flaw pairs under uniaxial compression. In: Proceedings of the 1st Canada-US rock mechanics symposium, Vancouver, Canada, pp 581–589

101. Wong LNY, Einstein HH (2009a) Crack coalescence in molded gypsum and Carrara marble: part 1. Macroscopic observations and interpretation. Rock Mech Rock Eng 42(3). pp 475–511

102. Wong LNY, Einstein HH (2009b) Crack coalescence in molded gypsum and Carrara marble: part 2—microscopic observations and interpretation. Rock Mech Rock Eng 42(3). pp 513–545

103. Wyllie D.C. (1999) Foundations on rock: engineering practice (2nd ed.) E & FN Spon, London

104. Wyllie, D.C. and Mah, C.W. (2004). Rock Slope Engineering: civil and mining, 4th ed., London, New York, Spon Press.

105. Xu and Benmokrane (1996) Strengthening of existing concrete dams using post-tensioned anchors: a state-of-the-art review Canadian Journal of Civil Engineering, 23 (6). pp 1151–1171

106. Yan (2008) Numerical modelling of brittle fracture and step-path failure: from laboratory to rock slope scale PhD Thesis Simon Fraser University, Burnaby, Canada

107. Yap, L. P. (1980). A study of the behaviour of vertical rock anchors using the finite element method PhD Thesis University of Aberdeen, United Kingdom

108. Zang. Y (2014) Modelling Hard Rock Pillar Using a Synthetic Rock Mass Approach PhD Thesis Simon Fraser University, Burnaby, Canada